
Doctoral Dissertations

Student Theses and Dissertations

Fall 2018

Delineation of a coal combustion residue landfill and underlying karst subsurface in Southwest Missouri using ERT and MASW surveys

Ruobai Zhao

Follow this and additional works at: https://scholarsmine.mst.edu/doctoral_dissertations



Part of the [Geological Engineering Commons](#), and the [Geophysics and Seismology Commons](#)

Department: Geosciences and Geological and Petroleum Engineering

Recommended Citation

Zhao, Ruobai, "Delineation of a coal combustion residue landfill and underlying karst subsurface in Southwest Missouri using ERT and MASW surveys" (2018). *Doctoral Dissertations*. 2857.
https://scholarsmine.mst.edu/doctoral_dissertations/2857

This thesis is brought to you by Scholars' Mine, a service of the Missouri S&T Library and Learning Resources. This work is protected by U. S. Copyright Law. Unauthorized use including reproduction for redistribution requires the permission of the copyright holder. For more information, please contact scholarsmine@mst.edu.

DELINEATION OF A COAL COMBUSTION RESIDUE LANDFILL AND UNDERLYING
KARST SUBSURFACE IN SOUTHWEST MISSOURI USING ERT AND MASW SURVEYS

by

RUOBAI ZHAO

A DISSERTATION

Presented to the Faculty of the Graduate School of the
MISSOURI UNIVERSITY OF SCIENCE AND TECHNOLOGY

In Partial Fulfillment of the Requirements for the Degree

DOCTOR OF PHILOSOPHY

in

GEOLOGICAL ENGINEERING

2018

Approved by:

Dr. Neil L. Anderson, Advisor
Dr. J. David Rogers
Dr. Lesley H. Sneed
Dr. Evgeniy V. Torgashov
Dr. Norbert H. Maerz

© 2018

Ruobai Zhao

All Rights Reserved

ABSTRACT

The safe containment of coal combustion residual (CCR) in landfills was addressed by the U.S. Environment Protection Agency (EPA) CCR rule published in 2015. The new rule affects new and existing U.S. based CCR landfills in terms of implementing safeguard systems for safe disposal and contamination control. Electrical resistivity tomography (ERT) and multichannel analysis of surface waves (MASW) data were acquired across and in proximity to a CCR landfill in southwest Missouri, USA, with the intent to identify potential karst features and seepage pathways.

Electrical resistivity tomography data were acquired using an automated 8-channel resistivity meter and multichannel analysis of surface waves data were acquired using a 24-channel Seistronix engineering seismograph and 4.5 Hz geophones. MASW data were acquired to aid the ERT data interpretation by providing engineering properties of subject materials. The outcome from the ERT survey were a suite of 2D and 3D resistivity images. ERT investigates the subsurface to a depth of approximately 100 ft. The outcome from the MASW survey were a suite of 1-D and 2-D (depth vs. shear wave velocity) profiles. MASW investigates the subsurface to a depth of approximately 100 ft. The variations in top-of-rock, variations in moisture content of the CCR, soil and bedrock, and seepage pathways and flow patterns, were successfully mapped.

The findings of this research indicate that the seepage pathways in close proximity to the landfill are from surface run-off and do not pose a threat to groundwater, and no evidence of karst features that could affect the structure stability of the CCR landfill in close proximity to and underneath the site was found.

ACKNOWLEDGMENTS

First and foremost, I would like to thank my Ph.D. advisor Dr. Neil Anderson for his tremendous support, both academically and financially, throughout this dissertation work and my Ph.D. years.

I would like to thank my committee member Dr. David Rogers for the guidance, financial support/scholarship, and courage he offered. I truly appreciate the daily interactions with him, which teaches me something new every day.

I would like to thank my committee members, Dr. Evgeniy Torgashov, Dr. Lesley Sneed and Dr. Norbert Maerz, for their time and guidance on the writing of this dissertation.

I would like to thank my fellow researchers who have contributed in any way for the making of this dissertation.

I would like to thank Dr. Katherine Grote for offering me a teaching assistantship. I would like to thank Office Support Assistant Sharon Lauck and my Graduate Study advisor Katherine Wagner for processing my paperwork and answering my countless questions.

I would like to thank my lovely wife Jing Sun, without whose sacrifice and tremendous support, I would not have been able to achieve what I have achieved. I would like to thank my young son Nolan for being my companion alongside the journey. I would like to thank my parents who provided emotional support and financial support.

TABLE OF CONTENTS

	Page
ABSTRACT.....	iii
ACKNOWLEDGMENTS	iv
LIST OF ILLUSTRATIONS.....	viii
LIST OF TABLES.....	xii
 SECTION	
1. INTRODUCTION.....	1
2. METHODS AND OBJECTIVES	4
2.1. METHODS	4
2.2. RESEARCH OBJECTIVES	5
3. CCR DISPOSAL IN LANDFILLS.....	7
3.1. BACKGROUND	7
3.2. SAFE CCR DISPOSAL AND REGULATIONS.....	9
3.3. CCR LANDFILL SYSTEM.....	13
3.3.1. Site Selection and Construction.	13
3.3.2. Components of CCR Landfills.	14
3.3.2.1. Cap cover system..	15
3.3.2.2. CCR deposit.....	19
3.3.2.3. Leachate control system.....	28
3.3.2.4. Composite liner system.....	31
3.3.2.5. Run-on and run-off control.	34

4. KARST AND GROUNDWATER.....	39
4.1. LAND SUBSIDENCE AND KARST.....	40
4.2. SINKHOLE TYPES	44
4.3. GROUNDWATER FLOW.....	46
4.3.1. Groundwater Flow in Non-Karst Formations.	47
4.3.2. Groundwater Flow in Karst Formations.....	48
5. ELECTRICAL RESISTIVITY TOMOGRAPHY AND MULTICHANNEL ANALYSES OF SURFACE WAVES.....	52
5.1. RESISTIVITY VARIATIONS OF THE EARTH SUBSURFACE MATERIALS.....	52
5.2. RESISTIVITY OF CCR, SOIL AND SAND.....	55
5.3. ELECTRICAL RESISTIVITY TOMOGRAPHY BASIC THEORY	55
5.4. MULTICHANNEL ANALYSES OF SURFACE WAVES	61
6. DATA PREPARATION	63
6.1. GEOLOGIC SETTING	63
6.2. DATA ACQUISITION PLAN AND LAYOUT	64
6.3. ERT DATA ACQUISITION AND PROCESSING.....	66
6.3.1. Pre-Survey Considerations.	66
6.3.2. Field Operations.	67
6.3.3. Common Data Acquisition Problems and Solutions.	75
6.3.4. ERT Data Processing.....	78
6.4. MASW DATA ACQUISITION AND PROCESSING	78
6.4.1. Field Operations.	78
6.4.2. MASW Data Processing.....	79

7. RESULTS AND DISCUSSIONS	82
8. CONCLUSIONS	108
BIBLIOGRAPHY	111
VITA	118

LIST OF ILLUSTRATIONS

Figure	Page
1.1. Percentage of beneficially used fly ash and CCR.....	1
1.2. The wet storage and dry storage of CCR disposals..	2
3.1. CCR storage in landfills.....	7
3.2. 2015 EPA CCR rule regarding safe CCR landfill deposals.....	10
3.3. Typical components of a solid waste landfill.	14
3.4. Illustrative diagram showing different systems above and below the CCR deposit.....	16
3.5. CCR landfill cap cover and installation.	17
3.6. A Geosynthetic cap cover system and prescriptive cap cover system.....	18
3.7. CCR production during coal combustion.	20
3.8. Bottom ash.	22
3.9. Boiler slag.	22
3.10. Photograph of FGD materials.	23
3.11. Fly ash.....	24
3.12. Fly ash particle size and color.....	25
3.13. Leachate drains through leachate pipes.	29
3.14. Photograph of a “chimney drain”.	30
3.15. Flow rate variations through different liner systems	32
3.16. Good seal vs. poor seal.	34
3.17. Most of the run-off flows down along the flanks of the CCR landfill.....	36
3.18. Landfill run-off control.	37

3.19. Illustrative diagram of seepage into the subsurface.	38
4.1. Karst features.	40
4.2. Photograph of land subsidence caused by water withdrawal in California.	41
4.3. Sinkholes in Missouri.	42
4.4. Photographs of sinkhole formed on a golf course built on karst terrain.	43
4.5. Illustrative diagram showing solution-widened joints and voids in the karst subsurface.	44
4.6. Different types of sinkholes.	45
4.7. Basic groundwater flow diagram.	47
4.8. Porosity, permeability and hydraulic gradient.	49
4.9. Dye tracing for groundwater monitoring.	51
5.1. Two types of conduction in the subsurface.	52
5.2. Resistivity values of common rocks, soil materials and chemicals.	53
5.3. Basic conductor diagram illustrating Ohm's law.	56
5.4. Basic diagram of a cylinder-shaped conductor.	57
5.5. Simple resistivity survey diagram.	59
5.6. Five commonly used ERT arrays.	60
5.7. Illustration of the dipole-dipole array.	60
5.8. Illustration of the Wenner array.	60
6.1. The study area is underlain by Mississippian limestone.	64
6.2. Illustrative ERT and MASW data acquisition locations.	65
6.3. ERT data acquisition equipment.	69
6.4. ERT field survey layout.	70
6.5. Installing stakes into the ground using a 5 lb hammer.	71

6.6. Attached electrode on stainless-steel stake.	71
6.7. Adding water onto the ground for effective conductivity.....	73
6.8. Raw field data were stored in the resistivity meter as Stg. files and converted into Dat. files on-site.	74
6.9. Common issues associated with ERT data acquisition in the field.	76
6.10. 24-channel Seistronix seismograph with 4.5 Hz geophones placed at 5 ft intervals.....	80
6.11. Generate 2-D MASW profile from 1-D MASW profiles.	81
7.1. Resistivity variations in the CCR deposit.	84
7.2. Illustrative diagram of the CCR landfill run-off directions.	85
7.3. Seepage pathways resulted from moisture seeping down into the pervasively fractured bedrock.....	87
7.4. Aerial view of the CCR landfill and the locations of the ERT traverses surrounding the landfill.	88
7.5. ERT profile acquired at the north toe.	91
7.6. ERT profiles acquired at the west toe of the landfill.	92
7.7. Run-off gets intercepted by man-made features.	93
7.8. ERT profiles acquired near the retention pond.	95
7.9. ERT profiles acquired near the southeast berm.	96
7.10. ERT profiles acquired at the east toe of the landfill.	98
7.11. ERT profile acquired at the northeast toe of the landfill.	99
7.12. ERT profiles acquired over a berm near the west toe of the landfill.	101
7.13. ERT profiles acquired at the east toe of the landfill.	102
7.14. 3-D ERT profiles 614-615, 615-616, 616-617.....	104
7.15. Moisture content comparison between ERT profile 8' and ERT profile 1.	105

7.16. ERT top-of-rock is consistent with MASW top-of-rock at ERT station 450 on 3-D ERT profile 600-601.....	106
7.17. MASW top-of-rock is 20 ft at ERT station 240.....	107

LIST OF TABLES

Table	Page
3.1. Comparison between EPA regulation and Missouri regulation CSR 80-11.010	11
3.2. Fly ash engineering properties	26
6.1. Common problems associated with ERT data acquisition and solutions	77

1. INTRODUCTION

Power plants utilize coal to generate electricity and steam and produce millions of tons of coal combustion residue (CCR) every year. In a recent document published by the U.S. EPA, in the year of 2012 alone, approximately 110 million tons of CCR were produced in 47 states and Puerto Rico from over 470 coal-fired electric utilities (U.S. EPA, 2015). The American Coal Ash Association (ACAA) reported that, as the second largest industrial waste stream, coal usage is expected to grow 3.4% over the next two decades, and the production of fly ash, which makes up approximately 80% of the CCR, is expected to increase by 2.6% through the year of 2033. CCR is reported to contain toxic metals (e.g., arsenic, mercury, lead, chromium), which can cause heart disease, cancer, respiratory diseases (Earthjustice.org, n.d.).

CCR has been beneficially used extensively in the civil industry (e.g., to produce concrete cement). In 2016, the recycling rate for CCR reached approximately 56% of the overall CCR production (ACAA, 2016), shown in Figure 1.1.

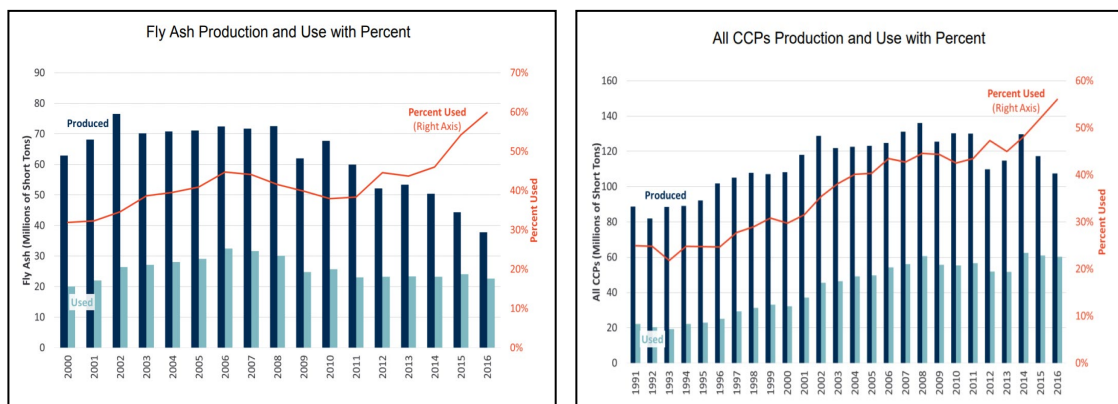


Figure 1.1. Percentage of beneficially used fly ash and CCR (ACAA, 2016).

CCR that is not immediately recycled for beneficial use is contained in CCR disposal sites (Figure 1.2), in either ash ponds (wet form) or landfills (dry form).

According to the U.S. EPA (2015), in 2012, the United States had over 310 CCR landfills in operation.



Figure 1.2. The wet storage and dry storage of CCR disposals. a) CCR disposal in an ash pond (Catawba Riverkeeper Foundation, 2018). b) CCR disposal in a landfill (Crum, 2018).

Many argue that without strict regulations to enforce the safe containment of CCR, CCR could potentially cause harm to humans, animals, and the environment by contact. The public has voiced their concerns over CCR landfills, or CCR disposal in general, regarding their safety and environmental impact. It is generally accepted that enforcing more stringent regulations regarding the placement, design, monitoring, and reporting of CCR landfill will help prevent or minimize potential negative CCR landfill

impacts (e.g., contamination to groundwater, structure failure). The U.S. EPA published a final rule in 2015 addressing these concerns. This 2015 EPA CCR rule, compared to many state regulations, is a more stringent regulation. Several states (e.g., Missouri) since then have announced the plan to adopt the minimum criteria listed in the new rule gradually. Many new and existing CCR landfills owners are advised to obtain professional engineering site assessments. For CCR landfills that were built and are operating over unstable areas (e.g., karst terrain), owners are advised to address several issues associated with karst that could affect landfill structure stability and groundwater.

2. METHODS AND OBJECTIVES

2.1. METHODS

This research was inspired and prompted by the increasing need from CCR landfill owners, especially those who operate on karst terrains, to obtain effective and accurate assessments over their sites. The utilization of the modern geophysical investigation techniques (ERT and MASW) was determined based on several factors:

1. Techniques with time-effective acquisition, processing, and interpretation mechanisms that help the owners adopt the new rule promptly are preferable.
2. Techniques that are non-invasive and cause no damage to the containment of the CCR are preferable.
3. Techniques that have been proved to be effective for karst terrain investigations, and sensitive to moisture content are preferable.
4. Techniques that are cost-effective are preferable as CCR landfills usually take up a large area of land hence require relatively more investigation time and labor.

ERT and MASW have been proven to be excellent tools for karst terrain investigations. The typical combined output from ERT and MASW are quality 1-D, 2-D, and 3-D images of the subsurface, where the bedrock depth, soil thickness, moist content variations, possible seepage pathways, and karst features could be identified. ERT and MASW data acquisitions can be conducted fairly quickly covering large areas of investigated surface and are non-invasive and not labor-intensive. Acquired ERT and MASW data can be processed and interpreted within reasonable periods of time, provided that the interpreter is experienced, and constraints are available. Utilizing both

ERT and MASW geophysical techniques provides reliable results by analyzing correlations between ERT data and MASW data.

Commonly used borehole logging, if utilized as the primary tool, will not be sufficient in this type of investigation. Traditional borehole logging aid engineers in understanding the subsurface material distribution by providing intuitive information of the subsurface, however, it generally requires extensive time, labor, and cost to thoroughly investigate large areas of land. It can be difficult to generate a continuous and extensive image of the subsurface with only borehole data.

It is worth mentioning that borehole logging could significantly aid the interpretations of ERT and MAST data. In areas where ERT and MASW data do not correlate well, borehole logging can be conducted at those specific areas to serve as a constraint for ERT and MASW interpretation. The interpretations of ERT and MASW data also depends heavily on the engineering judgment and local geology experience of the interpreter.

With the consideration of all the factors discussed, for this research, it was determined to use ERT as the primary investigating tool and MASW as the secondary investigation tool.

2.2. RESEARCH OBJECTIVES

The objective of this research is to image the subsurface underneath and in proximity to a CCR landfill for findings of any potential karst features and seepage pathways that could affect the landfill structure stability and groundwater. The objective of this research is also to provide insight into the understanding of seepage flow patterns

and causes of moisture content variations in the subsurface. This research specifically aims to:

1. Delineate variations in top-of-rock.
2. Delineate variations in moisture content of CCR, soil, and rock.
3. Delineate possible seepage pathways through, underneath, and around the CCR landfill.
4. Identify possible seepage flow patterns.
5. Identify possible subsurface karst features.
6. Demonstrate the impact of anthropogenic features on subsurface moisture content.

3. CCR DISPOSAL IN LANDFILLS

3.1. BACKGROUND

As the dry storage of CCR, CCR produced in the coal-burning process is transported to and disposed at on-site or off-site landfills (Figure 3.1). CCR previously stored in ash ponds (wet storage) may also be transferred to landfills once ponded CCR is dried. Although CCR landfills are generally termed as “dry storage,” it is common to lightly damp CCR with water and wetting agents before loading CCR onto trucks for disposal, as a caution for dust control. Other dust-control measures include minimizing activity during high wind and, maintaining a lower vehicle speed. Sometimes CCR is compacted before transport to reduce overall volume (William, Thierry, Schuller, & Subway, 1981).



Figure 3.1. CCR storage in landfills. a) Photograph of a CCR landfill (Teirstein, 2018). b) Photograph of CCR being dumped by trucks (Duke Energy, 2016).

The handling and transporting cost associated with CCR usually has a considerable impact on the location selection of CCR landfill disposals. In the United States, CCR landfill disposals are commonly built on the same property where the CCR is generated. It is preferred by CCR landfill owners to place CCR on-site rather than off-site, as the cost of transporting produced CCR to off-site locations can be considerably high. According to U.S. EPA, in the year 2012, approximately 80% of the CCR disposals were on-site disposals. It is also common for CCR landfill owners to consider expansions of the existing landfills once their current landfill capacity is met.

The proper construction and operation of CCR landfills with safeguard systems are crucial to the successful containment of CCR materials. At the time of this research, in the United States, CCR landfills are regulated as “solid waste” (RCRA Subtitle D) rather than “hazardous waste” (RCRA Subtitle C), stated in the 2015 EPA CCR rule. However, it is generally accepted that without any type of protective measures, such as a liner system, leachate control system, run-on, and run-off control system, it is easier for rainwater to infiltrate into the CCR deposit, and potentially percolate into the subsurface soil and rock. Such leachate can further get into groundwater.

Another factor that contributes to the safe CCR landfill disposals is the formation upon which the CCR landfill is constructed. Certain types of formation (e.g., wetlands, seismic impact zones, unstable areas) could adversely affect the containment of the CCR should CCR landfills be built in these areas without assessment and safeguarding. In some regions of the United States where karst formation is predominant, the underlain carbonate rocks are subject to karstification to form solution widened joints, fractures, and caves, which could facilitate the seepage of leachate into subsurface groundwater, as

leachate flows more freely and faster in karst enlarged fractures/pathways compared to in non-karst formations.

3.2. SAFE CCR DISPOSAL AND REGULATIONS

Newer CCR landfills are generally constructed and operated in a way to prevent or minimize both leachate production and leachate infiltration, while older CCR landfills may or may not be constructed in such a way to adequately address those issues, depending on the then-effective EPA and state regulations at the time of construction.

The U.S. EPA was prompted to propose a more stringent regulation to address the risks associated with CCR disposals, following one CCR disposal site spill incident in Tennessee. Web source Earthjustice.org reported that as the biggest toxic waste spill in U.S. history, occurred in 2008, when a CCR disposal site in Kingston, Tennessee spilled 1,100,000,000 gallons of toxic sludge across 30 acres, polluting the Emory and Clinch rivers, damaging 40 nearby homes, and resulting in impact of \$3 billion for cleanup costs.

The U.S. EPA eventually published a final CCR rule (U.S. EPA, 2015) on April 17, 2015, which took effect on October 19, 2015, to serve as the minimum criteria for safe CCR disposals. Under this updated EPA rule, CCR disposals are regulated as “solid waste” under Subtitle D of the Resource Conservation and Recovery Act (RCRA).

First, the 2015 EPA CCR rule (Figure 3.2) aims to address the formation impact on the safe disposal of CCR; the placement of CCR landfills is hence restricted for several areas. Second, to prevent leachate seepage into subsurface groundwater, new CCR landfills and existing CCR landfill seeking for lateral expansion, are required to install a liner system at the bottom of the CCR deposit. EPA requires explicitly the liner

system to be a composite liner system that consists of a geomembrane and a clay (at least 2 ft) with low permeability, or an equivalent composite liner system that has the same or lower permeability.

Further, new CCR landfills are now required to install leachate control systems for leachate collection and removal. All CCR landfills, new or existing, should have run-on and run-off control. Groundwater monitoring is also required for all CCR landfills (e.g., installing water monitoring wells to continuously monitor water quality).

Additionally, for CCR landfills that have wholly or partially ceased operation, a cap cover is required on areas that are no longer accepting new CCR, and owners must continue to monitor and maintain the landfill after closure for a certain amount of time.

CCR Landfill Requirements				
Requirement	Existing CCR Landfills		New CCR Landfills and Lateral Expansions	
	Required? ¹	Rule Section	Required? ¹	Rule Section
Location Restrictions:	√	§257.64	√	§257.60 - §257.64
Placement Above the Uppermost Aquifer			√	§257.60
Wetlands			√	§257.61
Fault Areas			√	§257.62
Seismic Impact Zones			√	§257.63
Unstable Areas	√	§257.64	√	§257.64
Floodplains ²	√	§257.3-1	√	§257.3-1
Endangered Species ²	√	§257.3-2	√	§257.3-2
Design Requirements:			√	§257.70
Composite Liner			√	§257.70 (b & c)
Leachate Collection and Removal System			√	§257.70 (d)
Groundwater Monitoring and Corrective Action	√	§257.90 - §257.98	√	§257.90 - §257.98
Weekly Inspections	√	§257.84 (a)	√	§257.84 (a)
Annual Inspections	√	§257.84 (b)	√	§257.84 (b)
Fugitive Dust Controls	√	§257.80	√	§257.80
Run-on, Run-off Controls	√	§257.81	√	§257.81
Surface Water Protection ²	√	§257.3-3	√	§257.3-3
Closure Requirements	√	§257.100 - §257.103	√	§257.100 - §257.103
Post-Closure Care	√	§257.104	√	§257.104
Recordkeeping Requirements	√	§257.105	√	§257.105
Notification Requirements	√	§257.106	√	§257.106
Publicly Accessible Internet Site Requirements	√	§257.107	√	§257.107
¹ √ = required, = not required. ² In existing regulations at 40 CFR part 257, subpart A.				

Figure 3.2. 2015 EPA CCR rule regarding safe CCR landfill disposals.

It is worth mentioning the 2015 EPA CCR rule is “self-implementing,” and EPA does not enforce the implementations of this rule (CCR landfills are state-regulated). EPA does, however, advise states to adopt the minimum criteria listed in this rule. This research was conducted at a CCR landfill located in Missouri. Therefore it is reasonable to compare Missouri regulations with the EPA CCR rule on CCR landfills (Table 3.1).

According to the Missouri Department of Natural Resources (MDNR, 2016), current Missouri regulations on CCR landfills are less stringent than EPA regulations, regarding groundwater separation, construction in seismic impact zones, liner and final cover requirements, groundwater corrective action, the length of the post-closure period, and inspections. However, in 2015 Missouri started to revise state regulations aiming to adopt the minimum requirements of the 2015 EPA CCR rule, and have asked affected CCR landfill owners in Missouri hence comply with EPA regulations without state or federal oversight. Nonetheless, it is reasonable to conclude that more and more states are likely to adopt the minimum criteria listed in the 2015 EPA CCR rule.

Table 3.1. Comparison between EPA regulation (80 FR 21301) and Missouri regulation CSR 80-11.010 (adopted from EPA and MDNR)

New CCR landfills (and existing CCR landfills seeking for lateral expansion)	EPA regulation (80 FR 21301)	Missouri regulation (CSR 80-11.010)
Placement above the uppermost aquifer	No less than 5 ft or prove no hydraulic connection	Requires 1 ft separation

Table 3.1. Comparison between EPA regulation (80 FR 21301) and Missouri regulation CSR 80-11.010 (adopted from EPA and MDNR) (cont.)

Placement in wetlands	Prohibited	Prohibited
Placement in fault areas	Within 200 ft of a fault that has had displacement in Holocene time	N/A
Placement in seismic impact zone	Prohibited	Prohibited within 200 ft of a fault that has had displacement in Holocene time
Placement in unstable areas	Prohibited (existing CCR landfill included)	Prove structure stability will not be affected
Liner system	Composite liner (geomembrane + 2 ft clay liner with K less than 1×10^{-7} cm/s) or equivalent composite liner	Composite liner (geomembrane + 2 ft clay liner) or 2 ft clay liner with K less 1×10^{-7} cm/s
Leachate collection and removal system	Required	Required
Groundwater monitoring	Required	Required
Cap cover	Required infiltration layer and an erosion layer, provided the infiltration layer has a permeability less than or equal to the bottom liner or natural subsoils K less than 1×10^{-5} cm/s	Required 1 ft compacted clay with K less than 1×10^{-5} cm/s +1 ft overlying soil layer
Run-on and run-off control	Required	Required

3.3. CCR LANDFILL SYSTEM

3.3.1. Site Selection and Construction. To minimize the formation impact on the safe disposal of CCR, the placement of CCR landfills is restricted for several areas by the 2015 EPA CCR rule (Missouri regulation is similar regarding placement restrictions). New CCR landfills and existing CCR landfills seeking lateral expansion, are now subject to the location restrictions for placement above the 1) uppermost aquifer, 2) in wetlands, 3) within fault areas, 4) in seismic impact zones, and 5) in unstable areas., For existing CCR landfills, they are subject to the location restriction for placement above unstable areas, providing the landfill is not aiming for lateral expansion.

Once the general location requirement is met, other factors such as the placement of various components of the CCR landfill should be considered before construction. Slopes of the topography should be taken into consideration for run-on control. Supporting facilities, such as leachate collection facilities, groundwater monitoring systems, drainage areas, and transportation roadways should be constructed to provide immediate access, and therefore ideally should be constructed in close proximity to the CCR deposit (Peppler, 2012).

The firm and consistent foundation is crucial to support the weight of the CCR deposit, and problems with expansive soil should be addressed. Following the corresponding codes, borings, in-situ and lab testings are carried out by geotechnical investigations for determination of optimum conditions of the material during placement. Normally, soil is wet and compacted to achieve 95% compaction to prevent or minimize future settlement and expansion, as well as to achieve low-permeability to prevent and minimize leachate seepage.

3.3.2. Components of CCR Landfills. A CCR landfill consists of its main component, CCR, and other safeguard systems (Figure 3.3). The safeguards meeting the requirement of the 2015 EPA rule should consist of a low-permeability cap cover (post-closure), a leachate control system, a bottom composite liner system, a run-on and run-off control system (e.g., drainage ditches, perimeter berms, stormwater retention), and groundwater monitoring system (e.g., the installation of upgradient and downgradient monitoring wells).

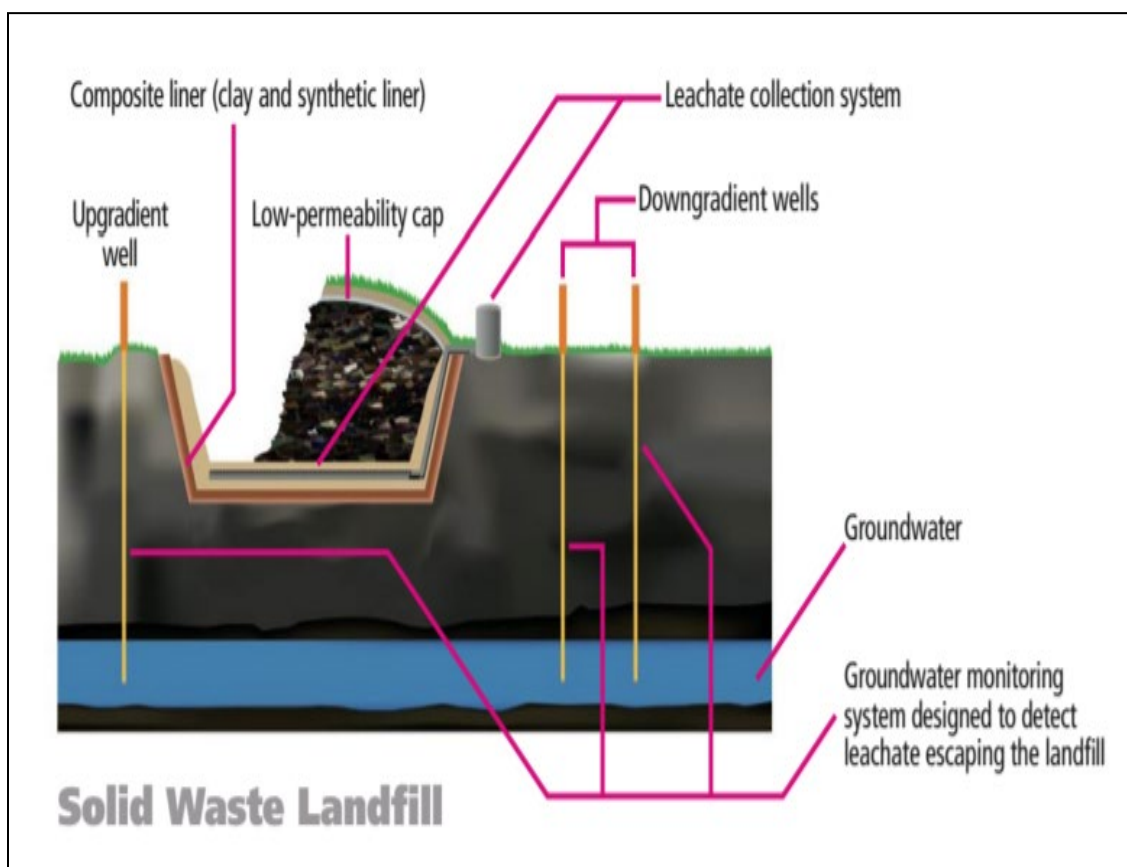


Figure 3.3. Typical components of a solid waste landfill (Tenenbaum, 2009).

3.3.2.1. Cap cover system. CCR landfill cap cover system (Figure 3.3 and Figure 3.4) is installed on top of the areas that ceased accepting new CCR. The purpose of the cap cover (also called “final cover” or “final cap”) is to limit rainwater contact with the CCR deposit, thus reducing leachate production. A cap cover is a layered system with low permeability aim to minimize precipitation infiltration into the CCR deposit, as well as to prevent CCR exposure to human and animals.

The cap cover systems for CCR landfills vary in design. The EPA rule (80 FR 21301), regulated under the RCRA Subtitle D for cap covers, requires an erosion layer and an infiltration layer to be installed as a minimum requirement. The erosion control layer must have earthen material capable of sustaining native plant growth with a minimum thickness of 6 inches (RCRA Subtitle D). The permeability of the infiltration layer should either be the equivalent permeability of any bottom liner or natural subsoils present, or less than 1×10^{-5} cm/s, whichever is less (80 FR 21301). Missouri regulates the cap cover under code CSR 80-11.010, which requires 1 ft of compacted clay with permeability less than 1×10^{-5} cm/s underlain by 1 ft of soil layer.

Generally, a soil layer with vegetation on top is utilized as the uppermost erosion layer in a CCR landfill cap cover (Figure 3.4 and Figure 3.5). The vegetation serves as erosion control and reduces water infiltration by evapotranspiration (Shanahan, 2004). The soil layer serves as a protective layer and nutrition source for vegetation growth.

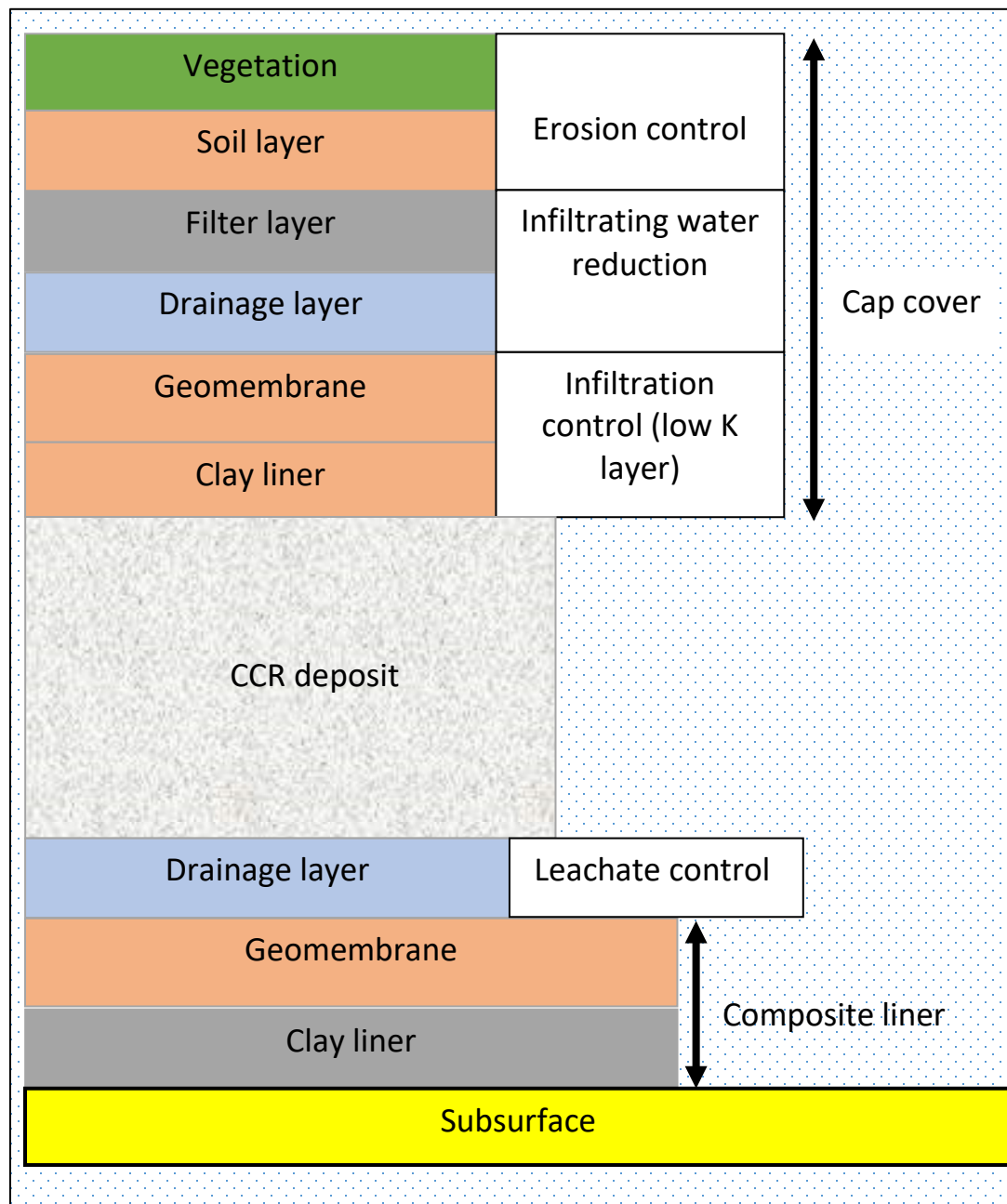


Figure 3.4. Illustrative diagram showing different systems above and below the CCR deposit.

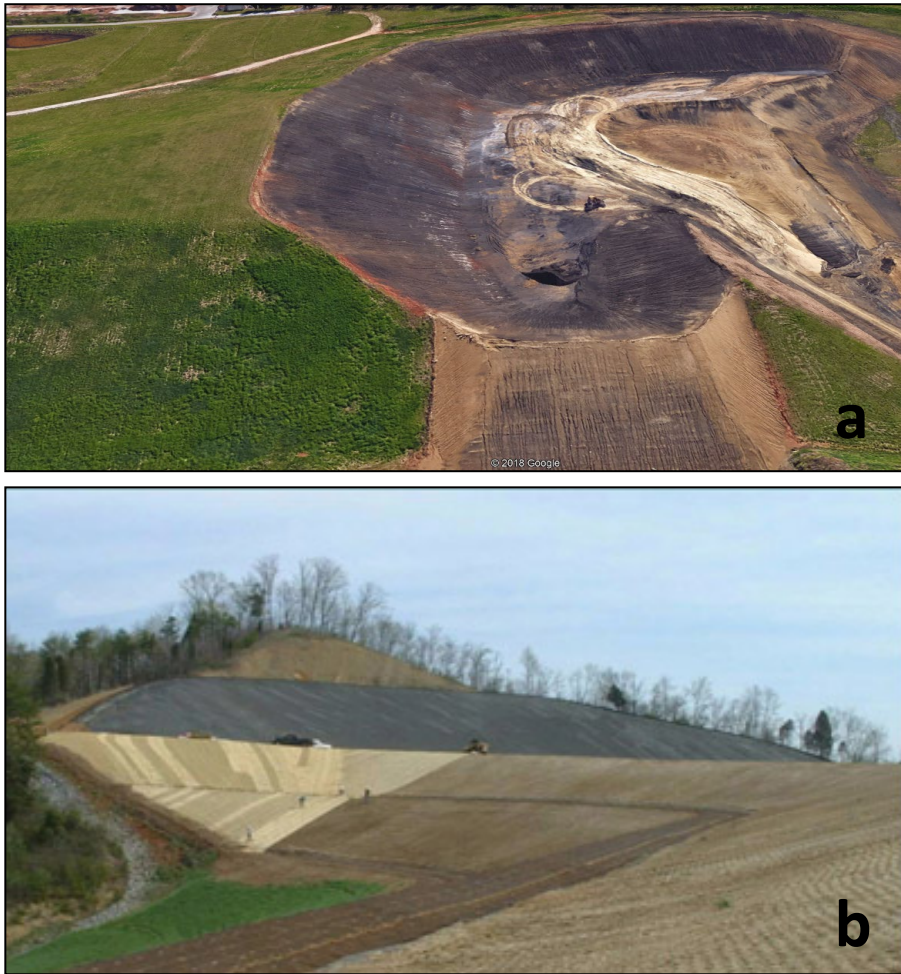


Figure 3.5. CCR landfill cap cover and installation. a) Google Earth image of a CCR landfill partially covered with “cap cover”. b) Soil layer is installed above the infiltration system for erosion control (Peppler, 2012).

The infiltration layer is also termed as the “low K” layer, which utilizes low permeability materials to prevent water infiltration into the CCR deposit. The 2015 EPA CCR rule does not require a composite liner system in the cap cover, provided that the infiltration layer meets the minimum permeability requirement. On the other hand, Missouri regulation requires the infiltration layer to be either a composite liner, such as a geomembrane sealed with at least 2 ft of clay that has permeability less than 1×10^{-5}

cm/s, or, as an alternative, a compacted clay layer with permeability less than 1×10^{-7} cm/s. In the meantime, other alternative cap cover systems have been developed that meet or exceed the 2015 EPA CCR requirement for cap covers, such as using solar panels as the top cover instead of the topsoil layer (Figure 3.6).

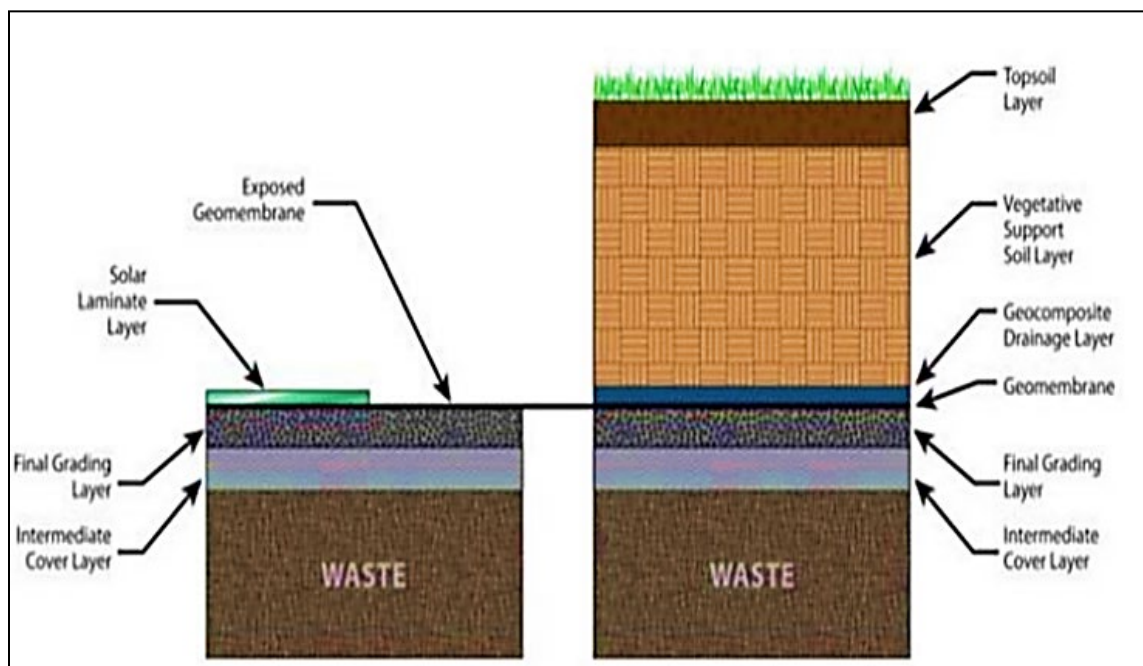


Figure 3.6. A Geosynthetic cap cover system (left) and prescriptive cap cover system (right) (Roberts, Flanders & Gumm, 2017).

Research has indicated that using a composite liner in the cap cover, usually the combination of geomembrane and clay, has a significant advantage over using a single clay liner or single geomembrane, in terms of preventing infiltration. The geomembrane is designed to have a very low permeability but is vulnerable to tears and holes, and the

clay liner can serve as a hydraulic and diffusional barrier at holes or breaks. Results show that the rate of flow into a single layer of clay liner with excellent permeability (1×10^{-8} cm/s), or into a single geomembrane layer with very few holes, is much greater than the flow rate into a composite layer system, even a low-quality one (Shanahan, 2004).

A drainage layer is typically installed between the topsoil layer and the infiltration layer. By gravitationally draining away water infiltrated through the upper soil, the amount of rainwater seeping down onto the infiltration layer is reduced. A 1 ft geosynthetic layer or 1 ft of sand with a permeability of 10^{-2} cm/s could be used as an example. The drainage layer is usually constructed at an angle to utilize gravity for drainage, and the fluid is discharged along CCR deposit flanks and to the toe of the landfill. To prevent the drainage layer from clogging, a filter layer is usually installed along with the drainage layer. The filter layer is normally made of geosynthetic filter fabric or 1 ft of sand and filters out the soil fines coming from the soil layer, which could potentially clog the drain.

3.3.2.2. CCR deposit. The components of the CCR disposed in the landfill vary among coal-burning facilities and are associated with the type of coal used. Generally, CCR is the solid mineral that is produced or left behind in the coal boiler in the coal combustion process, hence termed as “coal combustion residue.”

CCR generally consists of a significant portion of the mineral matter in the coal that is incombustible, while carbon and other combustible elements in the coal are oxidized or volatilized (William, Thiery, Schuller, & Subway, 1981). In the coal combustion process, produced CCR includes bottom ash, boiler slag, fly ash and flue gas desulfurization materials, as shown in Figure 3.7.

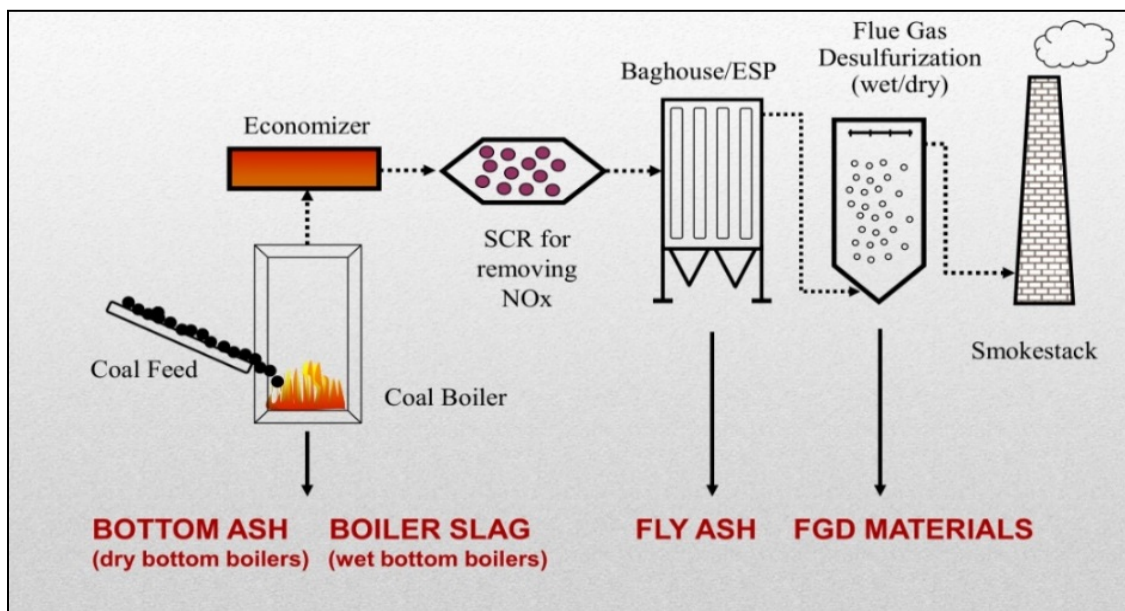


Figure 3.7. CCR production during coal combustion (Butalia, 2011).

Based on the particle size of the CCR, bottom ash and boiler slag are two types of CCR that have larger particles and settle in the coal boiler. According to the ACAA, bottom ash makes up approximately 20 percent of the total CCR produced in the coal combustion process.

The most common type of coal boiler used to burn coal to generate electricity is the dry bottom pulverized coal boiler (Recycled Materials Resource Center), in which pulverized coal similar to the size of baking flour is fed to the dry bottom coal boiler for combustion. Within the dry bottom coal boiler the temperature ranges from 1300 °C to 1700 °C and unburned ash is softened and melted (University of Kentucky Center for Applied Energy Research, 2017). Bottom ash is the ash found at the bottom of dry bottom coal boiler, which is a fine to coarse material and consists of dark agglomerated ash particles (Figure 3.8). These particles are not small enough to be carried away by

swirling air designed to transport unburned ash out of the coal boiler and hence accumulated at the bottom of the boiler (University of Kentucky Center for Applied Energy Research, 2017). The bottom ash is flushed out periodically by a hydraulic system and then goes through a sluice pipeline into ash ponds for disposal.

Bottom ash could be beneficially used (Figure 3.8), mainly in transportation applications such as structural fill, road base material, and as snow and ice control products (Recycled Materials Resource Center). Others argued that bottom ash is not as useful as fly ash, and could remain toxic when it is recycled (Palmer, 2015).

Boiler slag (Figure 3.9) is the wet form of bottom ash, produced when the temperature in a wet bottom coal boiler becomes high enough to melt the ash. The wet bottom coal boiler has a solid base with an orifice that can be opened to direct the molten ash to flow into a hopper filled with quenching water (Recycled Materials Resource Center). The water cools the molten ash into boiler slag, a glassy material that contains black, dense, hard angular particles (Butalia, 2011).

The main application (Figure 3.9) of boiler slag is blasting grit and roofing shingle granules. Other applications include structural fills, mineral filler, and snow and ice control (University of Kentucky Center for Applied Energy Research, 2017).

Flue gas desulfurization (FGD) materials (Figure 3.10) are produced in the air pollution control system, usually a “scrubber,” which sprays fine-ground sorbents such as limestone or lime onto flue gas to remove sulfur oxides. The limestone or lime reacts with the sulfur to form calcium sulfite that is processed to make FGD or synthetic gypsum. This by-product is predominantly silt-size particles (University of Kentucky Center for Applied Energy Research, 2017).

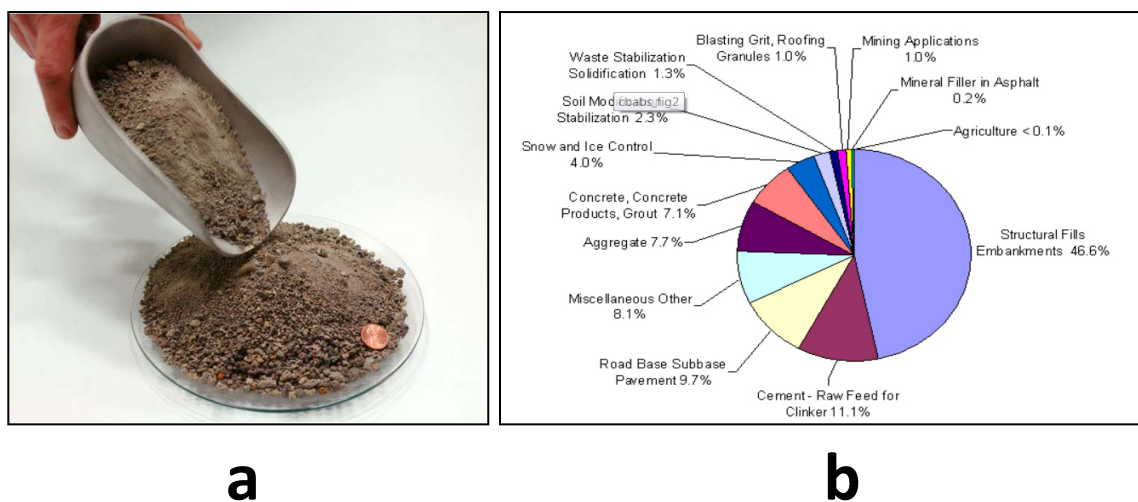


Figure 3.8. Bottom ash. a) Photograph of bottom ash. b) Bottom ash beneficial use (University of Kentucky Center for Applied Energy Research, 2017).

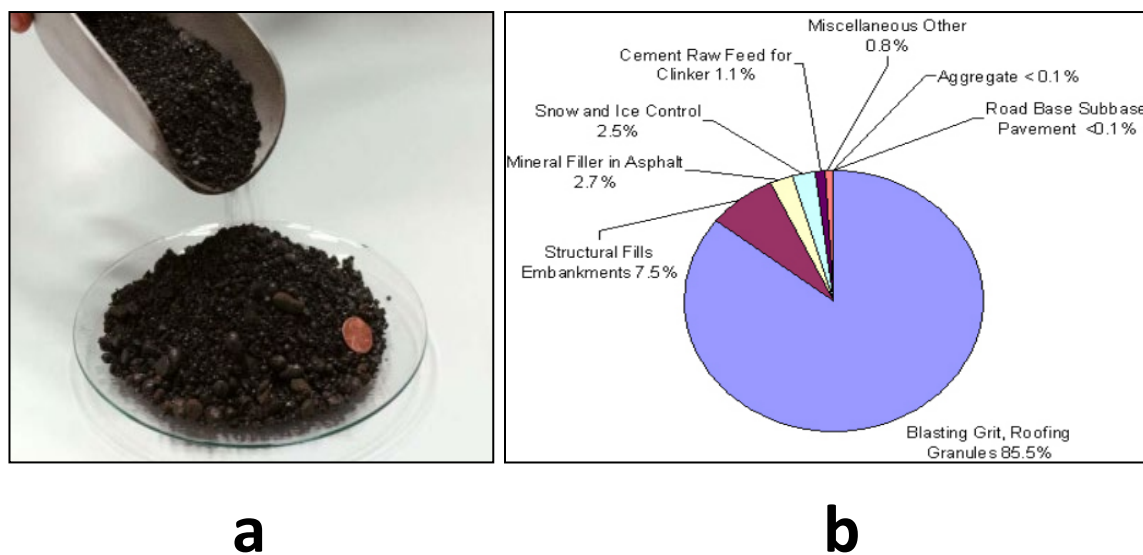


Figure 3.9. Boiler slag. a) Photograph of boiler slag. b) Boiler slag beneficial use (University of Kentucky Center for Applied Energy Research, 2017).



Figure 3.10. Photograph of FGD materials (University of Kentucky Center for Applied Energy Research, 2017).

The most commonly known CCR is fly ash, which is produced in the flue gas filtering process. In contrast to bottom ash and boiler slag that contains larger particles to be able to settle at the bottom of the boiler, fly ash is a fine powdery mineral (Figure 3.11) that contains smaller particles, and is the lightest form of CCR carried within flue gas. The small particles are usually a result of uncombusted mineral melting and could also contain unburned carbon (Butalia, 2011). As Figure 3.7 illustrates, fly ash is captured from flue gas by an emission system, which is either an electrostatic precipitator (ESP) that attracts the fly ash with opposing electrical charges (Palmer, 2015) or a “baghouse” that captures the fine fly ash material through fabric filtration. Studies have shown that ESP filters out approximately up to 99% of the fly ash (Palmer, 2015), and “baghouse” is as effective as the ESP (Whitehead Construction, 2017).

Dvorak et al., (1978) and EPRI (1979) (cited in William et al., 1981) reported that about 70% to 80% of produced CCR is fly ash, which is consistent with reports by the American Coal Ash Association (ACAA), who states that the overall produced CCR contains approximately 80% of fly ash. The ACAA also states that in the United States, the beneficial use of fly ash, in particular, can be found in over 50% of the overall concrete production.

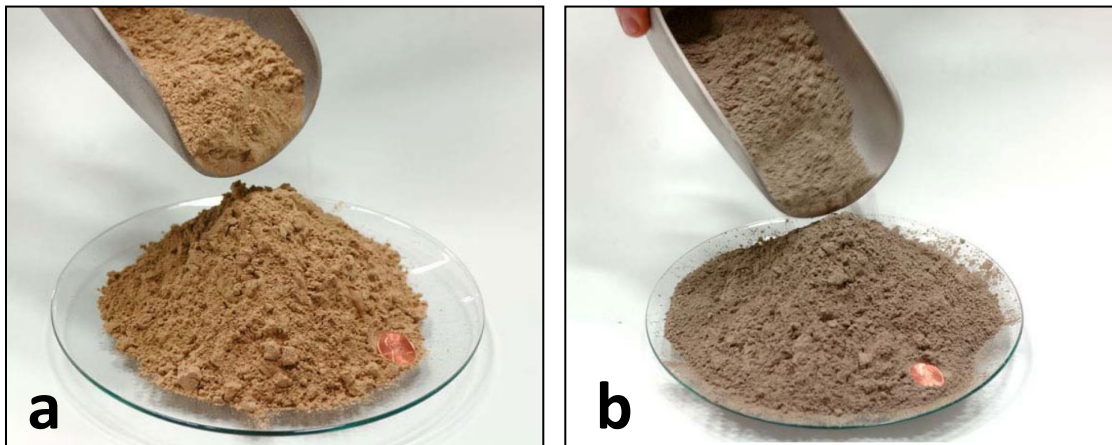


Figure 3.11. Fly ash. a) Class C fly ash .b) Class F fly ash (University of Kentucky Center for Applied Energy Research, 2017).

The physical and chemical properties and permeability of fly ash are the research focus in this dissertation with the consideration that fly ash makes up most of the CCR landfill deposit. Bottom ash and boiler slag is studied to a lesser extent to aid part of the ERT interpretations in the targeted landfill site.

Physically, fly ash is visually a powder in shape and a silt-like material, as shown in Figure 3.12. The particles in fly ash are predominantly silt-sized and spherical, either solid or hollow, and mostly glassy (amorphous) in nature (United States Department of Transportation, 2016). The color of fly ash ranges from grey to tan to reddish brown (William et al., 1981).

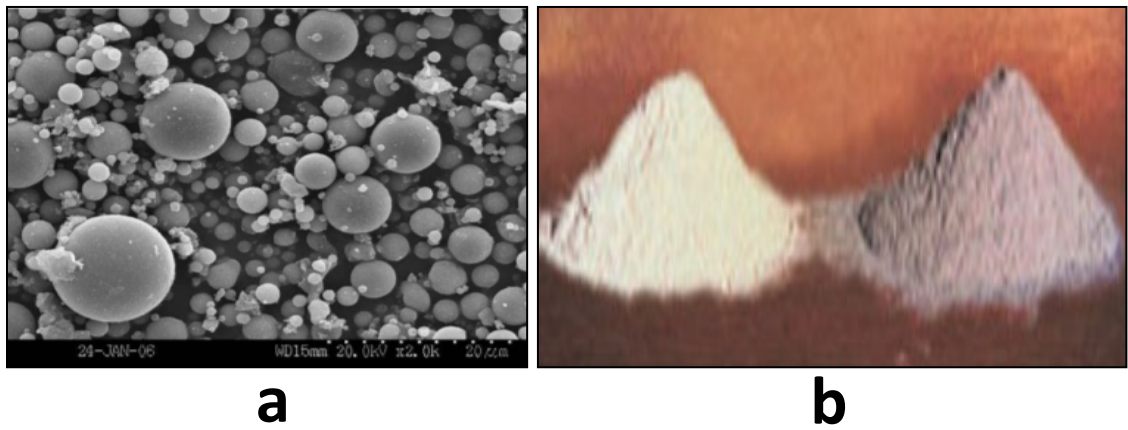


Figure 3.12. Fly ash particle size and color. a) Fly ash consists predominantly silt-sized and spherical particles. b) Typical fly ash color (United States Department of Transportation, 2016).

Fly ash normally has particles ranging in size from 0.001 to 0.1 mm (Butalia, 2011), with approximately 65% to 90% of the particles smaller than 0.01 mm (EPRI, 1979). In contrast, the particle size for bottom ash and boiler slag ranges typically from 0.1 to 10 mm. Fly ash has an approximate compressibility of 1.8 %, and a dry density ranges from 40 to 90 lb/ft³ (Table 3.2).

Table 3.2. Fly ash engineering properties (Butalia, 2011)

Typical Characteristics	Fly Ash
Particle Size (mm)	0.001-0.1
Compressibility (%)	1.8
Dry Density (lb/ft ³)	40-90
Permeability (cm/sec)	10^{-6} - 10^{-4}

Chemically, fly ash mainly consists of oxides of silicon, aluminum iron, and calcium, magnesium, potassium, sodium, titanium, and sulfur (United States Department of Transportation, 2016).

Permeability is one of the engineering properties that evaluates how well fluid can flow through a material, and it depends on the size of void spaces in the materials, as well as how well these void spaces connect with each other. As mentioned earlier, fly ash is the main component of the CCR, and hence the study on fly ash permeability is of significant importance in terms of preventing or minimizing leachate (run-off water infiltrating into the CCR deposit).

For fly ash, the permeability depends on the degree that fly ash is compacted, the distribution of fly ash grain size and how well the void spaces connect with each other. It is generally accepted that compacted fly ash has lower permeability than uncompacted fly ash. The spherical particles in fly ash make it relatively easy for fly ash to be well compacted, hence decreasing void spaces for flow to pass through.

According to the U.S. Department of Transportation, Federal Highway Administration (2016), for well-compacted fly ash, the permeability ranges from 10^{-4} cm/s to 10^{-6} cm/s.

Herrmann et al. (2009) found in a research involving 72 fly ash-sewage sludge mix samples that the permeability of fly ash-sewage sludge mixes was most influenced by compaction energy.

Chakradhar and Katoch (2016) argued that with proper compaction at optimum moisture content, fly ash achieves permeabilities of the order of 10^{-7} cm/s. They also claimed that the high alkaline conditions that prevail in fly ash do not allow the passing through of most of the toxic elements that are present in leachate.

Bern (1976), Dvorak et al. (1978), EPRI (1979), and Townsend and Hodgson (1973; as cited in William et al., 1981) concluded that generally fly ash has low permeability and compacted fly ash is less permeable than uncompacted fly ash.

Prashanth (2001) argued that adding uncompacted fly ash to soil generally increases the overall permeability of the fly ash-soil mixture. Other researchers conducted vertical and horizontal permeability tests on many fly ash and soil mixes with different fly ash content (ranging from 0% to 100%). Both the vertical permeability and horizontal permeability of the fly ash-soil mixes became higher when more fly ash was added to the mixes, while horizontal permeability values were larger than the vertical permeability values (Galupino & Dungca, 2015).

Kim (2015) studied the permeability values for compacted ash mixes of fly ash and bottom ash. The results revealed that with the increasing amount of fly ash in the mixes, the permeability of the fly ash and bottom ash mixes decreases slightly. The

permeability values indicate the ash mixtures are hydraulically conducted, similar to the sand/silt mixtures.

3.3.2.3. Leachate control system. Without the installation of the cap cover, rainwater could infiltrate into the CCR deposit more easily. On the other hand, an installed cap cover does not prevent all rainwater from infiltrating, and generally minimal infiltration into the CCR deposit is expected. The leachate control system is designed to collect and drain any successfully infiltrated leachate (water that carries toxic materials while it gets contacted with CCR deposit in the process of infiltration). The 2015 EPA CCR rule and Missouri regulation both require the installation of such leachate control system, for new CCR landfills and existing CCR landfills seeking lateral expansion.

The leachate is drained through a drainage layer, commonly installed beneath the CCR deposit (Figure 3.13). Also called the “leachate collection layer,” the drainage layer is normally made of geocomposite with perforated pipes. The leachate is then pumped into a leachate collection pond. The leachate collection system is a crucial part constructed under the CCR deposit. First, the leachate collection layer should use materials that have sufficient strength and thickness to support the above CCR structure. Second, because a final composite liner system underlies the leachate collection layer and acts as the last barrier between leachate and subsurface, the leachate collection system must maintain an effective drain to prevent or minimize the amount of leachate head forced upon the composite liner system.

Ponded water on the CCR deposit surface is not rare. The ponded water neither infiltrates into the drainage layer nor flows down the landfill flanks as run-off and accumulates typically at surface low points. Research conducted by Hardin and Perrotta

(2011) suggested that this ponded surface water on the CCR deposit is challenging to drain to the leachate collection layer by itself, due to reduced infiltration rate through compacted CCR deposit.

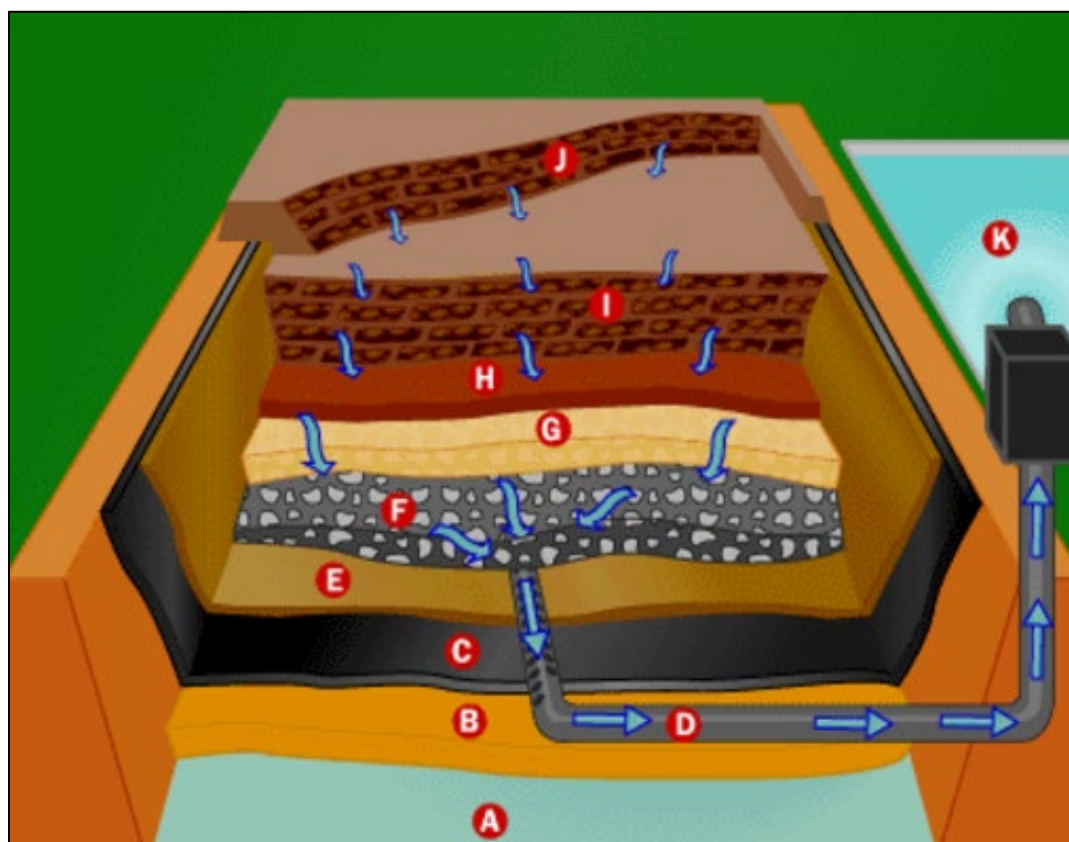


Figure 3.13. Leachate drains through leachate pipes (Freudebrich, 2000).

The 2015 EPA CCR rule also requires that the leachate collection be constructed in a way that minimizes clogging during the active life of the CCR landfill and 30-year post-closure care period. Cole and Kuhn (2017) claimed that bottom ash in the CCR contains pyrites and may clog the drainage layer with ochre formed by ferrous hydroxide,

and CCR fines in the surface contact water could also blind the leachate collection layer on the layer surface.

In order to drain surface ponded water and prevent clogging of the leachate collection system, it is common to utilize a system where the leachate collection layer connects to vertically perforated pipes (chimney drains) throughout the CCR deposit in an effort to drain the surface ponded water directly into leachate collection layer (Figure 3.14).



Figure 3.14. Photograph of a “chimney drain” (Bell, Daly & Shumpert, 2017).

3.3.2.4. Composite liner system. A composite liner system is installed below the drainage layer and is normally the last barrier to prevent any leftover infiltrated leachate from seeping further down into the underlying soil and bedrock. A composite liner typically consists of a geomembrane layer and a compacted clay liner and is required by the 2015 EPA CCR rule to have a geomembrane layer and at least 2 ft of clay with permeability less than 1×10^{-7} cm/s. Other composite liner systems are also permitted provided that the permeable effectiveness is the same or higher. Missouri regulation allows a single clay layer of at least 2 ft thick with a permeability of less than 1×10^{-7} cm/s, as an alternative to the EPA regulated liner system.

It is generally accepted that a single geomembrane layer or a single clay layer is not as effective as a composite layer system. Figure 3.15 illustrates the flow rate variations when fluid passes through different liner systems. Under the same circumstances, an excellent clay layer with the permeability of 1×10^{-8} cm/s has a passing flow rate of 110 L/ha/day compared to a passing flow rate of 3100 L/ha/day when using a good geomembrane layer with one hole/acre at 0.1 cm² in diameter. A poor composite liner with one hole/acre at 1 cm² has a passing flow rate of 7 L/ha/day, which in this case is much more effective than a single excellent clay or single good geomembrane layer (Shanahan, 2004).

An excellent geomembrane with virtually no tear or holes only has a passing flow rate of 0.1 L/ha/day, but realistically geomembrane is not immune to tears or holes. The standard for good geomembrane layer is defined as one hole per acre with good construction and QA/QC control (Shanahan, 2004).

Liner quality and type	Holes per acre	Rate of flow (gal/ac/day)	Rate of flow (L/ha/day)
Good FML	1 @ 0.1 cm ²	330	3,100
Excellent clay	1 x 10 ⁻⁸	12	110
Poor composite	30 @ 0.1 cm ²	19	180
Poor composite	1 @ 1 cm ²	0.8	7
Excellent FML	none	0.01	0.1

Figure 3.15. Flow rate variations through different liner systems (Shanahan, 2004)

An Empirical formula (Giroud et al., 1997) could be used to calculate the leakage flow rate through the composite layer system should a circular defect (hole) be found on the geomembrane. The equation demonstrates various factors that impact the leakage flow rate (e.g., leachate head above composite liner, clay liner thickness, and permeability, area of the hole, and seal condition between two layers):

$$Q/A = 0.976C_{q0}[1 + 0.1(h/t_s)^{0.95}]d^{0.2}h^{0.9}K_s^{0.74} \quad (1)$$

where

Q/A = leakage flow rate

C_{q0} = seal condition factor

h = leachate head above the composite liner

t_s = clay liner thickness

d = circular defect diameter

K_s = clay liner permeability

The leakage flow rate Q/A increases with the increasing of leachate head above the composite liner, which is reflected in the 2015 EPA CCR rule explicitly requiring the leachate control system to be designed to maintain less than 1 ft depth of leachate on top of the composite liner.

Secondly, leakage increases with increasing clay liner permeability and decreasing clay liner thickness, and these are reflected in the 2015 EPA CCR rule explicitly requiring the clay liner to have a minimum thickness of 2 ft and a permeability less than 1×10^{-7} cm/s.

The leakage rate also increases with increasing value of C_{qo} . C_{qo} describes the seal condition between the geomembrane and clay liner (Giround et al., 1997), where a smaller value of C_{qo} means a better seal between the geomembrane and the clay layer. Therefore, it is best for the geomembrane to be wrinkle free and the underlying clay to be smooth and properly compacted.

The poor seal between the geomembrane and clay facilitates more prominent leakage, as leakage tends to spread over the “vacant space” between the geomembrane and clay, and seeps down over a larger affected area. The leakage area is much less when the two layers are properly sealed, as shown in Figure 3.16.

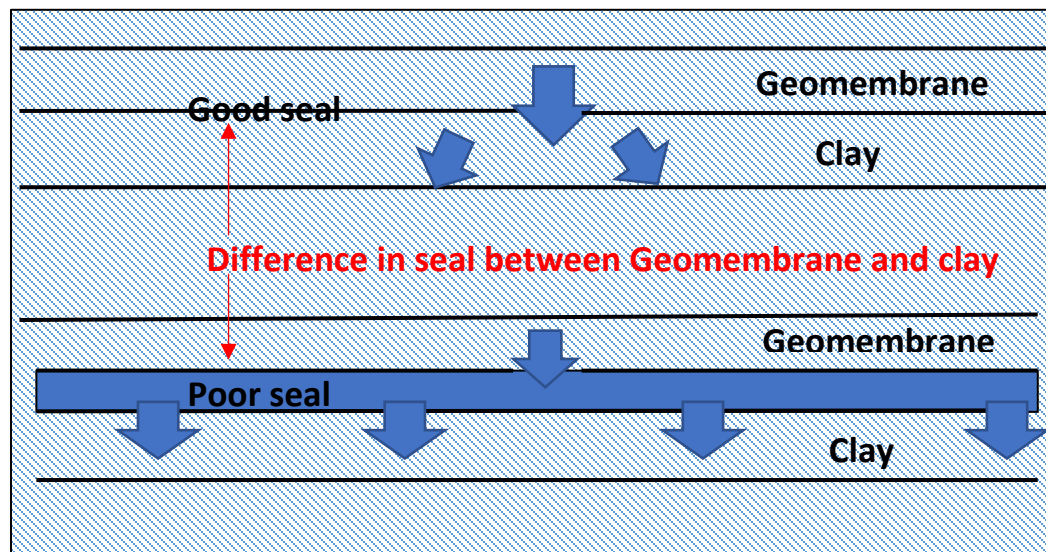


Figure 3.16. Good seal vs. poor seal.

3.3.2.5. Run-on and run-off control. The run-on and run-off control systems in CCR landfills are designed to minimize the amount of fluid that contacts the CCR, hence reducing the source of leachate production.

“Run-on” refers to any water drains over land onto any part of the CCR landfill (U.S. EPA, 80 FR 21301). The run-on control system diverts any water that may flow on the landfill and contact the CCR. The 2015 EPA CCR rule requires an effective run-on control system to prevent flow onto the active portion of the CCR landfill during peak discharge from a 24 hour, 25-year storm.

For run-on control, the topography of the placement of the CCR landfill should be considered prior to landfill construction. It is ideal to place the landfill away from any potential upgradient water source and to avoid placing the landfill in a topography low towards which the natural drainage drains. In places where topography around the landfill does not allow natural drainage away from the landfill, drainage ditches and berms

should be constructed at the upgradient of the landfill, to divert the upcoming flow. The berms should be constructed of enough thickness.

“Run-off” refers to any rainwater that precipitates onto the landfill and contacts the landfill. If the landfill is covered with cap cover, run-off rainwater infiltration into the CCR is minimized. Without cap cover, run-off rainwater infiltrates more easily into the CCR. The drainage layer in the cap cover and the drainage layer (leachate collection layer) underneath the CCR deposit are designed to drain the leachate and normally constructed at an angle.

A run-off system typically consists of berms, drainage ditches, and retention ponds. By design, most of the run-off rainwater should flow down along the flanks of the CCR landfill (Figure 3.17), which then gets intercepted by perimeter berms (normally made of on-site structure fill soil) constructed surrounding the landfill (Figure 3.18), and gets directed into stormwater retention pond through drainage ditches (Figure 3.18). The 2015 EPA CCR rule requires the run-off control to effectively collect run-off from a 24-hour, 25-year storm.

The materials used to construct drainage ditches are generally concrete or lined by gravel. The stormwater retention pond is for the successful containment of run-off and hence should be designed with enough capacity and well-lined per the 2015 EPA CCR rule. In the stormwater retention pond, water is tested for leachate chemicals after suspended soil particles settle. If water quality meets the requirement, it is then pumped away from the pond (Freudebrich, 2000).

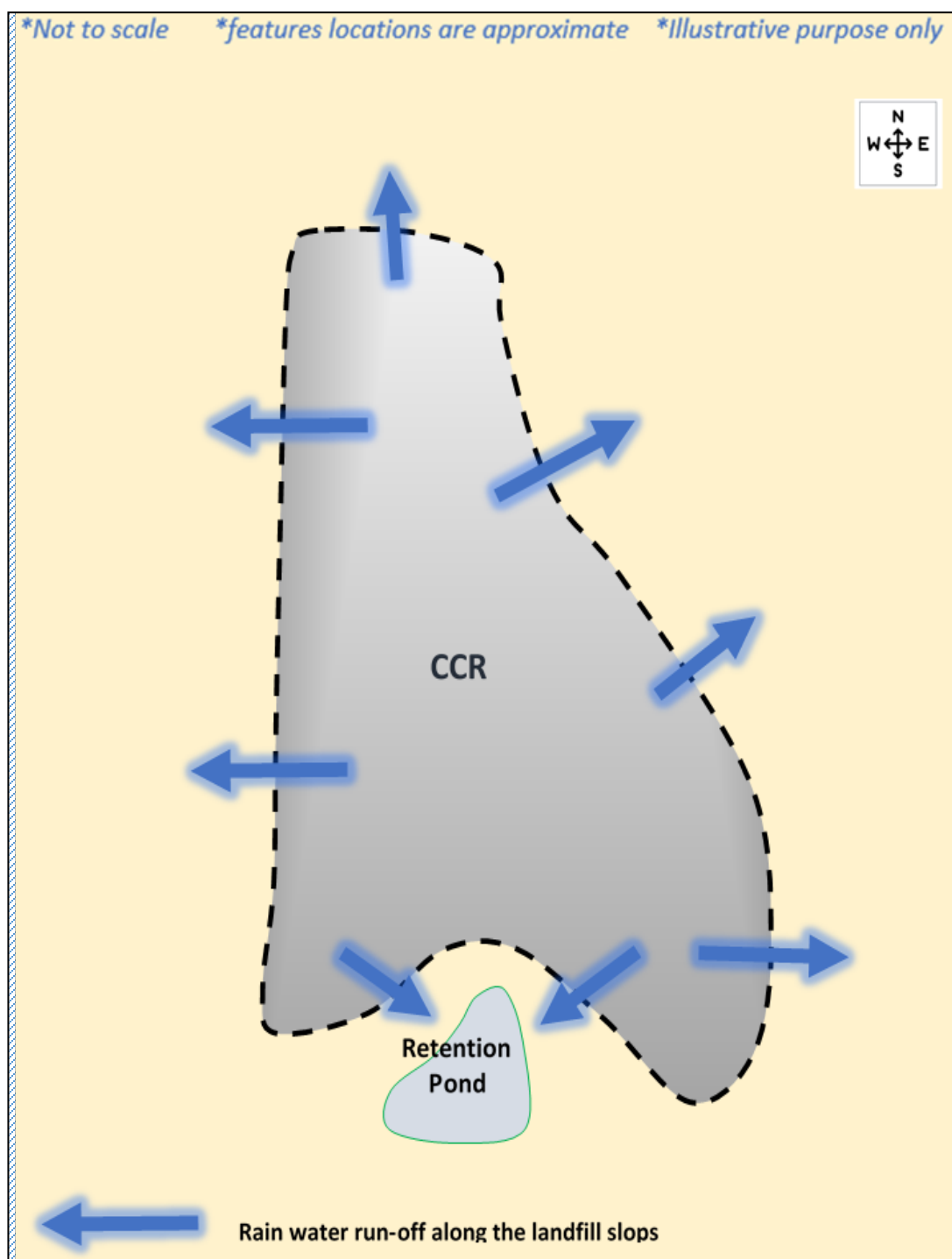


Figure 3.17. Most of the run-off flows down along the flanks of the CCR landfill.



Figure 3.18. Landfill run-off control. a) Perimeter clay berm constructed at the toe of the landfill to divert run-off into b) drainage ditches (Freudebrich, 2000).

The stormwater retention pond, or any water accumulation in general in the landfill, should be monitored with care, especially if the underlying subsurface is subject

to karstification. As Figure 3.19 illustrates, in the event of water accumulation above a subsurface that is pervasively fractured, or filled with solution-widened joints, water could potentially seep downward out of poorly lined retention ponds and into enlarged spaces of the subsurface into bedrock. It is accepted that the amount of potentially leaked seepage into the bedrock depends on the water head, the degree of fracture, as well as the overlying soil layer thickness and permeability. The design of the stormwater retention pond and any liner system play an essential role in preventing contained water from seeping into the subsurface.

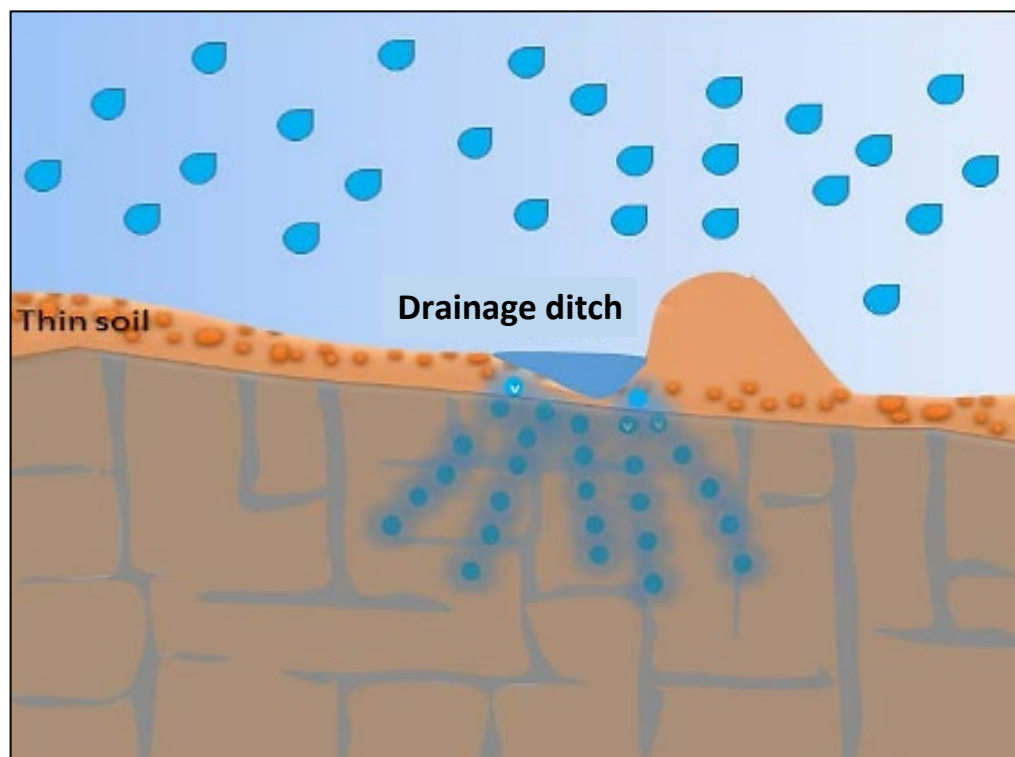


Figure 3.19. Illustrative diagram of seepage into the subsurface. In areas where underlying limestone rock is pervasively fractured, surface accumulated water, such as in a drainage ditch could seep down into the fractured bedrock (drawn by the author in 2015).

4. KARST AND GROUNDWATER

Karst is a unique topography that is characterized by sinkholes, subsurface channels, caverns, rocky ground, sinking streams, and springs. Karst is a result of subsurface rocks being dissolved by water (e.g., surface water and groundwater).

Karstification is an ongoing process. Initially, precipitation falls onto the surface soil and becomes acidic (mildly) due to the presence of carbon dioxide in the air and soil. The acidic water then infiltrates downward through soil pores into the bedrock fractures.

Bedrocks that are soluble, such as limestone and dolomite, are dissolved, and rock fractures become enlarged and deepened. These enlarged void spaces become connected and therefore provide an even more convenient path for acid water to flow through. As this process continues, generally over an extended period, cave passages and caverns are formed under the subsurface. Figure 4.1 illustrates the several different outcomes of karstification.

Soluble carbonate rock such as limestone and dolomite, is the most common type of bedrock that is subject to karstification. Karst topography is most evident in a humid area where underlying limestone is pure, thick, and fractured (Blair, 1986). More than 70% of the earth surface is sedimentary rock that consists of approximately 10-20% of limestone and dolomite (Pettijohn, 1975). Approximately 15% of the United States' surface consists of soluble limestone (Rosenberg, 2018). In Missouri, 59% of bedrock is thick carbonate rocks (MDNR, 2016).



Figure 4.1. Karst features. a) Caves and b) sinkhole and c) streamway formed as a result of karstification (British Geological Survey, NERC 2017).

4.1. LAND SUBSIDENCE AND KARST

Land subsidence refers to the gradual settlement or sudden collapse of the earth surface in the vertical direction. According to the United States Geological Survey

(USGS, 2017), a certain degree of land subsidence could be found over more than 17,000 square miles spreading across 45 U.S. States.

Land subsidence is a result of either natural tectonic plate movement, folding and faulting and earthquakes (Briney, 2017), or human activities such as water withdrawal. According to the USGS, in 2015, groundwater served as the source of more than 20 percent of total water withdraw, in the U.S. The most significant amount of groundwater usage is for irrigation, followed by public use. Figure 4.2 shows a typical land subsidence occurred in California due to groundwater withdraw.



Figure 4.2. Photograph of land subsidence caused by water withdrawal in California (USGS, 2015).

Karst is one of the common causes of land subsidence. One of the most common characteristics of karst terrain is the presence of sinkholes, which visually present as depressed or collapsed areas (USGS, 2015). As the karstification process carries on, the formed subsurface void might become significant to an extent to reach the top, hence causing land surface to gradually settle or suddenly collapse and creating a sinkhole.

According to the USGS, about 20 percent of U.S. land is susceptible to gradual land settle or sudden collapse. Out of the states that are highly vulnerable to sinkhole damages, Missouri is called by many the “the cave state,” and is characterized by the presence of 15,000 sinkholes, as shown in Figure 4.3 (MDNR, 2007). Sinkhole sizes and shapes vary significantly. Some are less than 1 ft deep, while others may be 100 ft deep, some have a shape that resembles a shallow bowl, while others have vertical walls (Kaufmann, 2007).

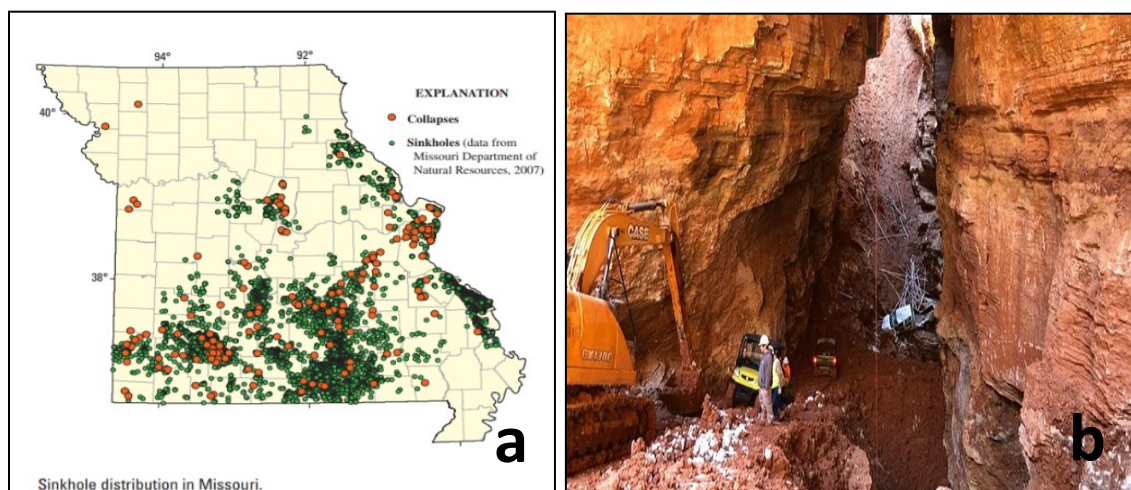


Figure 4.3. Sinkholes in Missouri. a) Sinkhole distributions in Missouri (MDNR, 2007). (b) Photograph of a truck that fell into a sinkhole in Missouri and caused injury (Western Taney County Fire Protection District, 2018).

Figure 4.4 illustrates a sinkhole formed on a golf course, which was built on karst terrain in southwest Missouri. In this area, water accumulated (e.g., small ponded water on the golf course) over fine-grained clay and fractured limestone rock, and then seeped down into the enlarged rock fractures while carrying clay. This process continued as the topsoil pipped down into the void space to the point a sinkhole formed.



Figure 4.4. Photographs of sinkhole formed on a golf course built on karst terrain. (photos were taken by the author in 2015).

4.2. SINKHOLE TYPES

The underlying carbonate bedrock in karst terrain generally consists of limestone, dolomite or gypsum and can be dissolved by the acidic rainwater seeps down through the overlying soil, thus creating solution-widened joints, caverns, and voids (Figure 4.5).

The gradual ground settlement is the more common subsidence compare to the sudden collapse of the land surface. When the soil above the bedrock spalls into the bedrock through openings and a portion of the soil settles into the void, this process is called “piping.” Subsidence of the land surface may occur gradually as the “piping” process continues where more and more sediments above the void settle into the vacant space (Figure 4.6).

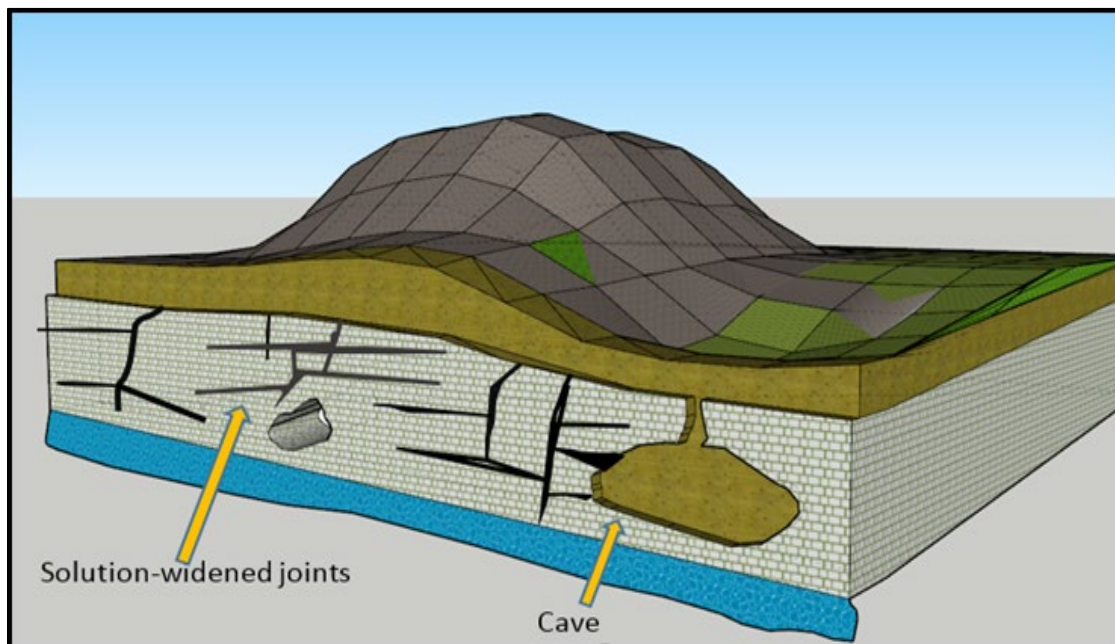


Figure 4.5. Illustrative diagram showing solution-widened joints and voids in the karst subsurface. The void has caused ground settlement through soil “piping” (drawn by the author in 2016).

Not as common as gradual ground settlement, another potential failure associated with sinkholes in karst terrain is the sudden collapse of the structure. This cover-collapse sinkhole does not happen very often but can be catastrophic. The sudden collapse occurs when the cohesive sediments spall into the void and form a structural arch that causes the void to migrate upward to the extent that the void reaches the ground surface (Figure 4.6).

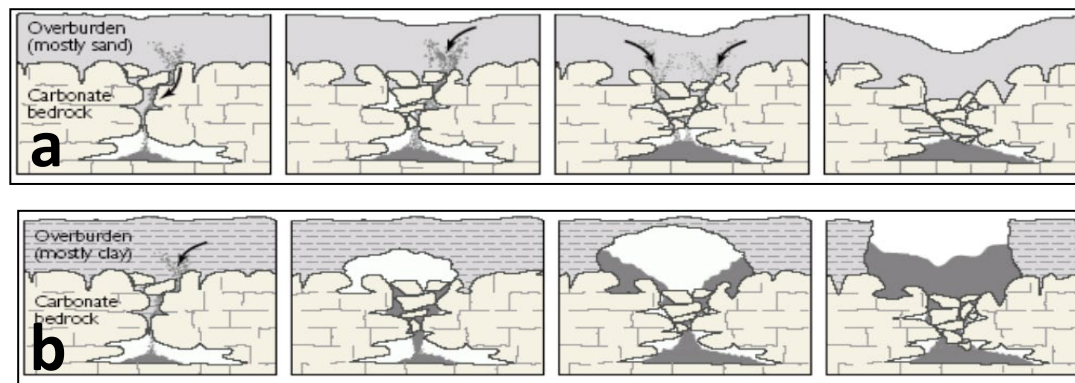


Figure 4.6. Different types of sinkholes. a) Gradual land subsidence caused by “piping”. b) Catastrophic collapse sinkhole (USGS, 2017).

More often, human activity plays a vital role in the development of sinkholes. For example, human activity prevents water from flowing freely, and thus water accumulates. For example, a newly built roadway might intercept natural water drainage and water accumulated by the edge of the roadway, and the ponded water percolates downwards into the soluble rock and causes the gradual settlement of the land.

However, water accumulation does not always cause land subsidence. Anderson N also claimed that another critical factor that contributes to “piping” is the overlying soil thickness and how much fine clay-sized particles are in the soil layer (Anderson N, personal communication, 2017).

4.3. GROUNDWATER FLOW

Groundwater refers to the water stored inside soil and sand formations in the ground. It initially comes from precipitation. While some of the rainwater falls onto the ground surface and form streams, some of the rainwater soaks down into the ground.

The underlying soil and rock enable the water to flow through them because of the existence of cracks and fractures in sand and rock, as well as the pores in the soil. Water keeps flowing downward until the formation becomes impermeable when water accumulates and starts to fill up empty spaces above the impermeable formation.

The zone with empty spaces and cracks that are entirely filled up with water is called the “saturated zone,” where water pressure is higher than atmospheric pressure ($P_w > P_a$), and the water contained in the zone is referred to as “groundwater” (Figure 4.7).

In the shallow subsurface where usually soil exists, water does not fill up all the spaces because air is contained in these empty spaces ($P_a > P_w$). This zone is called the “unsaturated zone” or “vadose zone.” The interval between the “saturated zone” and the “unsaturated zone” where $P_a = P_w$, is called the “water table.” A part of the “vadose zone” above the water table where $P_a > P_w$ is still saturated with water and called the “capillary

fringe” due to capillarity. Depending on the grain size of the sediments, the height of the capillary fringe varies.

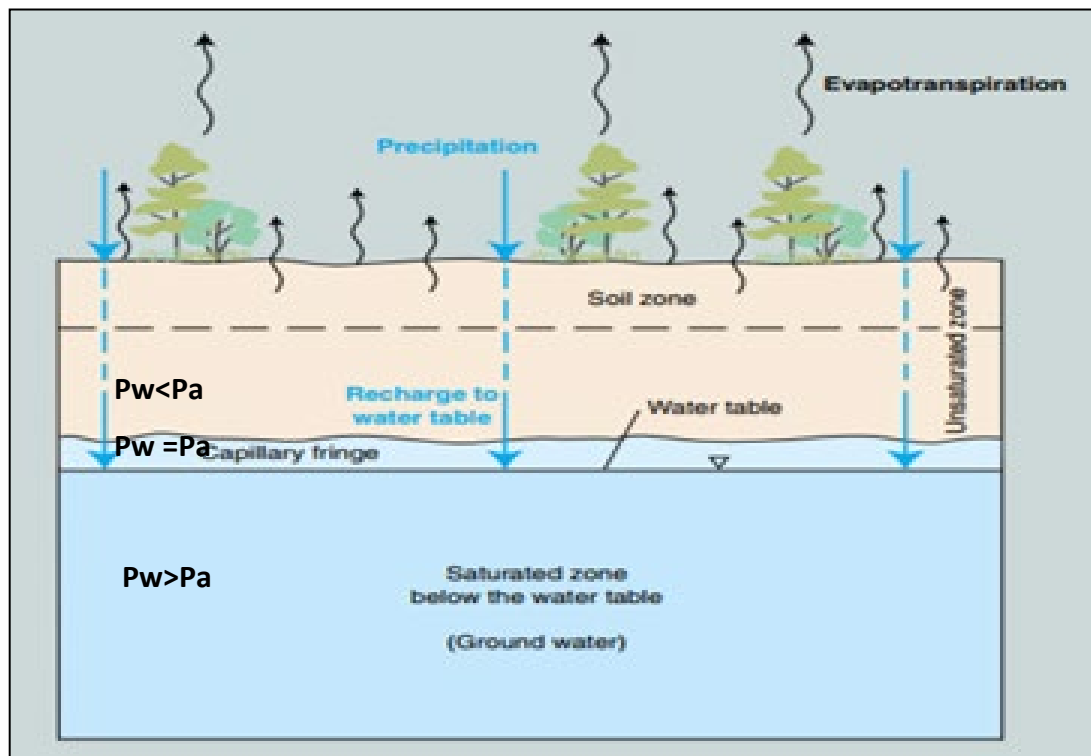


Figure 4.7. Basic groundwater flow diagram (Alley, Reilly & Franke, 1999).

4.3.1. Groundwater Flow in Non-Karst Formations. In a non-karst, or granular formation, groundwater flows in a relatively straightforward fashion. The flow direction/path is generally identifiable and often consistent, mimicking land topography trends.

The speed of groundwater flow in a non-karst formation is also relatively slow, as it could be a few centimeters per day (Rogers, personal communication 2017).

Groundwater flows through soil pores and small fractures in the granular rock, and several factors control its flow rate. For one, how fast groundwater flows in granular formation is dependent on porosity but not solely. Porosity is a measure of how big the void spaces are as compared to the total volume of the soil and sand and is defined as the fraction of the volume of the voids divided by overall volume.

The flow rate also largely depends on permeability, which is a measure of how well the void spaces in sand and rock are connected, and how easily water flows through sand and soil. It is very common to see materials with large void spaces inside them (high porosity) but with little to no permeability because those voids are not well or not all interconnected.

The permeability of the formation can be assumed uniform in granular formation, groundwater flow rate is then ideally dependent on the hydraulic gradient. Figure 4.8 illustrates the hydraulic gradient, which is calculated by dividing the vertical difference between the two hydraulic heads by the length of the path. The hydraulic gradient is expressed as a fraction and is often called “Darcy slope.”

4.3.2. Groundwater Flow in Karst Formations. Karst formations, contrary to on-karst formation, are characterized by complex groundwater flow behavior due to the existence of karst features such as sinkholes, channels and solution-widened joints. As opposed to granular bedrocks that consist of loose sand and small fractures, karst rocks contain void spaces dissolved by acid water, much like interconnected conduits. Groundwater in karst formation flows through those branching out conduits. Therefore, the direction of such flow is not easy to identify.

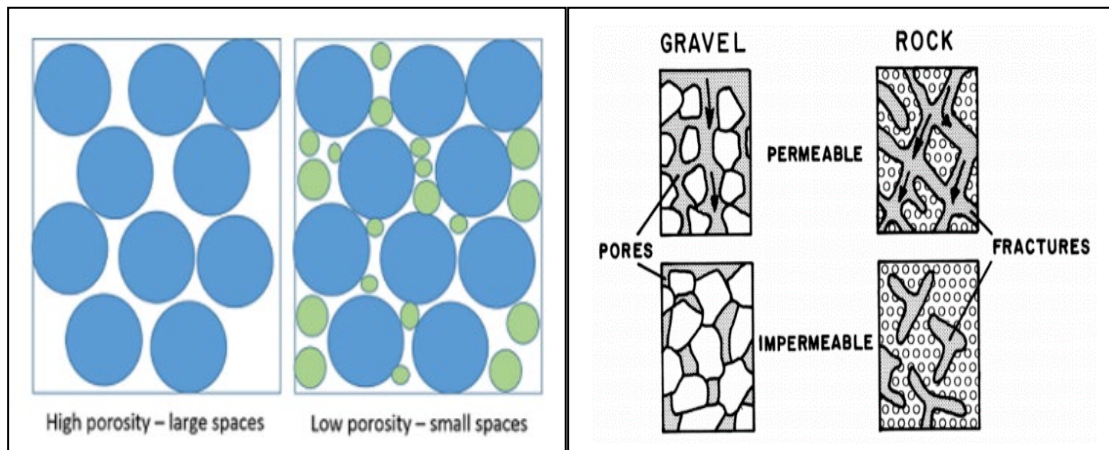
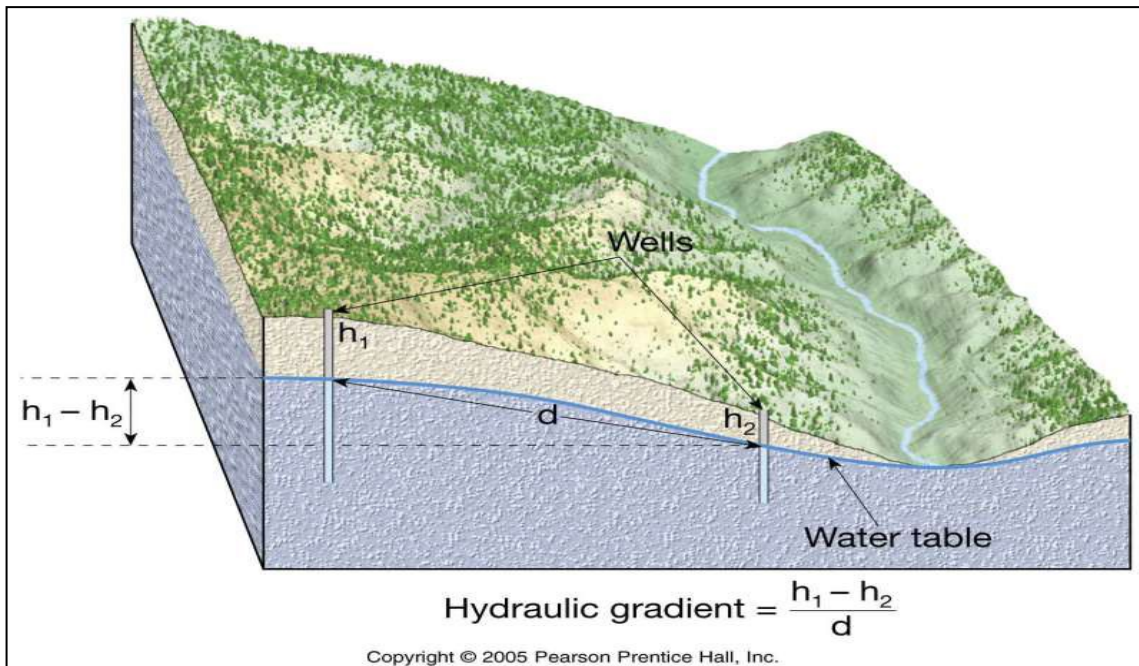
**a****b****c**

Figure 4.8. Porosity, permeability and hydraulic gradient. a) Porosity difference in a material (Clark & Briar, 2001). b) Permeability difference in materials (Clark & Briar, 2001). c) Hydraulic gradient (Rogers, 2016).

Groundwater in karst formation is more vulnerable to contamination due to the unique characteristics of karst groundwater flow.

Firstly, surface water is capable of flowing in a rapid fashion into the karst subsurface and gets into groundwater. For example, water recharges through a massive sinkhole instead of flowing through soil pores into the subsurface. Meanwhile, sinkholes offer little to no filtration to filter out contaminants that water may carry, while the soil layer in a granular formation can act as a filter material to trap those contaminants through soil pores.

Secondly, according to Mull (1993), the hydrologic significance of karst groundwater flow (conduit flow) is the rapid introduction and movement of water through the aquifer system. Water flow rate in karst formations is much faster than that in granular formations, and as water drains through enlarged conduits, the conduits provide no filtration.

Lastly, the flow pattern in karst formation is unpredictable, as water flows along branched-out fractures of which the directions are not clear, and for this reason, it is generally accepted that monitoring of karst groundwater flow behavior is difficult. Traditional water monitoring wells in karst formations do not work as effectively as in granular formations, as they often times miss the actual openings of karst groundwater flow.

However, several measures could be taken to help improve the karst groundwater monitoring effort. The most common practice is to use dye to trace karst groundwater flow, similar to using dye to trace a fluid leak in vehicles. Typically, fluorescent dyes used are not toxic and are soluble in water but do not react with water, soil, and rock

(Kincaid, 2003). Figure 4.9 illustrates the use of fluorescent dyes to trace the karst groundwater flow. By using dye, the direction of karst groundwater can be identified and any discharge locations can be determined. However, since the fluorescent dyes become diluted (e.g., a small amount of injection), visibility of the dye becomes limited. Under such circumstances, a fluorometer, which measures the fluorescence difference of a water sample, is often used (Kincaid, 2003).

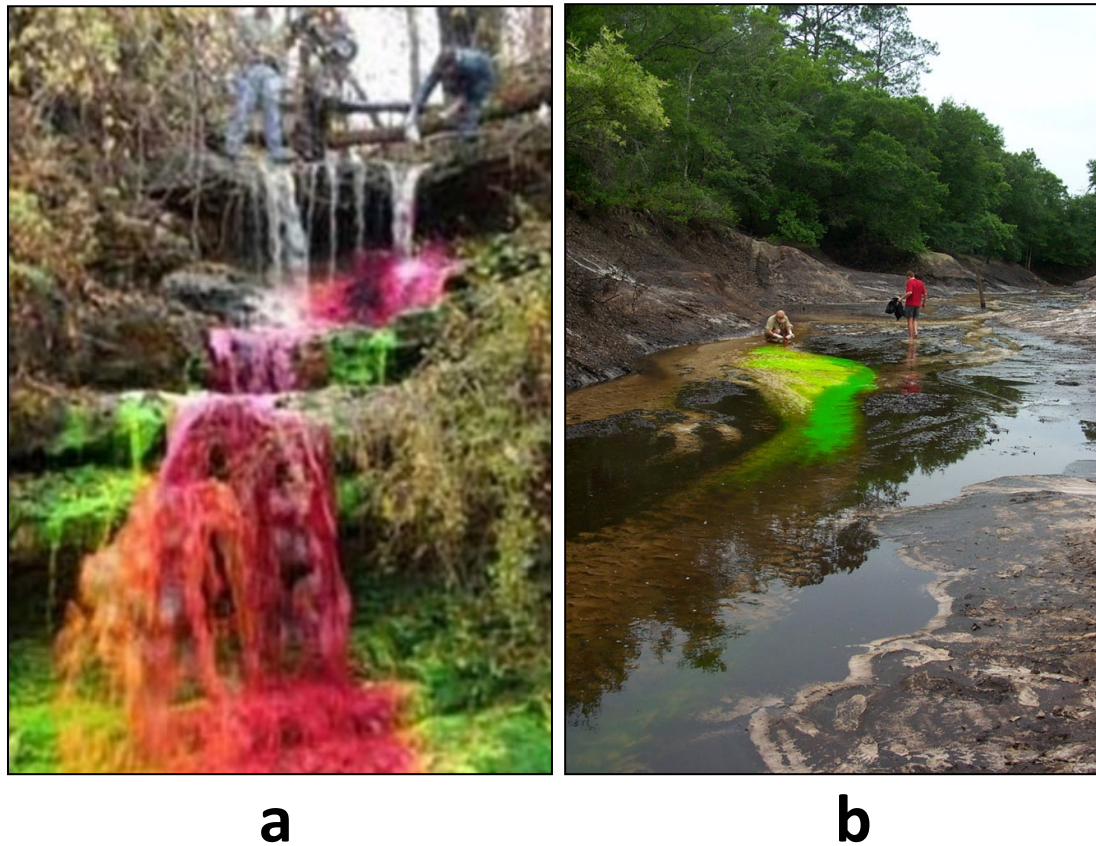


Figure 4.9. Dye tracing for groundwater monitoring. a) Fluorescent dyes being mixed with water at a recharge point (MDNR, 2016) and (b) dye moving downstream in a tracing effort (Kincaid, 2003).

5. ELECTRICAL RESISTIVITY TOMOGRAPHY AND MULTICHANNEL ANALYSES OF SURFACE WAVES

5.1. RESISTIVITY VARIATIONS OF THE EARTH SUBSURFACE MATERIALS

Electronic conduction and electrolytic conduction are two types of conduction that allow electrical current to pass through a conductor. Figure 5.1 illustrates the two types of conduction in the subsurface. Earth subsurface materials can be viewed as a huge conductor, and electrolytic conduction is considered the main conduction caused by the movement of ions carried by groundwater. Electronic conduction, on the other hand, refers to the free movement of electrons in metallic ores.

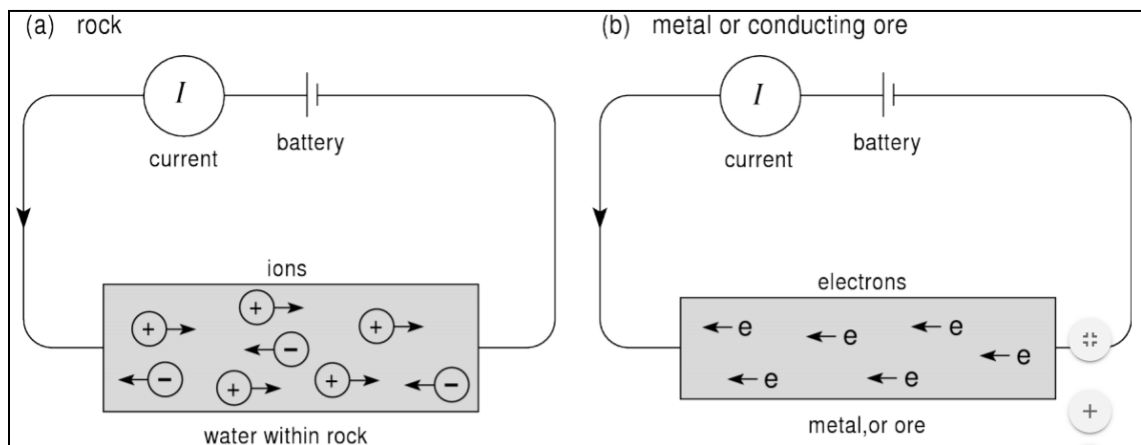


Figure 5.1. Two types of conduction in the subsurface. (a) Electrolytic conduction and (b) electronic conduction (Marshall, 2006).

Resistivity is an intrinsic property of a particular conductor material, and it varies for different earth materials. Figure 5.2 lists the resistivity ranges of some of the most common earth materials, where substantial resistivity variations can be seen.

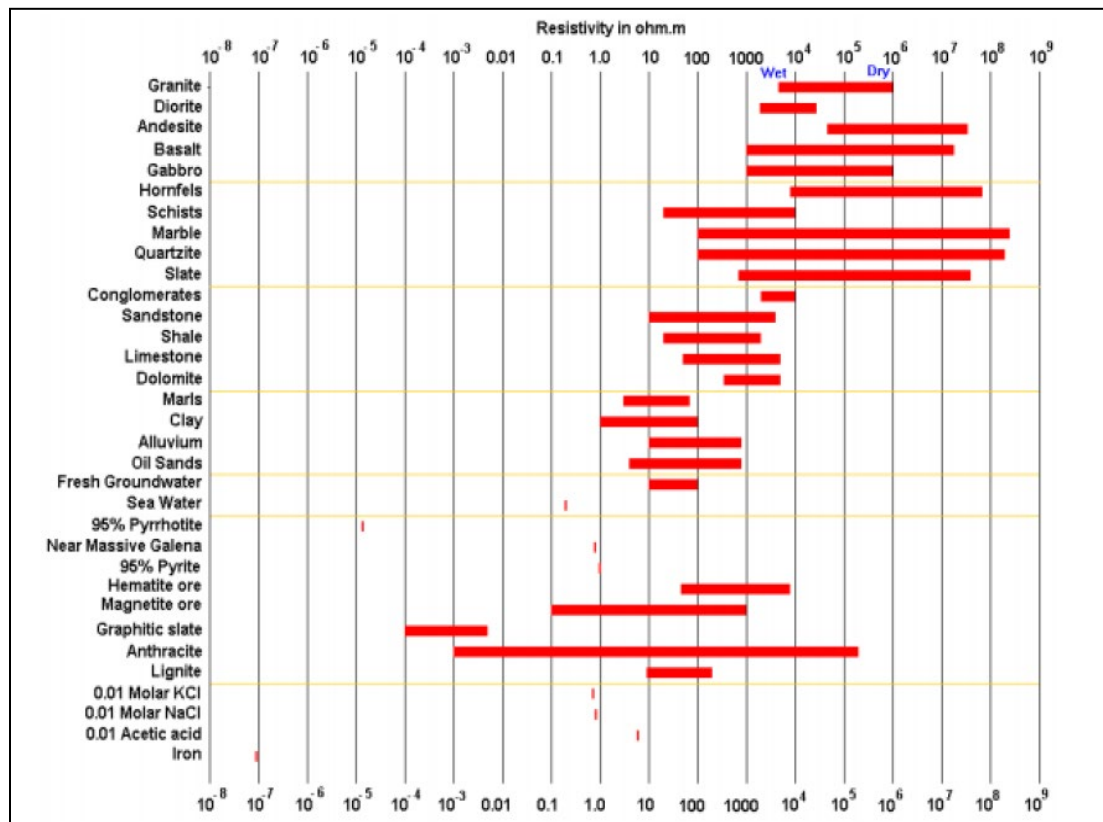


Figure 5.2. Resistivity values of common rocks, soil materials and chemicals (Keller and Frischknecht, 1966).

Saline water, which contains a significant amount of moving ions (electrolytic conduction), has very low resistivity values. Therefore earth materials that contain a good amount of saline water generally have low resistivity values. However, the resistivity of an earth material is highly dependent on the porosity, degree of fracture, and water saturation of that material, and therefore even within the same material, resistivity can vary largely. Mathematically, the resistivity of rocks and sediments is defined by Archie's Law, which is an empirical model:

$$\rho = a\rho_w\varphi^{-m}S_w^{-n} \quad (2)$$

where

$a = 0.5-2.5$ (empirical constant)

m = cementation (empirical constant), normally 1.3 to 2.0

ρ_w = resistivity of fluid

φ = porosity

$n = 2$ if S_w is equal or larger than 0.3

S_w = water saturation

Soils usually have lower resistivity values than rocks, as they are generally more porous with higher moisture content than rocks. Resistivity values of soils can vary, and clay soils generally have lower resistivity values than that of sandy soils. Similarly, rocks that are more porous with higher moisture content have lower resistivity values, than rocks that are less porous with lower moisture content. Among rocks, younger rocks tend to have lower resistivity values since they generally contain more fractures and pore space to allow saline water to flow in. In contrast, older rocks tend to have higher resistivity values since they contain fewer fractures and pore spaces.

Generally, air is very resistant to current flow, and therefore a subsurface air-filled void could have very high resistivity values. However, the resistivity value is also dependent on the conductivity of surrounding rock formations (Anderson et al., 2006). ERT is generally considered efficient in detecting of subsurface air-filled voids (Anderson N, personal communications, 2016).

Electrical resistivity tomography is often sufficient to identify air-filled voids that are present at a shallower depth (less than 20 ft) and are relatively big (Anderson, N., personal communication, 2017). Voids at deeper depths (greater than 50 ft) generally are considered as having minimal effect on structural stability.

5.2. RESISTIVITY OF CCR, SOIL AND SAND

When utilizing ERT to investigate the CCR landfill and subsurface underneath and in proximity, electrical current flows via electrolytic conduction through moisture content in the CCR, soil, and rock. CCR, soil, and rock that is more saturated generally has lower resistivity values than those that are less saturated. Rock is generally less porous than soil and CCR, therefore, it usually has higher resistivity values than that of soil and CCR. On the ERT profile, the resistivity contrasts are used to map the contact between rock and soil, or rock and soil/CCR (top-of-rock). However, it is generally difficult to confidently map top of rock in places where shallow bedrock was pervasively fractured and moist. Hence it was characterized by resistivity values that are comparable to that of overlying moist soil. Additionally, CCR and soils are similar in terms of porosity and permeability and therefore could have comparable resistivity values.

5.3. ELECTRICAL RESISTIVITY TOMOGRAPHY BASIC THEORY

ERT (Electrical resistivity tomography) investigates the earth subsurface via electrical resistivity measurements by viewing the earth as a huge conductor. This concept is based on the theory of Ohm's law, as Figure 5.3 illustrates, when an electrical current (I) is flowing through a conductor by the force of potential (V), due to the

resistance that conductor material exhibits towards the current, a potential difference (V) will occur from both ends of the conductor. The resistance (R) of the conductor describes how difficult electrical current flows through the conductor.

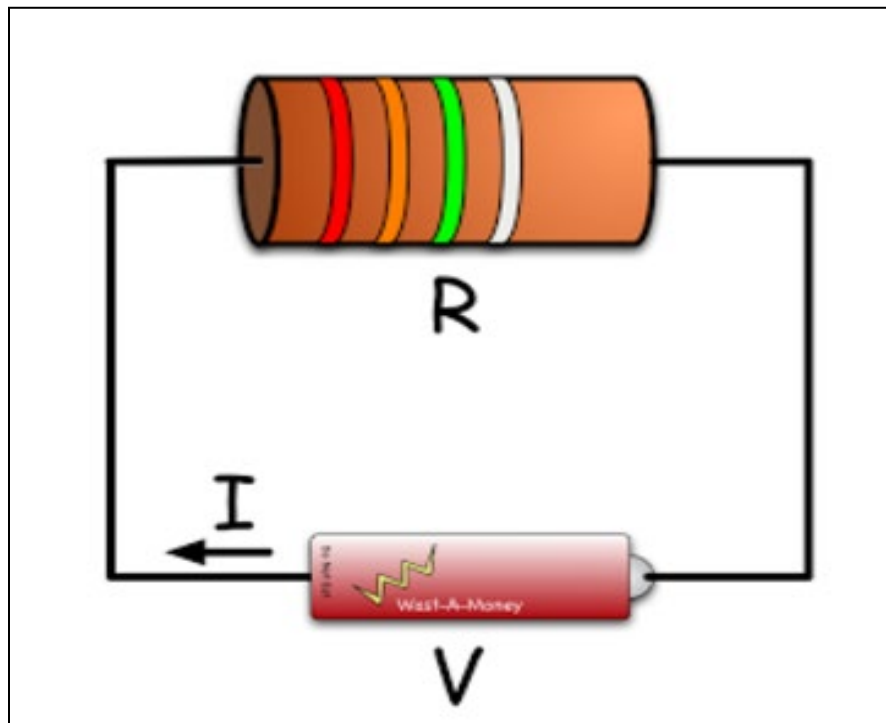


Figure 5.3. Basic conductor diagram illustrating Ohm's law (Delseaphysics1).

Ohm's law can be mathematically expressed as:

$$\Delta V = IR \quad (3)$$

where

ΔV = potential difference

I = current

R = resistance

Resistance (R) and resistivity (ρ) are not to be confused with each other.

Resistance (R) is related to conductor shape and conductor properties. As Figure 5.4 illustrates, in a cylinder-shaped conductor, resistance (R) is related to the length (L) of the conductor and the cross-sectional area where current (I) flows through. Resistance (R) is also related to conductor properties, i.e., resistivity (ρ), which is a measure of the conductor material's ability to resist the passing through of electrical current.

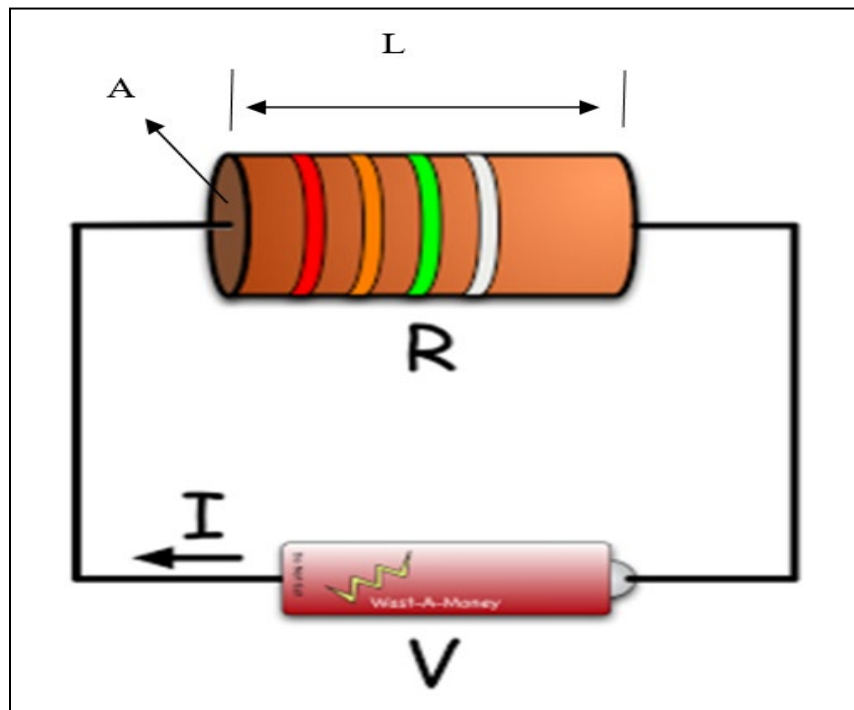


Figure 5.4. Basic diagram of a cylinder-shaped conductor (Delseaphysics1).

The mathematical relationship can be expressed as:

$$R = \rho \frac{L}{A} \quad (4)$$

where

ρ = resistivity

L = length of the conductor

A = conductor cross-sectional area

As Figure 5.5 illustrates, the most straightforward resistivity survey can be conducted by mounting two electrodes (C1 and C2) into the ground. The subsurface is treated as a conductor, and an electrical current (I) is injected via the two electrodes into the subsurface. The electrical current flows in the subsurface in a curved path, because electrical current follows the path of least resistance.

Because of the resistance to that electrical current exhibited by the earth material, the potential difference (V) is then measured using a voltmeter. Based on Equation (3) and Equation (4), resistivity values can be derived. Since electrical current (I) is known, and potential difference (V) is measured. With both parameters known, resistance (R) is derived. With known conductor length (L) and cross-sectional area (A), the resistivity (ρ) can be then calculated.

The geometric factor K varies for different electrode array configurations. The commonly used arrays are dipole-dipole, Wenner, Schlumberger, pole-dipole, and pole-pole (Figure 5.6).

The two most commonly used arrays are the dipole-dipole and Wenner arrays. According to Loke (2004), the dipole-dipole array has the advantage of imaging lateral resistivity contrast, such as vertical features like voids, because it is very sensitive to horizontal changes in resistivity. In a dipole-dipole array, two current-injecting electrodes

(C1, C2) are placed with an interval of “a” and two potential electrodes (P1, P2) are placed with an interval of “a” (Figure 5.7). The distance between the injecting pair and potential pair is “na.” It is suggested by Loke (2004) to use a resistivity meter that is highly sensitive and has good noise rejection circuitry. It is also suggested to ensure effective electrode-ground contact.

The Wenner array (Figure 5.8), on the other hand, is sensitive to vertical changes in resistivity, so it is an excellent array to image horizontal features. It also has the strongest signal strength to be used in a noisy environment. Wenner array has a decent depth of investigation compared to other arrays.

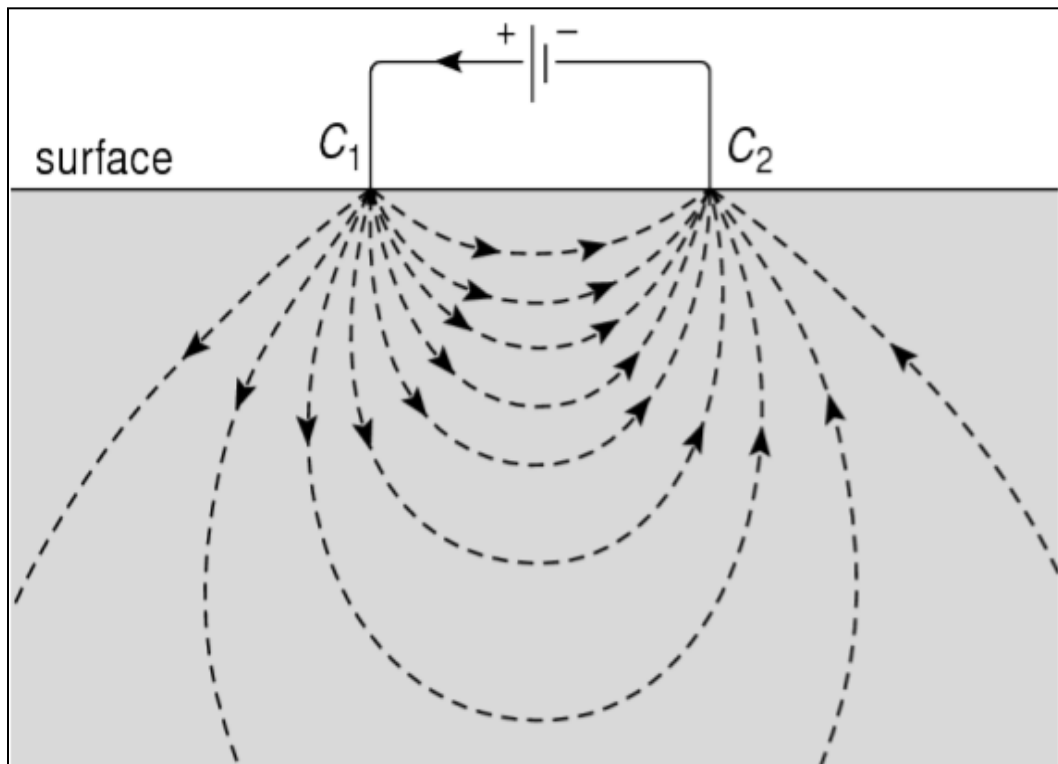


Figure 5.5. Simple resistivity survey diagram (Marshall, 2006).

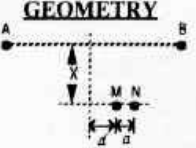
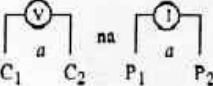
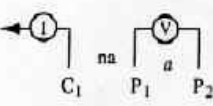
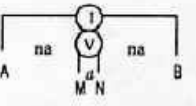
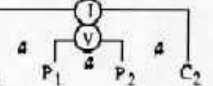
ARRAY	GEOMETRY	K	DISPLAY	USE
<u>GRADIENT</u>		See Fig. 31	Plan contours of ρ_a	Profiling
<u>DIPOLE-DIPOLE</u>		$\pi n(n+1)/(n+2)a$	ρ_a vs n	Sounding-Profiling
<u>POLE-DIPOLE</u>		$2\pi n(n+1)a$	ρ_a vs n	Sounding-Profiling
<u>SCHLUMBERGER</u>		$\pi n(n+1)a$	ρ_a vs $(n+1/2)a = AB/2$	Sounding
<u>WENNER</u>		$2\pi a$	ρ_a vs a	Sounding

Figure 5.6. Five commonly used ERT arrays (Marshall, 2006).

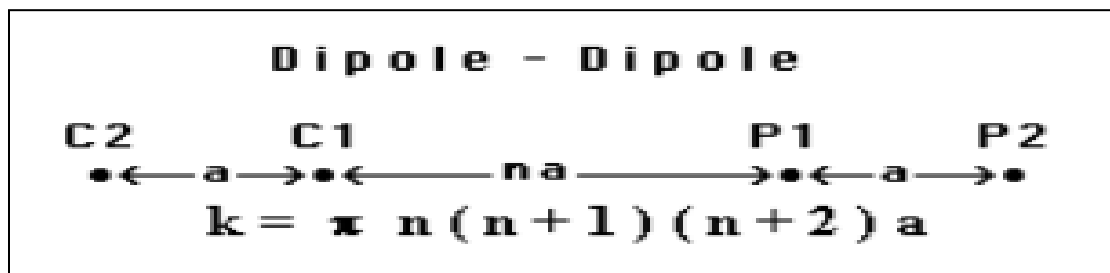


Figure 5.7. Illustration of the dipole-dipole array (Loke, 2004).

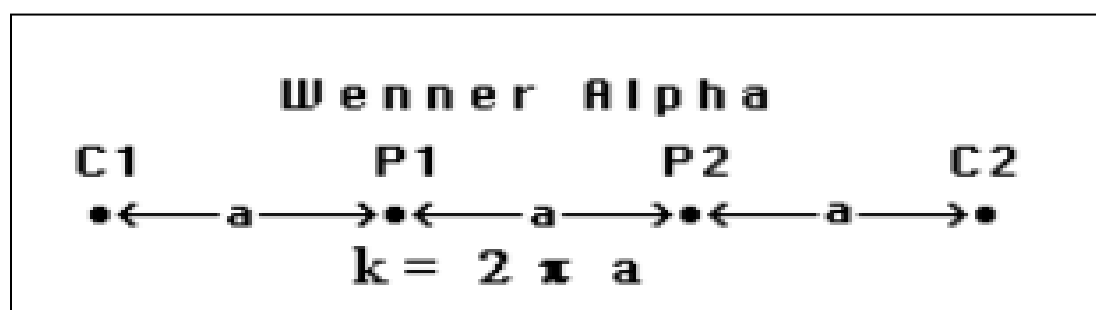


Figure 5.8. Illustration of the Wenner array (Loke, 2004).

5.4. MULTICHANNEL ANALYSES OF SURFACE WAVES

The multichannel analyses of surface waves (MASW) is a geophysical tool that measures spatial variations in the average shear wave velocity of the subsurface materials. In a MASW survey, active Rayleigh wave energy (used in this research) is generated by certain sources and has a higher frequency.

Common energy sources include dropping weight, sledgehammers, and explosives. Active Rayleigh wave energy provides higher vertical resolution for shallower depth of investigation and resolution drops with increasing depth. Rayleigh wave energy passes through the subsurface materials in a dispersive manner as different frequencies travel with different velocities that are dependent on the average shear wave velocity of the subsurface materials. Active Rayleigh wave data are then recorded with surface receivers (geophones) and then processed by MASW software to estimate the average shear wave velocity over certain depth ranges of the subsurface. The output of the MASW survey is a 1-D shear wave velocity profile of the subsurface materials. 2-D profiles can be generated if multiple MASW data are acquired along a traverse.

When using MASW to survey the CCR landfill, shear wave velocities normally increases with increasing depth, as overlying coal ash and soil are generally less rigid (lower shear wave velocity) than underlying rock (higher shear wave velocity). It is generally difficult to separate CCR from soil in terms of shear wave velocity (Anderson, N., personal communication, 2017).

Similar to ERT survey, MASW survey is non-invasive and cost-effective. MASW requires little labor, and survey equipment is relatively lightweight and can be transferred between different survey locations fairly quickly. Data can be processed rapidly, and interpreted data are reasonably reliable if constraints are available to the interpreter.

6. DATA PREPARATION

6.1. GEOLOGIC SETTING

The CCR landfill site is located in southwest Missouri, USA (Figure 6.1), situated on the Springfield Plateau, where land is underlain by Paleozoic carbonate rocks that are subject to karstification.

The local bedrock comprised of Mississippian age limestones with intercalated beds of chert and impure flint, and some sandstones and shales (Shepard, 1898). The uppermost and surface bedrock unit is Osagean series Burlington-Keokuk limestone, which is susceptible to karstification. Boring control, MASW control and ERT control data have suggested that the upper Burlington-Keokuk limestone is pervasively fractured in the general study area. The Burlington-Keokuk limestone is overlain by unconsolidated residual materials that comprise red clay, silt, and rock fragments as a result of bedrock weathering (Vandike & Sherman, 1994). Under the Burlington-Keokuk formation are the Elsey formation and Reeds Spring formation, which comprises of Osagen series carbonates and cherty carbonates and are underlain by the Pierson formation.

The Springfield Plateau aquifer is the uppermost continuous aquifer in this area. It is an unconfined, or water-table, aquifer (Vandike & Sherman, 1994). It generally extends from the base of Burlington-Keokuk Formation limestone to the Elsey-Reeds Spring formation.

Site observation indicated the site topography consisted of weathered upper Burlington-Keokuk Formation limestone rocks emerging from red clay soil and silt, and

covers the surface. The Burlington limestone is made of almost entirely on the remains of various fossils and is unusually course-grained, crystalline, crinoidal limestone (Gottfried, n.d.). The upper Burlington-Keokuk limestone is generally more weathered with solution-widened joints and becomes more rigid and less weathered with increasing depth (Anderson N., personal communication, 2017). Some water may be suspended and stored in the limestone formation (solution-widened joints, conduits) above groundwater (Anderson N., personal communication, 2017).

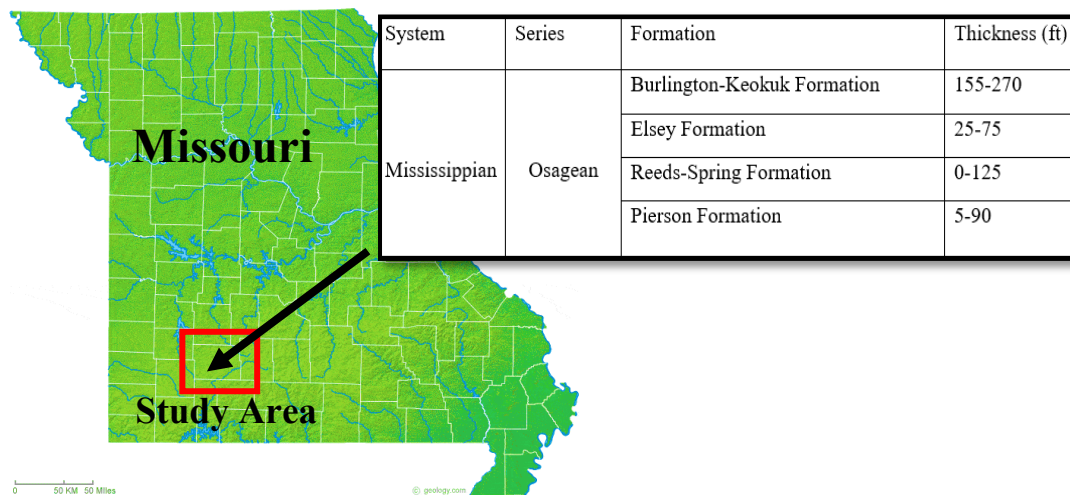


Figure 6.1. The study area is underlain by Mississippian limestone. The upper bedrocks are predominantly pervasively fractured Burlington-Keokuk limestone.

6.2. DATA ACQUISITION PLAN AND LAYOUT

The ERT and MASW investigations were conducted and focused on the northern part of the targeted area where the CCR contains mostly fly ash, and scrubber sludge and

bottom ash, and was covered with a cap cover (compacted clay and topsoil). An automated 8-channel resistivity meter SuperSting R8 and a 24-channel Seistronix engineering seismograph were used to acquire ERT and MASW data, respectively. Figure 6.2 illustrates the ERT and MASW data acquisition layout.

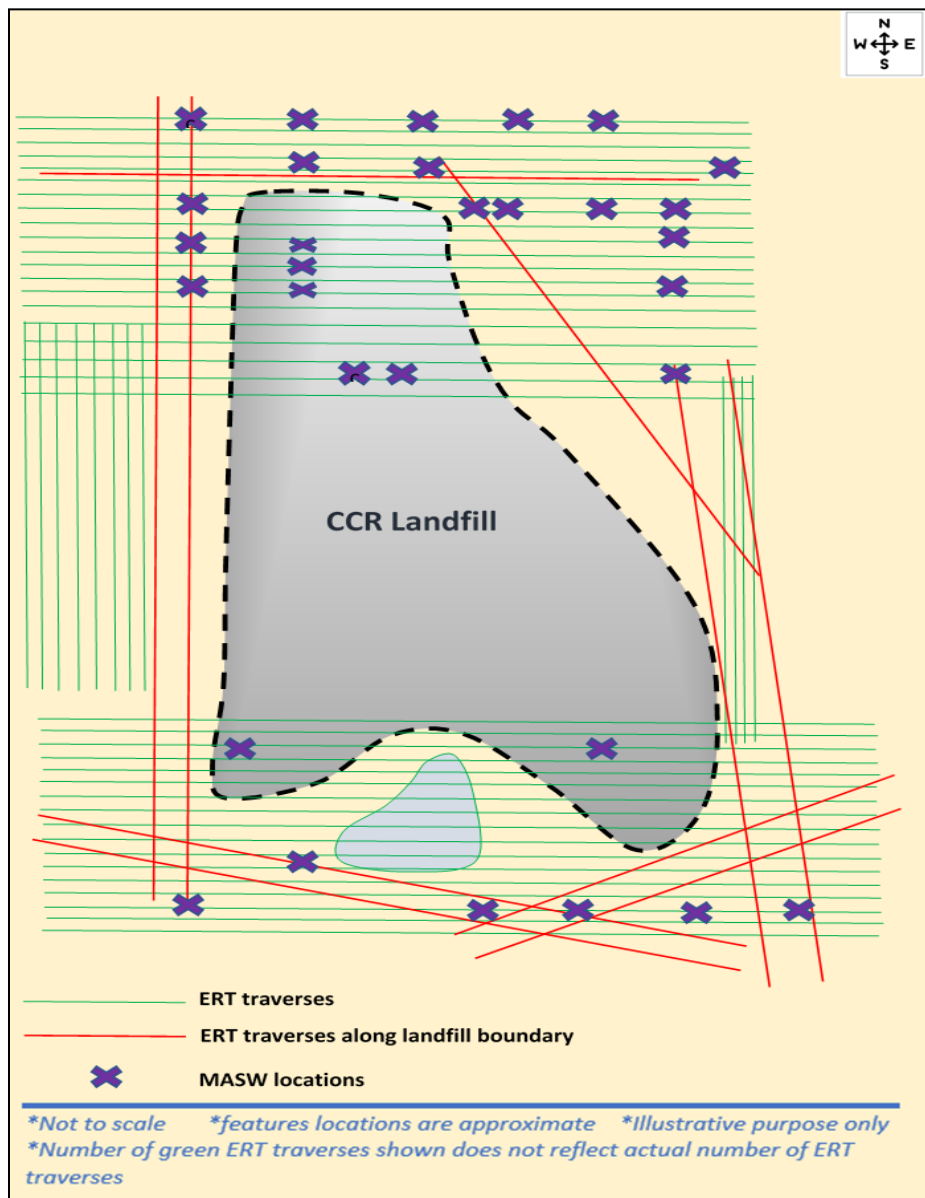


Figure 6.2. Illustrative ERT and MASW data acquisition locations.

On the north side the landfill, ERT data were acquired along 56 west-east oriented ERT traverses with 20 ft spacing. On the south side of the landfill, ERT data were acquired along 29 west-east oriented ERT traverses with a spacing of 20 ft. Those west-east oriented ERT traverses are marked in green in Figure 6.2.

In order to identify possible seepage pathways and determine seepage flow/moisture content variations, the following ERT profiles were acquired specifically for this purpose:

1. Ten ERT profiles were acquired immediately adjacent to the approximate boundary/toe of the CCR landfill, which are marked in “red” with the intent to provide a general idea of the CCR landfill site, and as a groundwater monitoring effort.

2. On the west side of the landfill, ERT data were acquired along 8 north-south oriented ERT traverses with a spacing of 20 ft. Those north-south oriented ERT traverses are marked in green in Figure 6.2.

3. On the east side of the landfill, ERT data were acquired along four north-south oriented ERT traverses with a spacing of 20 ft. Those north-south oriented ERT traverses are marked in green as shown in Figure 6.2.

MASW data were acquired along west-east oriented ERT traverses with mostly 200 ft intervals, with the exception that some locations were shifted due to accessibility. MASW locations are marked with “X.”

6.3. ERT DATA ACQUISITION AND PROCESSING

6.3.1. Pre-Survey Considerations. The use of 20 ft spacing between the ERT profiles acquired along west-east oriented traverses, was a consideration of the resources

available at the time of conducting this investigation. Although decreasing the spacing between each ERT profiles (2-D) yields better resolution on later processed 3-D ERT profiles, a significant increase in acquisition time and more extensive labor would have been required. According to the resistivity meter (SuperSting R8) manufacture AGI, it is generally accepted that 20 ft spacing is sufficient to provide adequate and quality details of the subsurface.

The order of electrode spacing affects the lateral resolution on the ERT profile. As lateral resolution generally decreases with increasing depth, vertical resolution also decreases with increasing depth and is comparable to lateral resolution. Minimum length of the ERT array was determined to be 835 ft, with the understanding that maximum investigating coverage is achieved only in the central third of the ERT array.

Considering the size of the survey area and accessibility issues in certain areas, lengths of acquired ERT profiles varied. Generally, several “roll-alongs” of one ERT array was conducted to make up one ERT profile and achieve the desired investigating coverage. Generally, as ERT array length increases, the depth of investigation increases. The maximum achievable depth of investigation is usually 20% of the array length (distance between the very first electrode and the very last electrode). In this study, the investigation depth was approximately 170 ft ($835 \times 20\% = 167$). The dipole-dipole array was utilized for all the ERT profiles, with the consideration that this type of array, compared to other arrays, provides excellent lateral resistivity contrast with reasonably faster acquisition time.

6.3.2. Field Operations. ERT data acquisition equipment was loaded onto a truck to be transported to the determined survey location. As shown in Figure 6.3, the primary

equipment included an automated 8-channel resistivity meter SuperSting R8 system, two switch boxes, multiple cables attached with electrodes, and a large number of stainless-steel stakes (depend on array length). Other equipment included rub bands, batteries, and a laptop computer.

Eight ERT cables with a total of 168 electrodes were pre-determined to be used for each ERT array. Each ERT array covered an investigating length of 835 ft ($168 \times 5 = 835$). Shorter arrays with fewer cables were used in places where a shorter coverage was needed (e.g., at the end of the ERT transverse after a few “roll-alongs”).

The resistivity meter controlled the electrodes (e.g., injecting current and measuring voltage) by attaching to two switch boxes connected to 8 cables. Figure 6.4 illustrates the connection configuration of the 835 ft ERT array.

The acquisition setup started with rolling a tape measure along the ERT traverse. As previously determined, 168 stainless-steel stakes were then driven into the ground with 5 ft intervals, using a 5 lb hammer (Figure 6.5). The stakes were routinely cleaned and sharpened to ensure excellent conductivity and were carefully examined each time prior to installation.

The conduction between the electrodes to the subsurface was achieved by attaching 168 electrodes (8 cables) to the 168 stakes using rubber bands (Figure 6.6). The rubber band was found to be a better choice over metal spring because it took less effort and time (e.g., easy to put on and take off, lightweight, takes up less space) to achieve a reliable connection. Nonetheless, the connections were carefully examined to ensure no loose connections were present.



Figure 6.3. ERT data acquisition equipment (Photos were taken by the author in 2015-2016).



Figure 6.4. ERT field survey layout. Two switch boxes were connected to the resistivity meter, cables 1 to 4 were switched by switch box 1, and cables 5 to 8 were switched by switch box 2.



Figure 6.5. Installing stakes into the ground using a 5 lb hammer.



Figure 6.6. Attached electrode on stainless-steel stake.

To ensure sufficient conductivity, water was manually added onto stake-ground contact (Figure 6.7). In areas that could be accessed by a truck, a water hose connected to a big water tank mounted on the truck was used. More than often, water was added using a bucket because of accessibility issues in the area.

The pre-acquisition setup took 1-1.5 hours to complete, and any loose connections that occurred during or after this process were carefully examined by conducting a contact resistance test for quality control. Loose connections could have been a result of human mistakes but were mostly caused by wind disturbance and animals interactions. The contact resistance test measured the resistivity between stake 1 and stake 2, stake 2 and stake 3 and so on, and the resistivity values should be overall consistent. Extremely high or low values most likely were attributed to the following:

- Electrodes not properly connected to the stainless-steel stakes (e.g., rubber band malfunction)
- Separate cables not correctly connected to each other
- Loose Connections at the switch boxes
- Stakes having poor contact with the ground (e.g., not firmly pushed into the ground, an insufficient amount of water added)

The potential cause of the abnormal resistivity values was carefully examined, and proper action was taken, followed by a second contact resistance test. The final data acquisition process then began, and field crew routinely checked physical connections and monitored readings on the resistivity meter during the process. Once data acquisition was completed, raw data was then transferred to a laptop computer. Initially, the raw field data were stored in the resistivity meter as Stg. Files and converted into Dat. files on-site

(Figure 6.8). The Dat. files provided general resistivity images of the subsurface and enabled crew members to examine potential data acquisition errors. This was only to ensure the collected were of satisfactory quality, the ERT profiles at this point did not present the actual resistivity image of the subsurface. Data acquired in the field were later further processed in the lab.



Figure 6.7. Adding water onto the ground for effective conductivity.

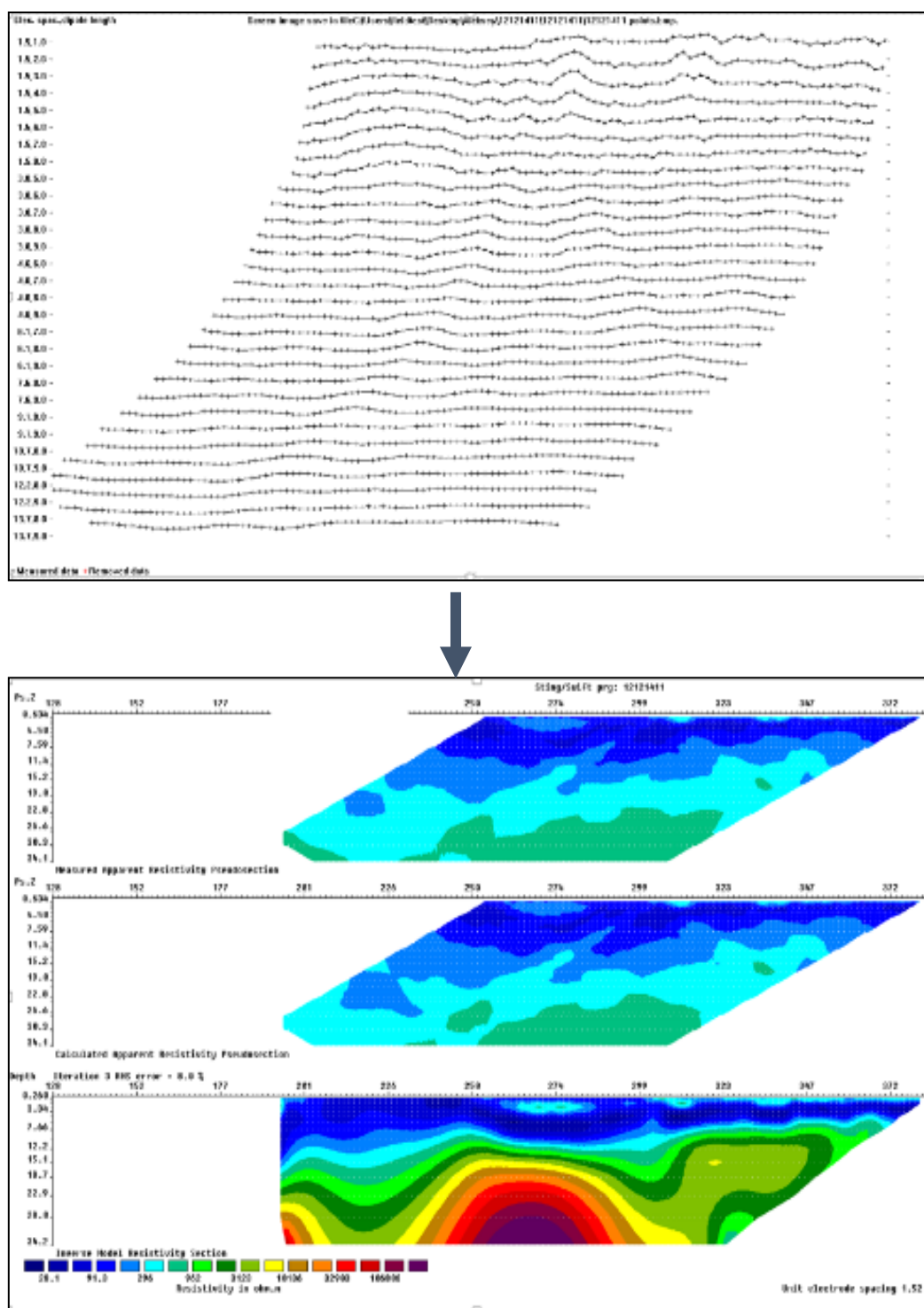


Figure 6.8. Raw field data were stored in the resistivity meter as Stg. files and converted into Dat. files on-site.

6.3.3. Common Data Acquisition Problems and Solutions. Generally, ERT data were acquired along proposed ERT traverses with a speed of more than 1200 ft/ day. Potential problems encountered that could jeopardize the acquisition speed and data quality were carefully studied, and solutions were offered.

Regularly, the resistivity meter collects data for several hours (approximately 2.5 hours per array in this research). Therefore, the effectiveness of data acquisition decreases significantly once a second correcting acquisition is required. Figure 6.9 illustrates the common problems in field data acquisition; Table 6.1 lists the suggested solutions.

The most common problem is the unsatisfactory connection/conduction, as it is generally difficult to firmly drive stakes into the ground when the ground is hard and dry. Inexperienced crew members may only drive the stakes in a few inches without realizing the connection between the stakes and the ground is not of satisfaction. Experienced crew members would use portable drills to drill holes in the hard/dry ground prior to pushing stakes in, an adequate amount of water onto the put onto the stake/ground contact surface.

Uneven ground, slopes, and overgrown vegetation may slow down the acquisition equipment installation process. These areas typically have limited truck access and often are difficult to walk on. As a precaution, it is advisable to walk slowly and carry the resistivity meter, stakes, cables, and batteries separately.

Ideally, overgrown vegetation should be cleared out prior to data acquisition. Overgrown vegetation could affect the connection between electrodes and stakes once leaves and such get in between.



Figure 6.9. Common issues associated with ERT data acquisition in the field.

Table 6.1. Common issues associated with ERT data acquisition and solutions

Problems	Effect	Solution
Hard Ground	Stakes are unable to be driven into the ground	Use drill to drill holes
Dry Ground	Poor conductivity between stakes and ground	Pour water over stake and ground contacting area
Uneven Ground & Slopes & Hills	Difficult to walk on and set up equipment	Walk cautiously and slow down
Rock Piles	Very difficult to drive stakes in Very poor conductivity	Pick out rocks and make space/ Pour a significant amount of water around contacting area
Overgrown Grassy Ground	Stakes are difficult to locate May cause tripping and other injuries	Clear the grassy spot with a truck or other tools
Rain	Moisture damage to equipment	Cover equipment and connectors with tarp and plastic covers
Poisonous Animals & Herbs	Cause injury/ could be fatal	Work cautiously and prepare first-aid kit
Fences & Obstacles	Unable to get through to set up equipment	Use tools to cut & clear fences and obstacles before setting up

The electrodes, resistivity meter, batteries, and switch boxes should be protected from rain and moisture at all times. Data acquisition during heavy rainstorm should be avoided. Typically, weather conditions were checked prior to acquisition. For possible

light rain, the electrodes were covered with plastic covers. Resistivity meters, batteries and switch boxes are covered with tarps. Plastic covers should also be applied to cable connecting points. In areas such as small creeks and ditches, the plastic cover is to be applied onto any portion of the equipment (usually the cables) that have contact with water, in order to prevent moisture damage. In areas where more significant water body is present, ERT data is usually acquired over these areas using marine cables.

6.3.4. ERT Data Processing. Raw ERT data (apparent resistivity data) acquired at the site were processed using software RES2DINV. The RES2DINV software was used to invert the acquired apparent resistivity data and generate an optimum resistivity image of the investigation target.

Model parameters were estimated based on the observed data, and the model response was synthetic data that can be calculated from the mathematical relationships defining the model for a given set of model parameters (Loke, 2004). The mathematical link between the model parameters and the model response for the 2-D and 3-D resistivity models is provided by the finite-difference (Dey and Morrison 1979a) or finite-element methods (Silvester and Ferrari, 1990). The output is 2-D electrical resistivity image of the subsurface. An estimate of the extent to which the output 2-D image correlates with the input apparent resistivity data is provided as a percent error.

6.4. MASW DATA ACQUISITION AND PROCESSING

6.4.1. Field Operations. MASW data were acquired using a 24-channel Seistronix seismograph with 4.5 Hz geophones placed at 5 ft intervals to achieve an investigation depth of approximately 100 ft (Figure 6.10). A sledgehammer, and

sometimes a dropping weight mounted on a vehicle were used as sources to generate the wave energy. Multiple MASW profiles were employed at mostly 200 ft intervals. The investigating depth of the MASW survey is roughly the same as the geophone array length, which is approximately 100 ft. The acquired data were checked frequently, and 2.5 ft geophone spacing was used instead of 5 ft if the data set with 5 ft spacing did not provide a quality result. The Seistronix seismograph and laptop were placed at the back of the vehicle so that equipment can be transferred to the next location fairly quickly.

6.4.2. MASW Data Processing. MASW field data was processed using software SURFSEIS. The fundamental-mode dispersion curves were estimated for each record. The curves then were inverted to obtain 1-D (depth) vs. (shear-wave velocity) profiles (Kansas Geological Survey, 2014). 1-D profiles can be assembled into 2-D profile if multiple 1-D profiles are acquired along a traverse in a close range within each other (Figure 6.11).

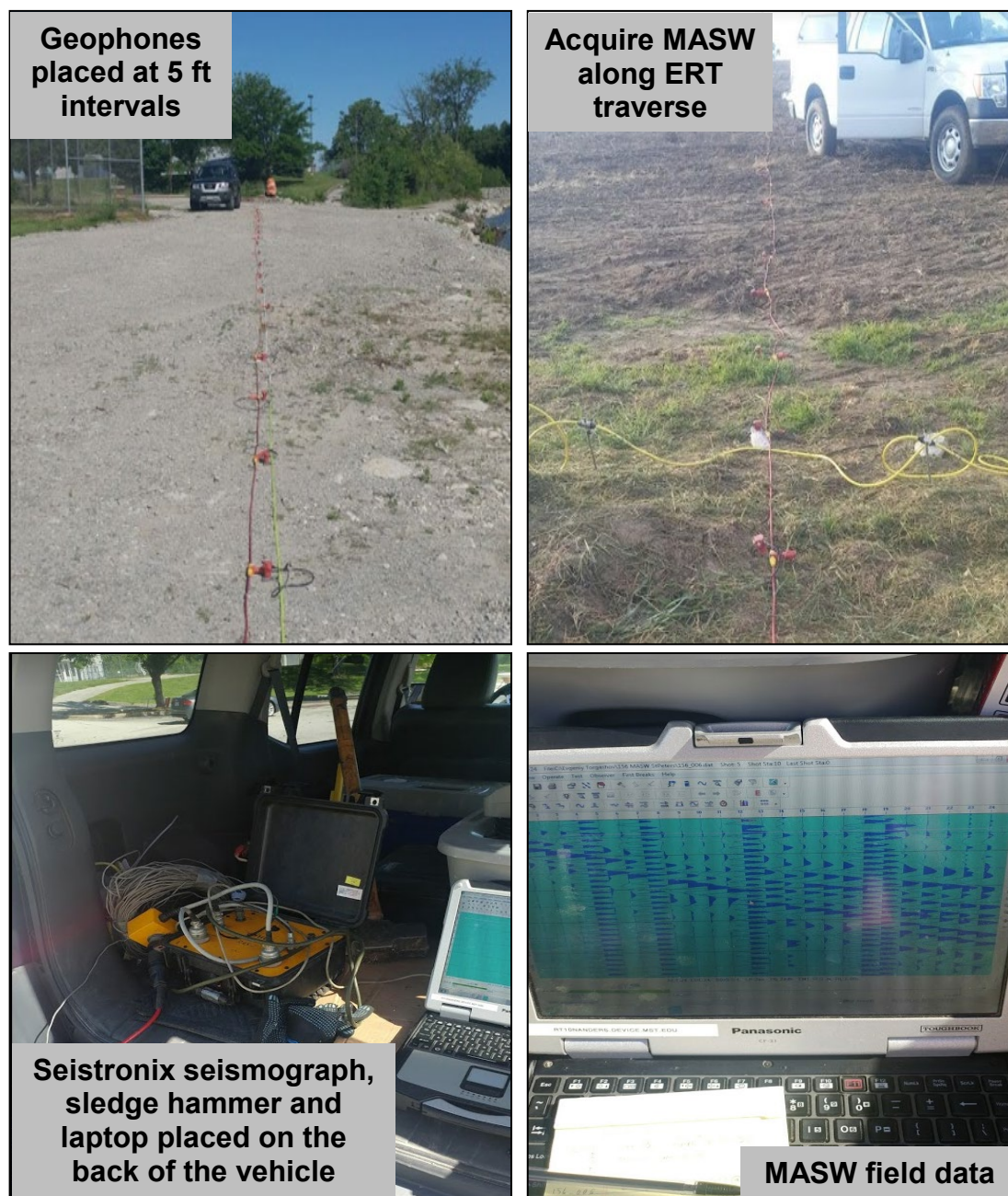


Figure 6.10. 24-channel Seistronix seismograph with 4.5 Hz geophones placed at 5 ft intervals.

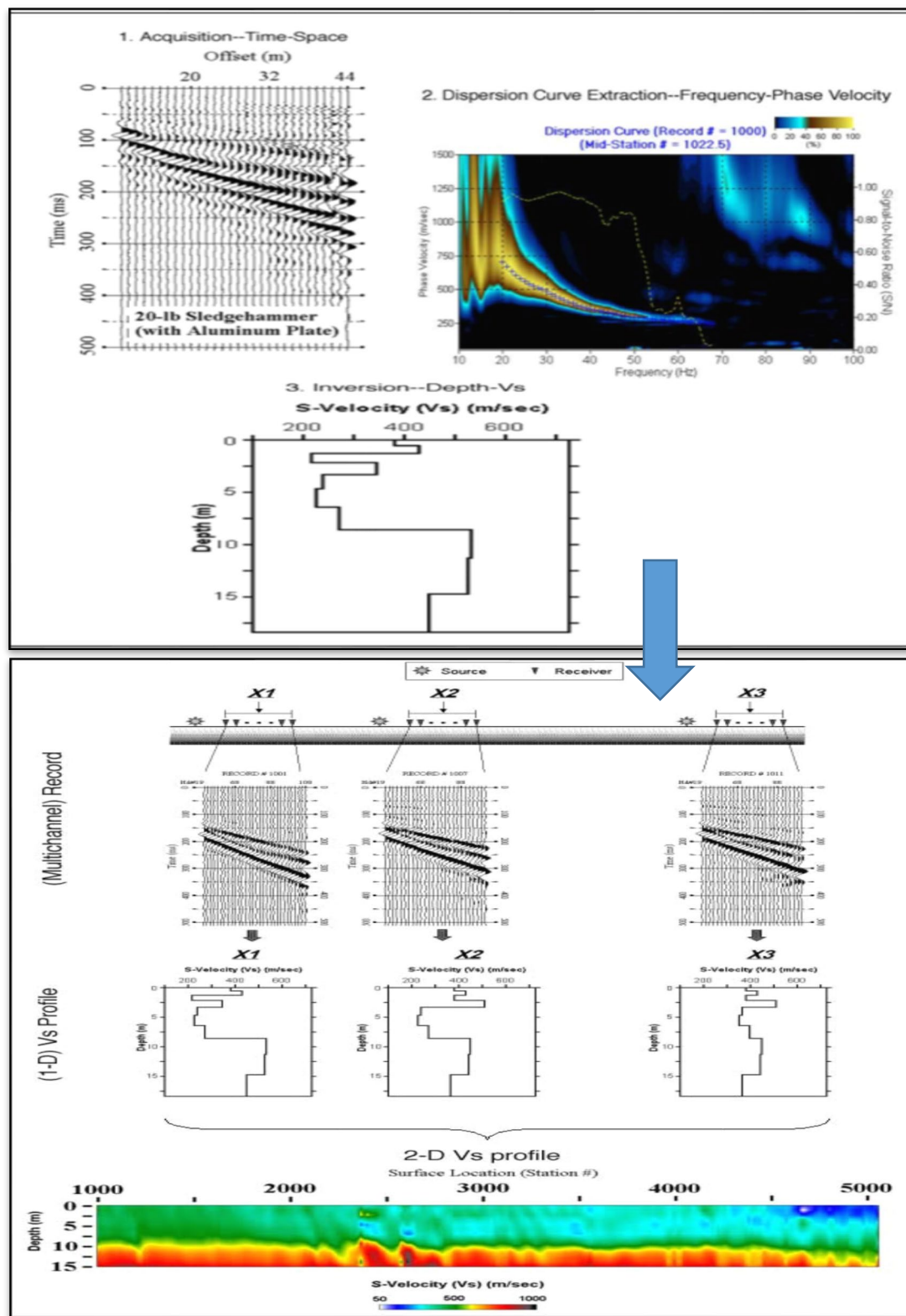


Figure 6.11. Generate 2-D MASW profile from 1-D MASW profiles (Kansas Geological Survey, 2014).

7. RESULTS AND DISCUSSIONS

Typically, the resistivity values of the CCR, soil, and bedrock are dependent on their moisture content. CCR and soil are typically more porous than rock therefore generally display lower resistivity values. CCR, soil and rock with higher moisture content are characterized by lower resistivity values than CCR, soil and rock with lower moisture content.

In this study, the top-of rock was difficult to confidently map in places on the ERT profiles where shallow bedrock was pervasively fractured and moist from run-off. Hence it was characterized by resistivity values that are comparable to that of overlying moist soil.

Herein, soil that has resistivity values higher than 125 ohm-m will be interpreted as “dry soil”, soil that has resistivity values less than 125 ohm-m will be interpreted as “moist soil”. Bedrock that has resistivity values greater than 900 ohm-m will be interpreted as “dry bedrock”, bedrock that has resistivity values from 125 ohm-m to 900 ohm-m will be interpreted as “moist bedrock”, and bedrock that has resistivity values less than 125 ohm-m will be interpreted as “very moist bedrock”.

For interpretation purposes, it is important to note that, even a thin film of saline moisture on soil grains or on grains of CCR will transmit significant current.

3-D ERT profile 633-634 (Figure 7.1) is a synthetic profile along an assumed traverse in between the actual traverses 633 and 634. The top-of-rock is highlighted in black. The uppermost portion of the deposit is generally dry and is characterized by resistivity values between approximately 50 ohm-m to 250 ohm-m. This portion is interpreted as the cap cover material. Below the interpreted cap cover, resistivity values

of the CCR deposit decrease to approximately 10 ohm-m with increasing CCR burial depth. As mentioned previously, the cap cover placed on top of the CCR does not prevent all the run-off from infiltrating into the CCR, and it is expected that some run-off will seep through and leachate is periodically drained through the leachate collection system. Based on the resistivity variations through the CCR deposit, it appears that some of the run-off has infiltrated through the cap cover into the deposit to the bottom liner.

The CCR disposed at the site mainly contains fly ash, bottom ash, and flue gas desulfurization (FGD) materials. Site history indicates that bottom ash was disposed infrequently (every few years), and CCR in the landfill is mainly fly ash and FGD materials. FGD materials were disposed mainly at the lower portion in the CCR deposit. When flue gas was produced, limestone or lime was added to the flue gas to act with sulfur, therefore it is reasonable to believe the CCR deposit contains a certain amount of calcium sulfate, which is the product of such desulfurization process. Calcium sulfate is highly conductive and the low resistivity values in the CCR deposit could also be the result of electronic conduction through calcium sulfate rather than electrolytic conduction through moisture content. Moreover, when the CCR was piled up it contained moisture as a result of prewetting (part of the dust control process), which might also be the reason of the low resistivity values.

The CCR landfill is equipped with both run-on and run-off systems per the regulations established by the Missouri Department of Natural Resources (MDNR) Solid Waste Management Program (SWMP). Site history indicates that the topography around the landfill is such that only the north of the landfill contributes run-on. Clay berms and drainage ditches were constructed to channel this run-on into a large swale located on the

west of the landfill. Additionally, the surface of the east and south sides of the landfill slope away from the landfill, therefore run-on does not come from these directions. The CCR landfill slopes with a narrow crown on top, hence most of the run-off flows down the flanks of the CCR landfill onto the perimeter berms at the toe (Figure 7.2). The perimeter berms divert run-off to be channeled through drainage ditches into a stormwater retention pond at the south.

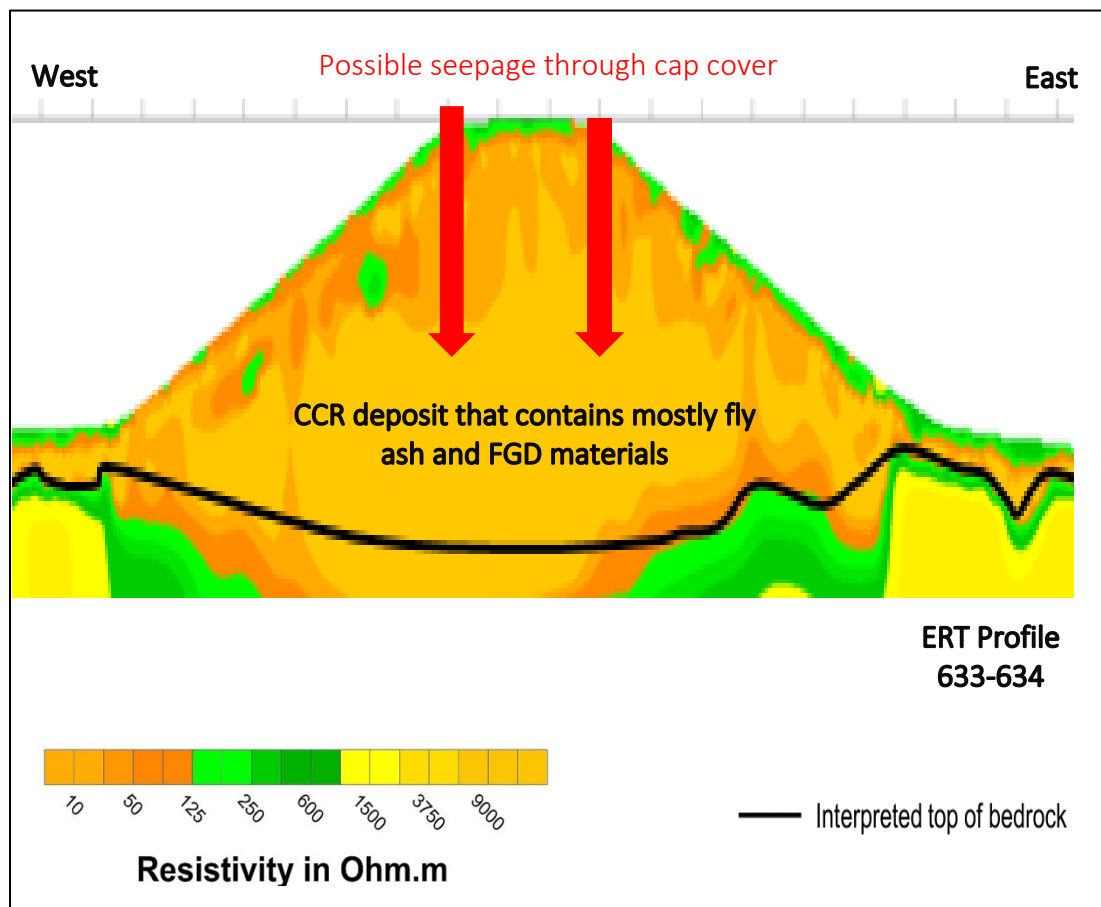


Figure 7.1. Resistivity variations in the CCR deposit.

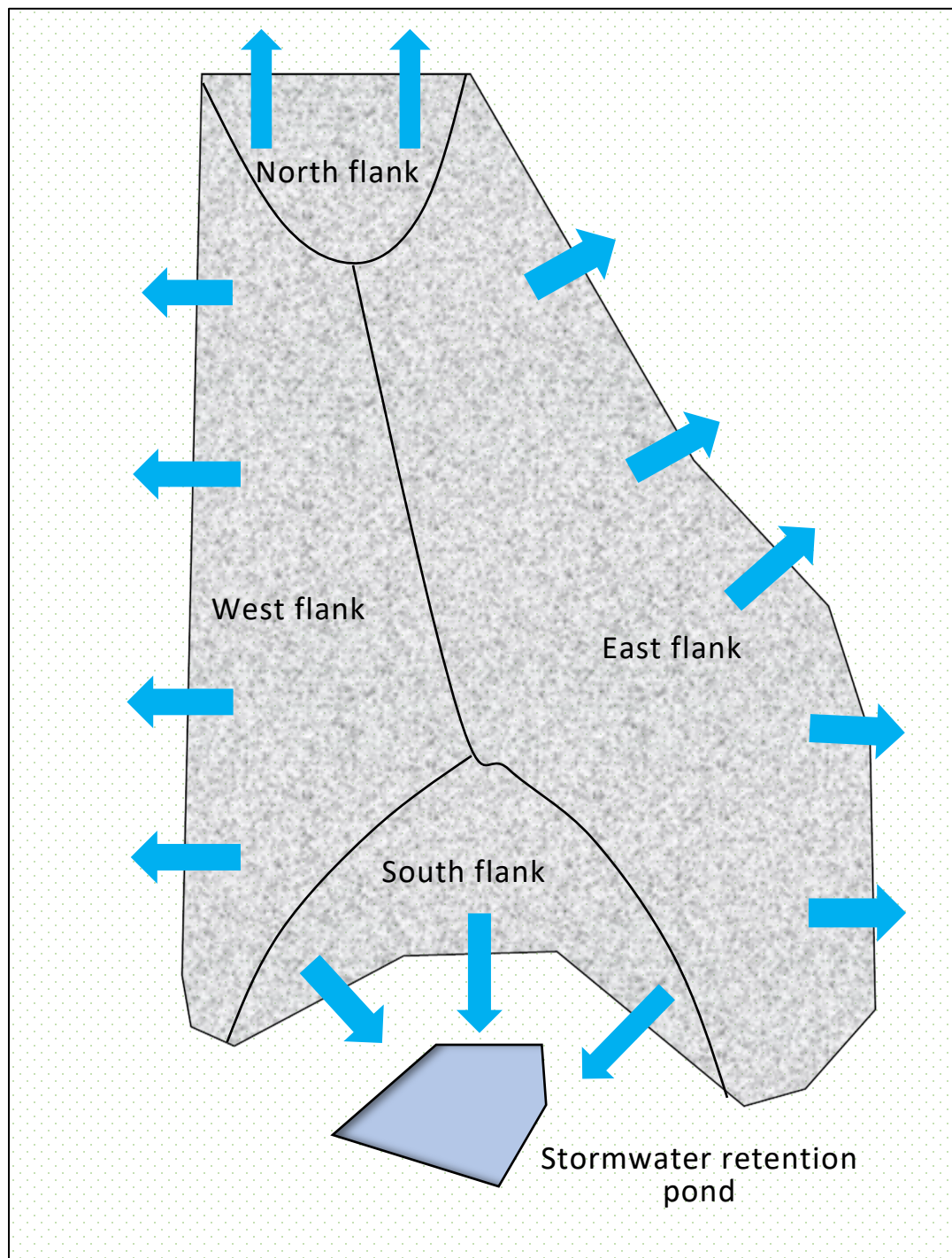


Figure 7.2. Illustrative diagram of the CCR landfill run-off directions. Run-off mostly flows down along the flanks of the landfill to the toe, then into drainage ditches connected to the stormwater retention pond.

Possible seepage pathways in proximity to the CCR landfill are identified on the 3-D profile 633-634 (Figure 7.3).

The seepage pathway identified near the west toe of the landfill, appears to be attributed to run-off flowing down the west flank of the landfill and concentrating in the drainage ditches along a roadway, where moisture infiltrates into the permeable soil and upper pervasively fractured bedrock.

The seepage pathway in proximity to the east toe of the landfill appears to be attributed to run-off flowing down the east flank of the landfill and getting intercepted by a diverting berm, moisture from the temporary concentration of the run-off likely seeps down into the upper pervasively fractured bedrock through the permeable soil.

Subsurface soil and bedrock immediately adjacent to the toe of the landfill appear to have the highest moisture content (seepage volume). As distance from the landfill toe increases, moisture content of the subsurface generally decreases, suggesting the seepage flow at the toe is mostly vertical with some lateral flow away from the landfill along the soil-uppermost bedrock intervals. Additionally, possible seepage at the toe of the landfill that appears to flow inward towards the CCR deposit are also identified. Site history indicates that the CCR landfill was constructed on a south-trending channel with a structure low, and it appears that run-off accumulating at the toe seeps vertically into the soil and fractured bedrock with some seepage flows laterally along the soil-uppermost fractured bedrock layer, towards the structure low beneath the CCR deposit.

The ten ERT profiles acquired surrounding the landfill (Figure 7.4, 1 through 10 highlighted in yellow), and the seven ERT profiles acquired at the west side and east toe

of the landfill (Figure 7.4, 1' through 8' highlighted in red) were to identify possible subsurface seepage pathways along the outer toe of the landfill.

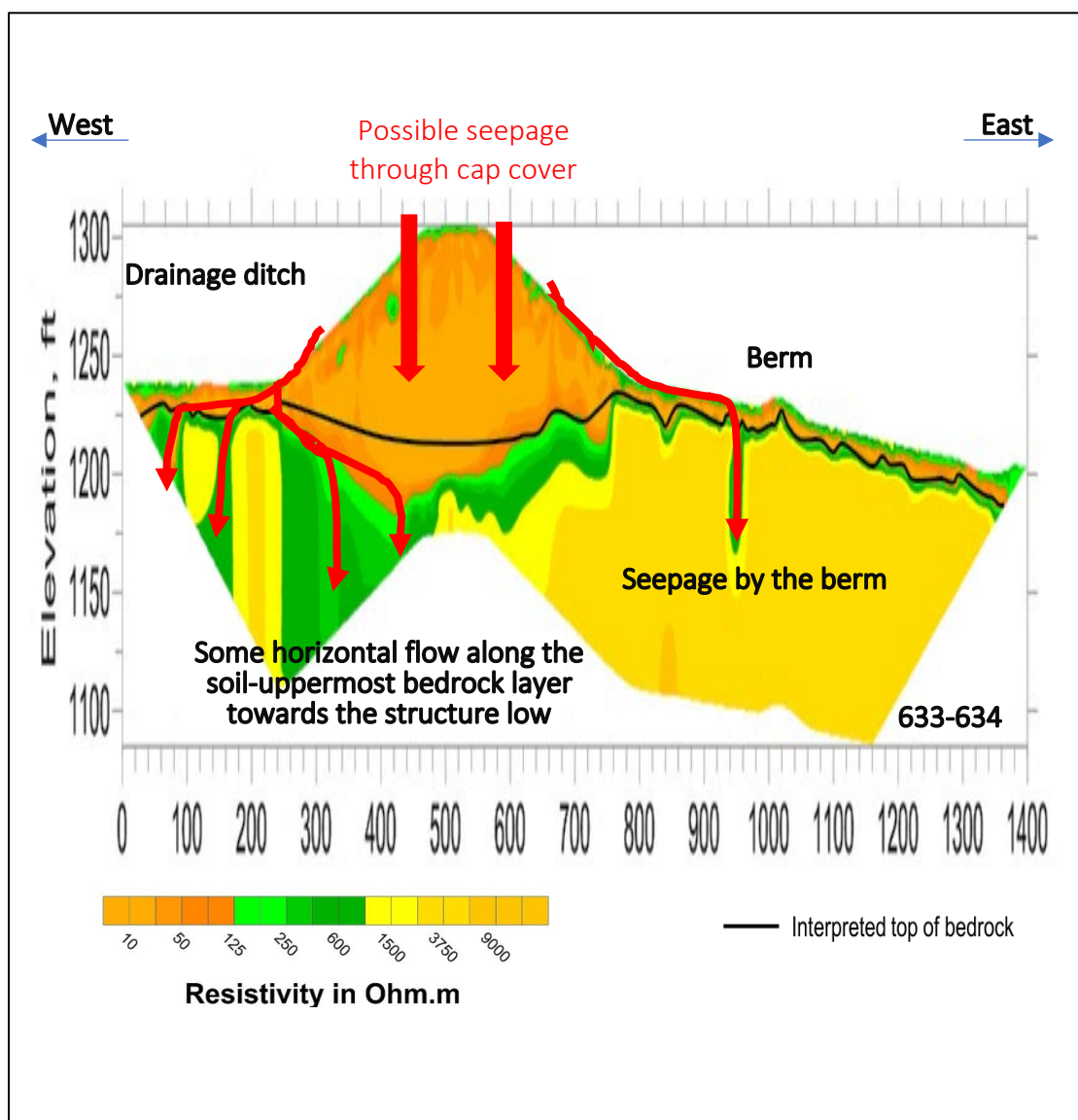


Figure 7.3. Seepage pathways resulted from moisture seeping down into the pervasively fractured bedrock.

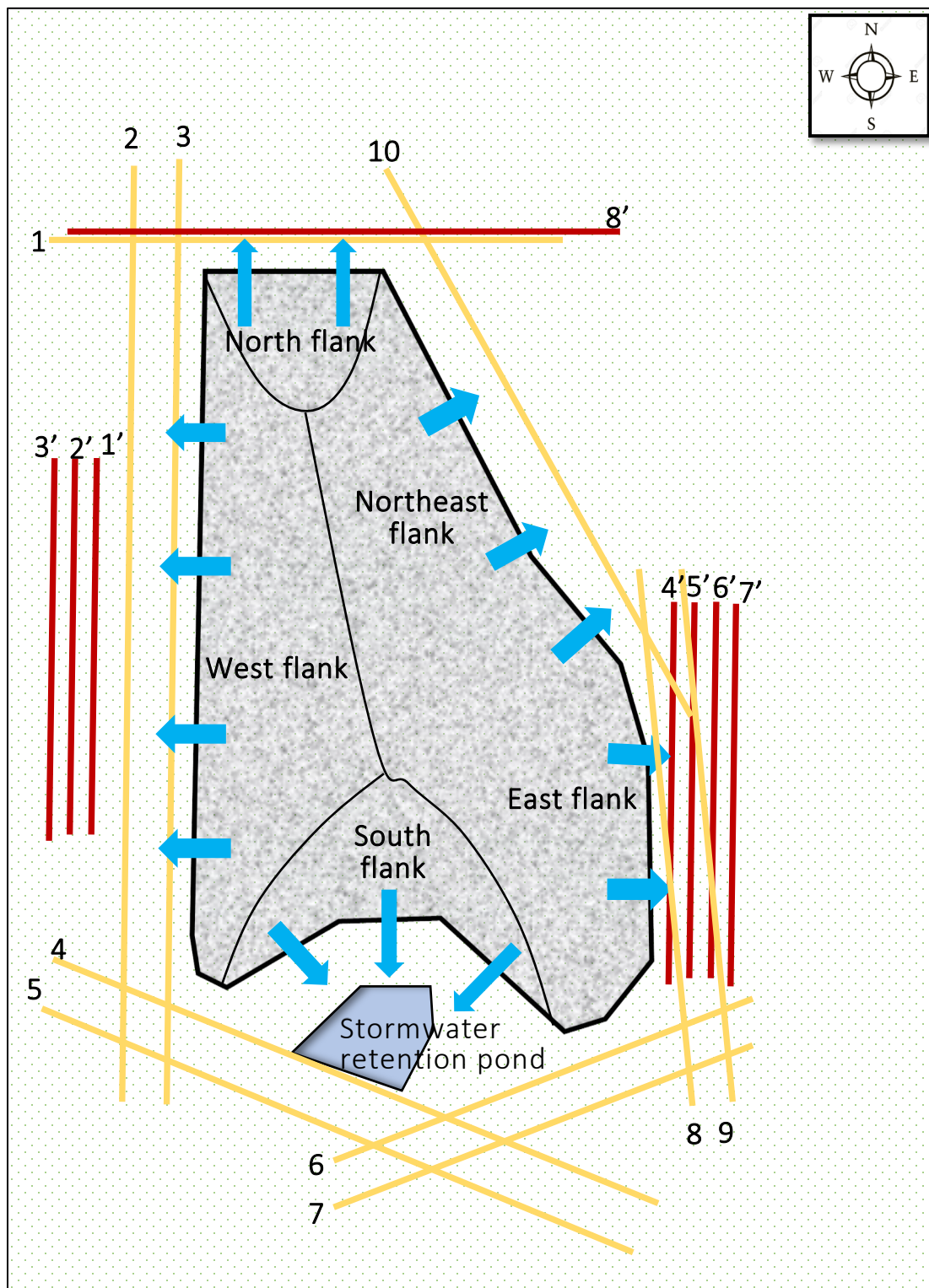


Figure 7.4. Aerial view of the CCR landfill and the locations of the ERT traverses surrounding the landfill.

Interpreted ERT profile 1 (Figure 7.5) was acquired in proximity to the north toe of the landfill. The interpreted soil-rock contact (top-of-rock) is highlighted in black. As noted, the top-of-rock cannot be confidently mapped as the upper bedrock is pervasively fractured and moist hence it is characterized by comparable resistivity values to that of overlying moist soil. The soil layer is interpreted as approximately 20 ft. thick, which is consistent with boring control, MASW (multichannel analysis of the surface waves) control and ERT control acquired elsewhere in the greater study area. The soil is classified as dry soil (resistivities > 125 ohm-m) and moist soil (resistivities < 125 ohm-m). Generally, dry soils overly moist soils. Interpreted uppermost bedrock is approximately 20 ft. below the ground surface. The bedrock is classified as dry rock (resistivities > 900 ohm-m), moist rock (125 ohm-m $<$ resistivities < 900 ohm-m), and very moist rock (resistivities < 125 ohm-m). Generally, the uppermost bedrocks are very moist and they overly moist rocks and dry rocks.

Four possible prominent seepage pathways were identified on ERT profile 1. Prominent seepage pathways were located in areas where moisture has infiltrated into the pervasively fractured Burlington-Keokuk limestone.

- Seepage pathway 1 is attributed to moisture seeping through a north-south oriented drainage ditch that channels run-off to the south towards the stormwater retention pond.
- Seepage pathway 2 is attributed to run-off from the north flank of the CCR landfill. Some run-off from the north flank of the CCR landfill seeps through the permeable soils and into bedrock at the toe of the landfill (outer edge of the

clay seal). Most of the run-off is designed to flow through the drainage ditches towards the stormwater retention pond.

- Seepage pathway 3 is attributed to surface rainwater flowing along a topographic low.
- Seepage pathway 4 is attributed to rainwater flowing along the topographic low and temporarily accumulating at a natural surface drainage path

Overall, bedrock that contains higher moisture content is immediately adjacent to the north toe of the landfill, bedrock moisture content generally decreases with increasing distance away from the north toe of the landfill.

Interpreted ERT profiles 2 and 3 (Figure 7.6) were acquired in proximity to the west toe of the landfill. Five possible prominent seepage pathways were identified on ERT profiles 2 and 3:

- Seepage pathway 1 (ERT profiles 2) is attributed to run-off from the west flank of the landfill that extends from ERT station 240 to ERT station 1120.
- Seepage pathway 2 (ERT profiles 2) is attributed to run-off from the west flank of the landfill that temporarily accumulated by the berm. Run-off is channeled towards the south retention pond, by the constructed perimeter berm (Figure 7.7) that extended roughly between station 1100- station 1600.
- Seepage pathway 3 (ERT profile 3) is attributed to run-off being channeled through a drainage path (Figure 7.7).
- Seepage pathway 4 (ERT profile 3) is attributed to run-off from the west flank of the landfill and surface rainwater being channeled through the drainage ditch along the roadway.

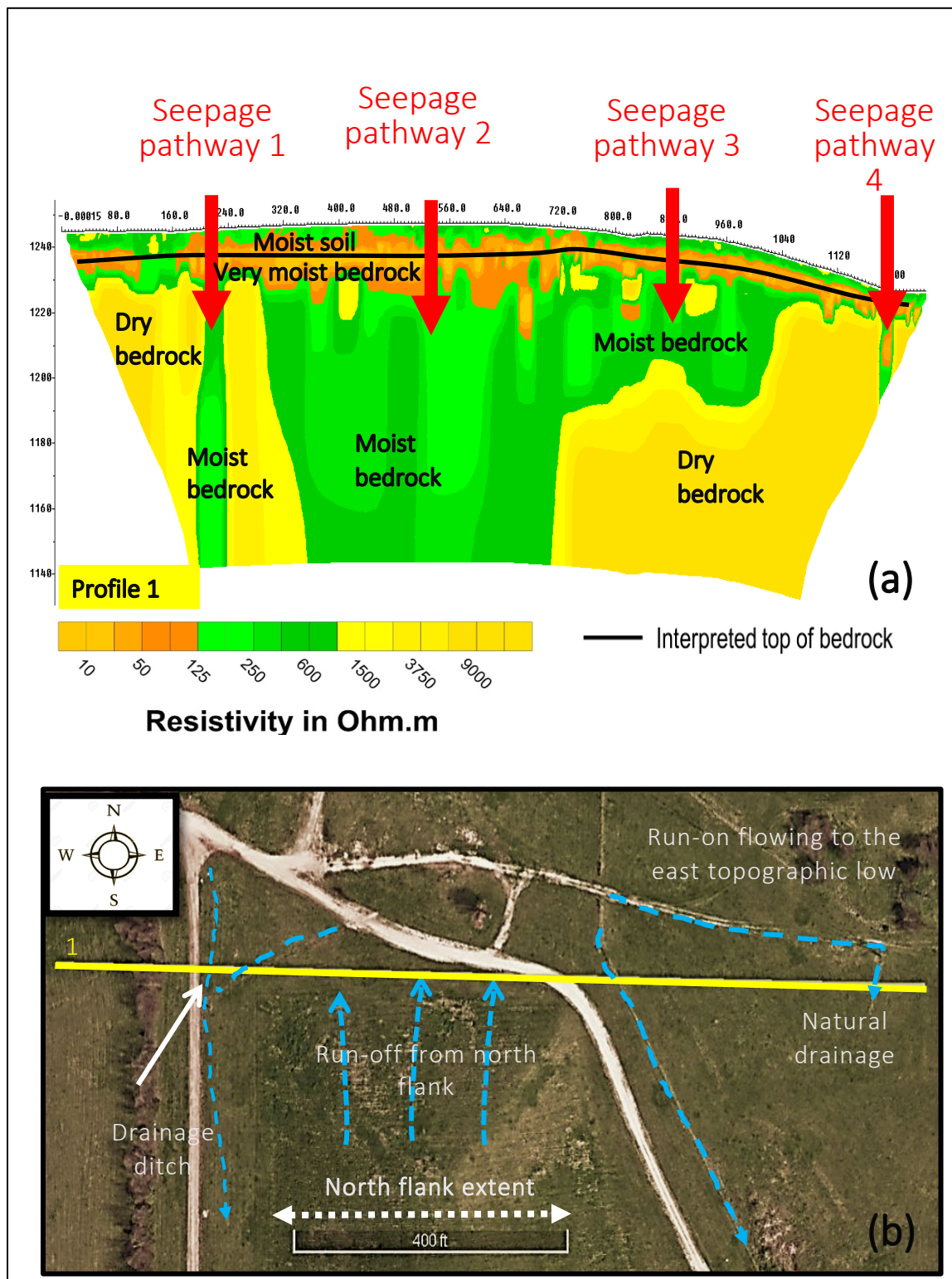


Figure 7.5. ERT profile acquired at the north toe. (a) Interpreted ERT profile 1 and (b) aerial view (Google Earth image) showing the north flank of the landfill and ERT traverse 1.

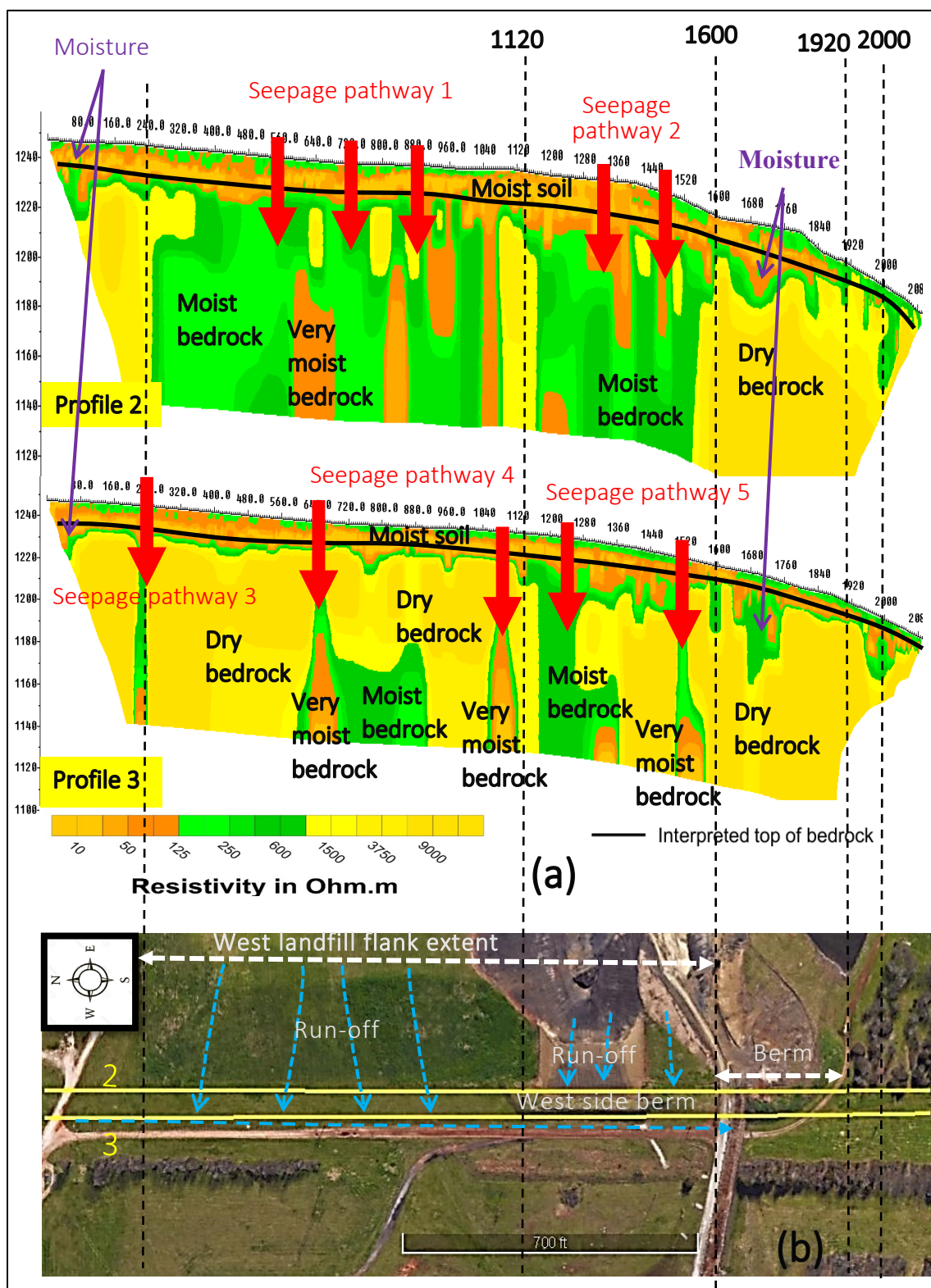


Figure 7.6. ERT profiles acquired at the west toe of the landfill. (a) Interpreted ERT profiles 2, 3. (b) Aerial view (Google Earth image) of the west flank/toe of the landfill and ERT traverses 2, 3.

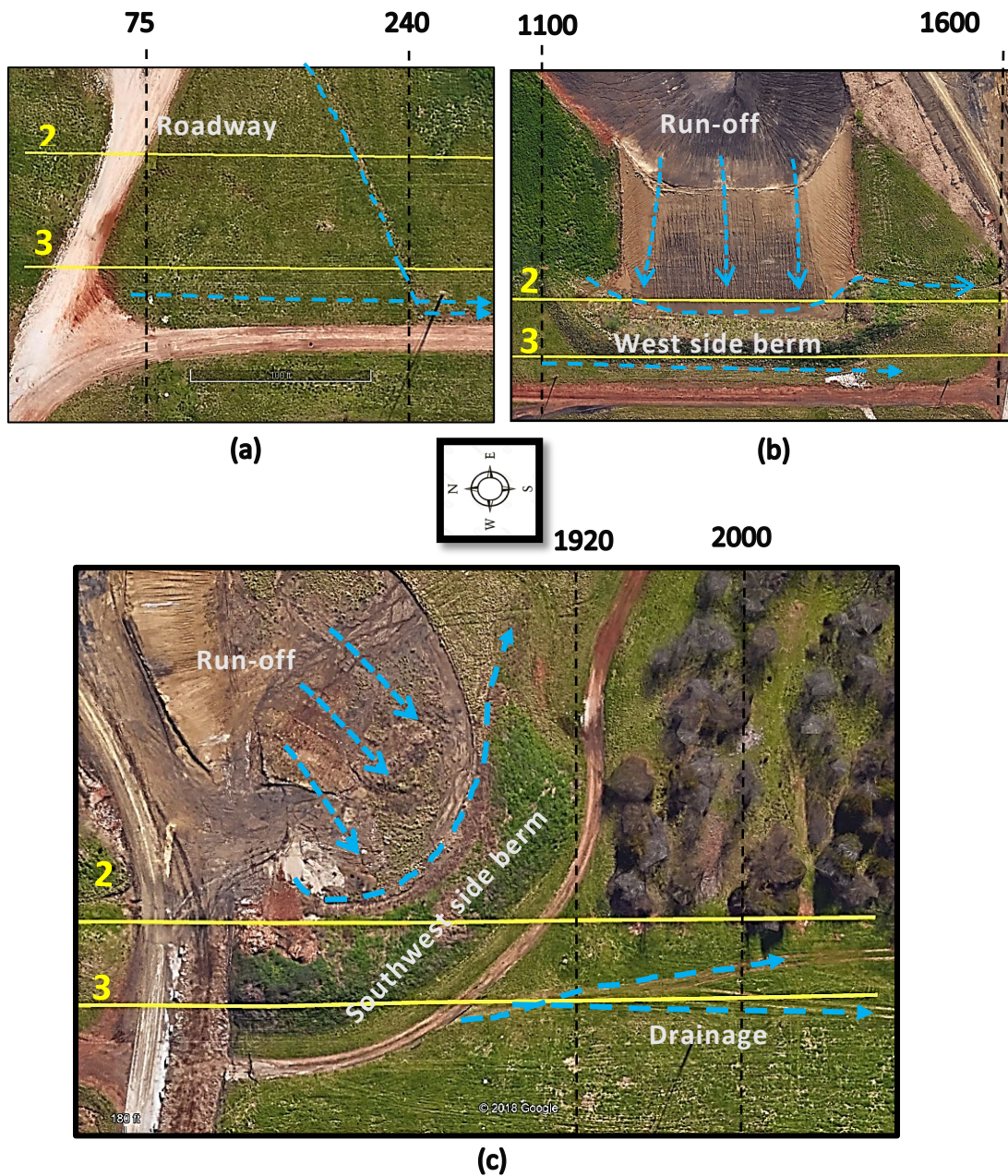


Figure 7.7. Run-off gets intercepted by man-made features.

- Seepage pathway 5 (ERT profile 3) is attributed to run-off from the west flank of the landfill and surface rainwater being channeled through the drainage ditch along the roadway.

Overall, bedrock contains higher moisture content under the subsurface immediately adjacent to the west toe of the landfill, and bedrock moisture content generally decreases with increasing distance away from the toe.

Interpreted ERT profiles 4 and 5 (Figure 7.8) were acquired in proximity to the south stormwater retention pond. The interpreted soil-rock contact (top-of-rock) is highlighted in black. Two possible prominent seepage pathways were identified on ERT profiles 4:

- Seepage pathway 1 is attributed to moisture from surface rainwater being channeled and accumulated by the roadway and berm.
- Seepage pathway 2 is attributed to moisture from run-off and surface rainwater being channeled inside the berm as well as along the roadway, into the stormwater retention pond.

Overall, bedrock with higher moisture content is found to be immediately adjacent to the south toe of the landfill, and bedrock moisture content generally decreases with increasing distance away from the south toe.

Interpreted ERT profiles 6 and 7 (Figure 7.9) were acquired in proximity to the southeast perimeter berm. The interpreted soil-rock contact (top-of-rock) is highlighted in black. Three possible prominent seepage pathways were identified on ERT profiles 6 and 7:

- Seepage pathway 1 is attributed to moisture from southeast landfill flank run-off channeled along the perimeter berm.
- Seepage pathways 2 and 3 are attributed to moisture from surface rainwater channeled along a berm that locates southeast to the perimeter berm.

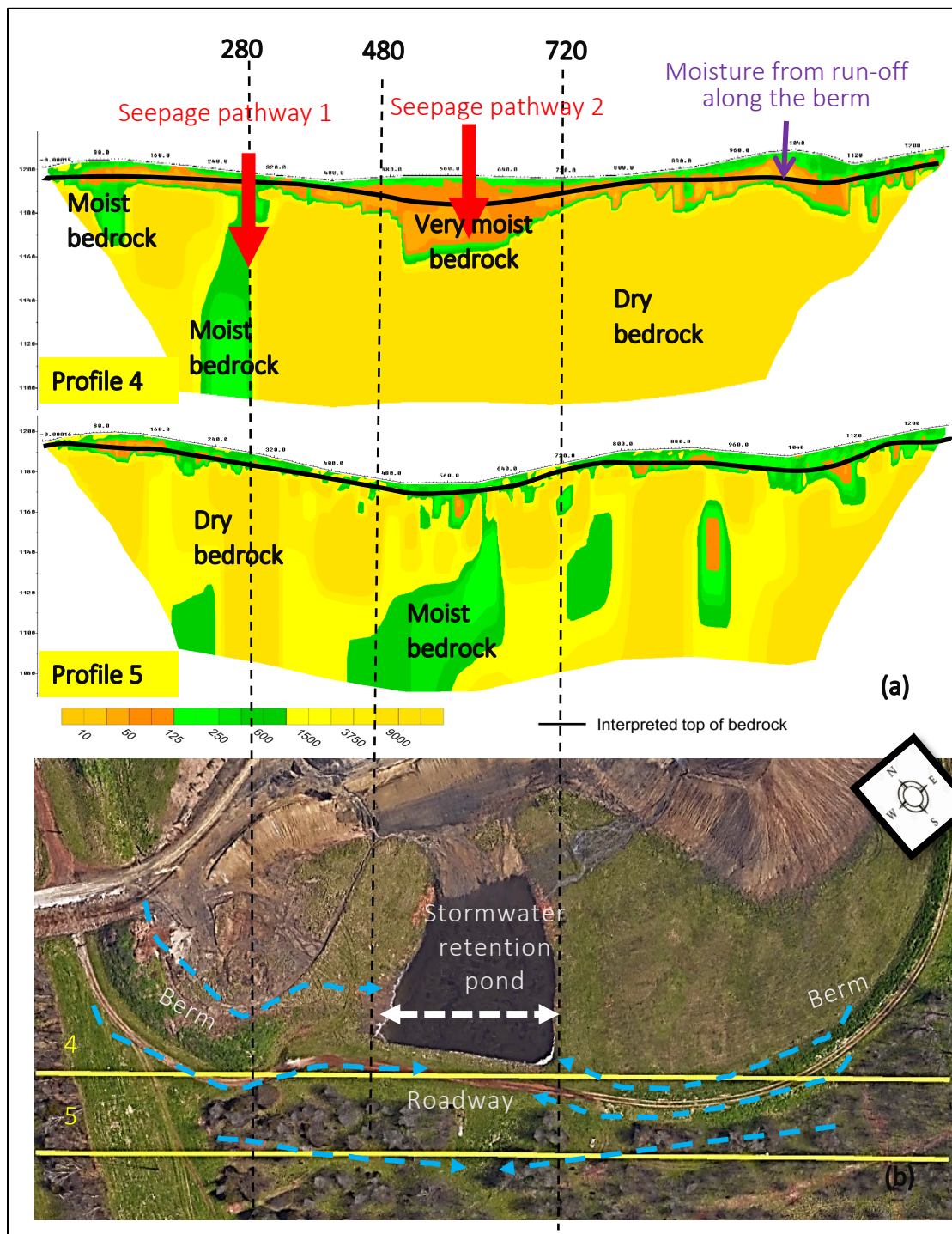


Figure 7.8. ERT profiles acquired near the retention pond. (a) Interpreted ERT profiles 4, 5 and (b) aerial view (Google Earth image) of the south stormwater retention pond and ERT traverses 4, 5.

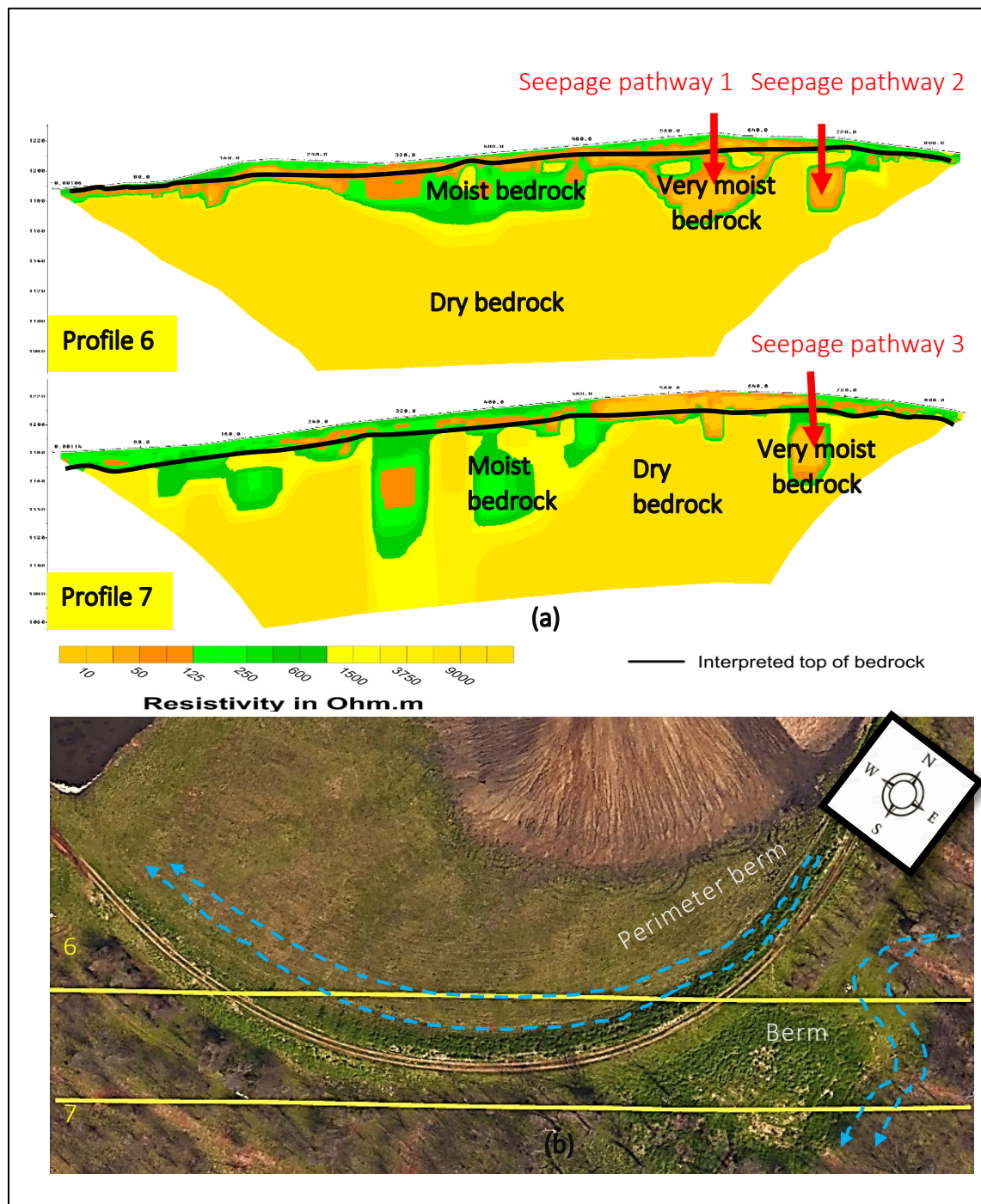


Figure 7.9. ERT profiles acquired near the southeast berm. (a) Interpreted ERT profiles 6, 7 and (b) aerial view (Google Earth image) of the southeast perimeter berm and ERT traverses 6, 7.

Overall, bedrock with higher moisture content is found to be immediately adjacent to the southeast toe of the landfill, and bedrock moisture content generally decreases with increasing distance away from the southeast toe.

Interpreted ERT profiles 8 and 9 (Figure 7.10) were acquired in proximity to the east side toe of the landfill. The interpreted soil-rock contact (top-of-rock) is highlighted in black. Three possible prominent seepage pathways were identified on ERT profiles 8 and 9:

- Seepage pathway 1 (ERT profile 8) is attributed to moisture from run-off from the east flank of the landfill channeling away by the perimeter berm into the south stormwater retention pond.
- Seepage pathway 2 (ERT profile 9) is attributed to surface rainwater accumulated by the roadway and vegetation.
- Seepage pathway 3 (ERT profile 9) is attributed to surface rainwater accumulated by the vegetation.

Overall, bedrock with higher moisture content is found to be immediately adjacent to the east toe of the landfill, and bedrock moisture content generally decreases with increasing distance away from the east toe.

Interpreted ERT profile 10 (Figure 7.11) was acquired in proximity to the northeast toe of the landfill. The interpreted soil-rock contact (top-of-rock) is highlighted in black. Two possible prominent seepage pathways were identified on ERT profile 10:

- Seepage pathway 1 is attributed to run-off from the northeast flank of the landfill channeling away through the drainage ditch.

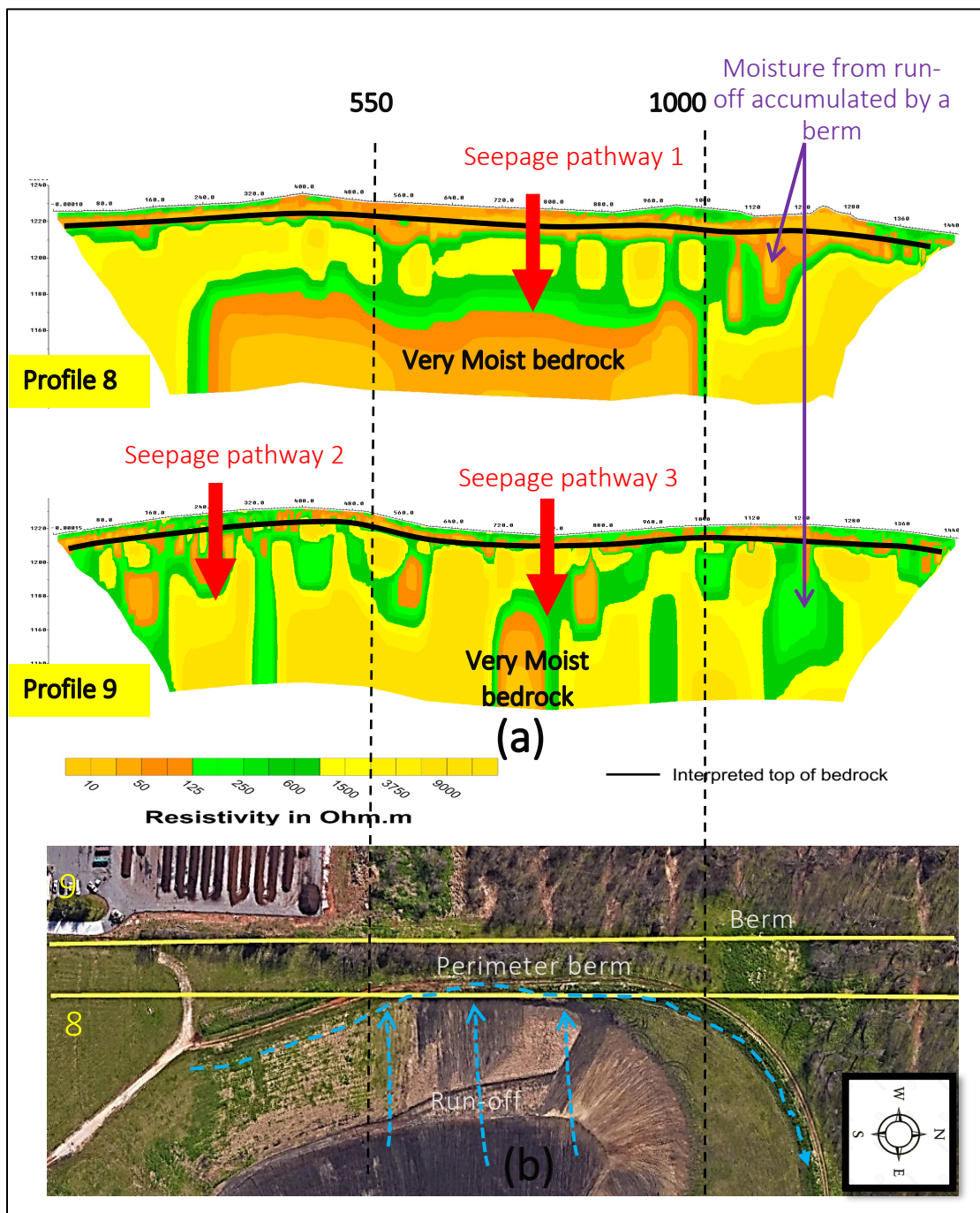


Figure 7.10. ERT profiles acquired at the east toe of the landfill. (a) Interpreted ERT profiles 8, 9 and (b) aerial view (Google Earth image) of the east side flank/toe of the landfill and ERT traverses 8, 9.

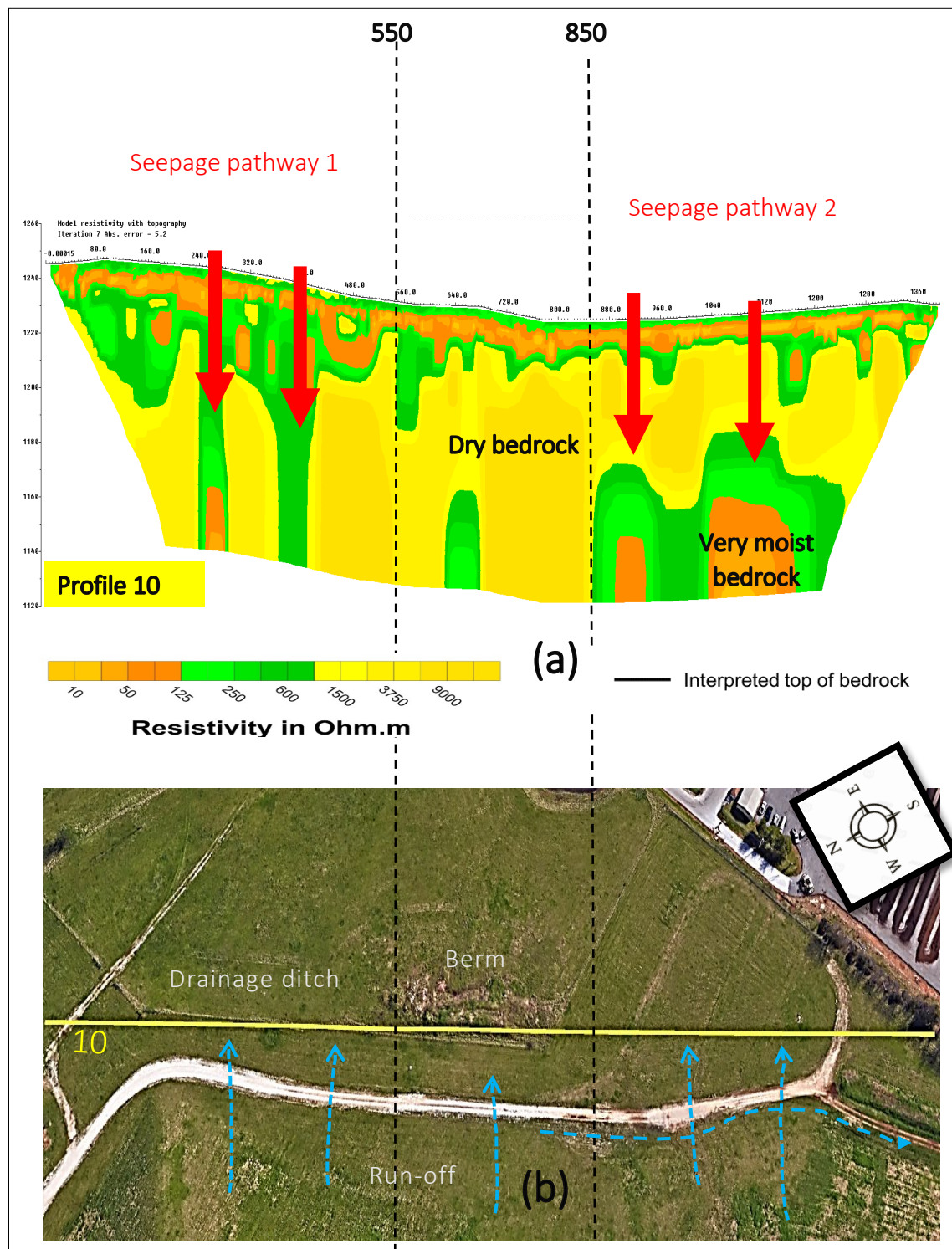


Figure 7.11. ERT profile acquired at the northeast toe of the landfill. (a) Interpreted ERT profile 10 and (b) aerial view (Google Earth image) of the northeast flank/toe of the landfill and ERT traverse 10.

- Seepage pathway 2 is attributed to run-off from the northeast flank of the landfill.

The subsurface between seepage pathway 1 and 2 has relatively less moisture, likely because of the berm acted as a low permeable barrier.

Interpreted ERT profiles 1', 2' and 3' (Figure 7.12) were acquired in proximity to the west side toe of the landfill with 20 ft intervals. The interpreted soil-rock contact (top-of-rock) is highlighted in black.

Moisture content in the subsurface on ERT profiles 1', 2' and 3' is attributed to run-off from the west flank of the landfill. The seepage boundary on the three ERT profiles correlates well with the boundary of the berm. Run-off appears to be intercepted by the berm, accumulated and seeped down into the subsurface.

Overall, bedrock with higher moisture content is in close proximity to the west toe of the landfill, and bedrock moisture content generally decreases with increasing distance away from the west toe. Bedrock moisture content on each profile also decreases with distance away from the berm.

Interpreted ERT profiles 4', 5' and 6' and 7' (Figure 7.13) were acquired in proximity to the east side toe of the landfill with 20 ft intervals. The interpreted soil-rock contact (top-of-rock) is highlighted in black. Moisture content in the subsurface on ERT profiles 4', 5' and 6' and 7' is attributed to run-off from the east flank of the landfill. Run-off appears to be intercepted by the perimeter berm, accumulated and seeped down into the subsurface. Overall, bedrock with higher moisture content is in close proximity to the east toe of the landfill/perimeter berm, and bedrock moisture content generally decreases with increasing distance away from the east toe/perimeter berm.

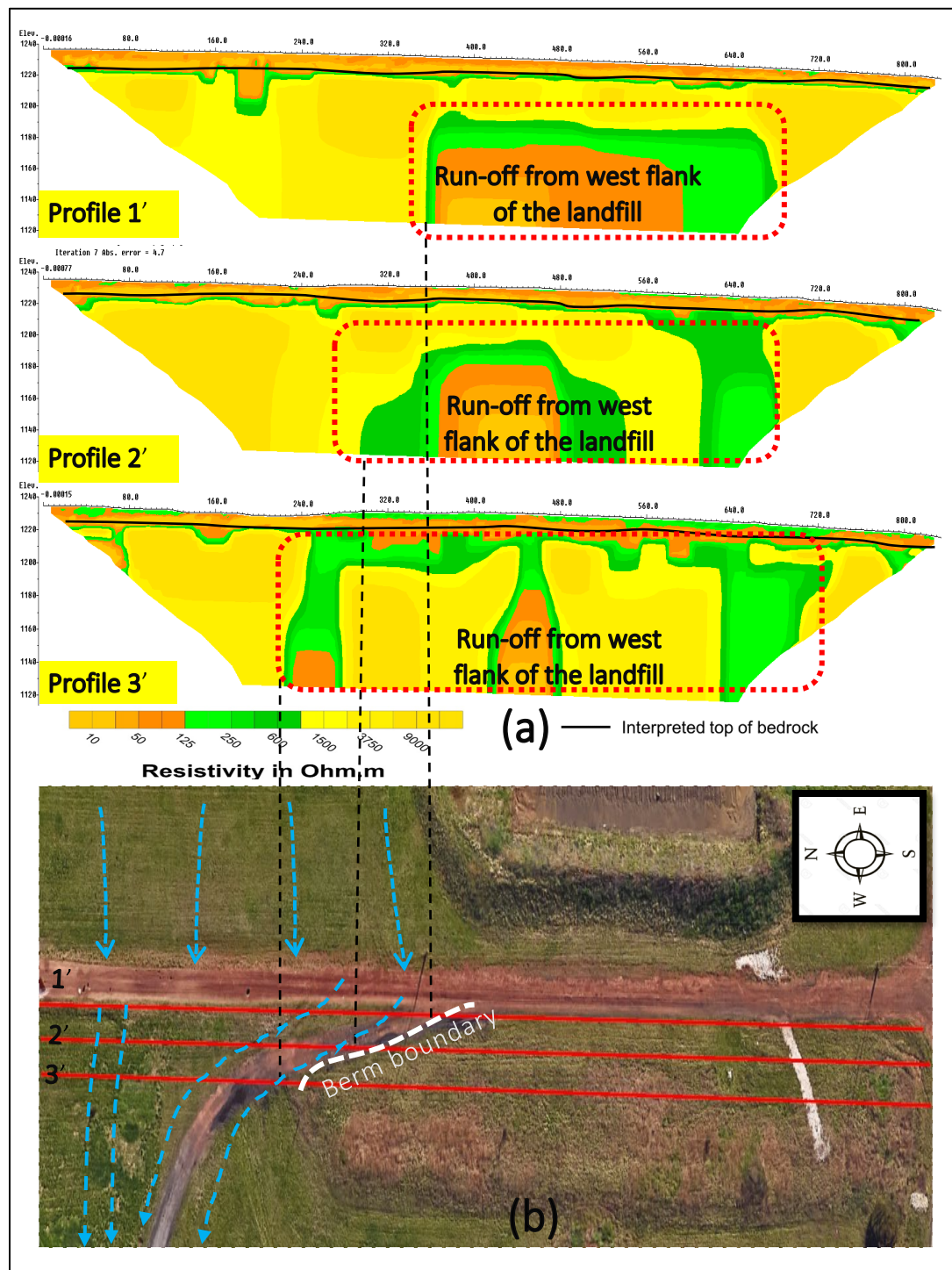


Figure 7.12. ERT profiles acquired over a berm near the west toe of the landfill. (a) Interpreted ERT profiles 1', 2' and 3' and (b) Aerial view (Google Earth image) of ERT traverses 1', 2' and 3' and the berm in proximity to the west toe of the landfill.

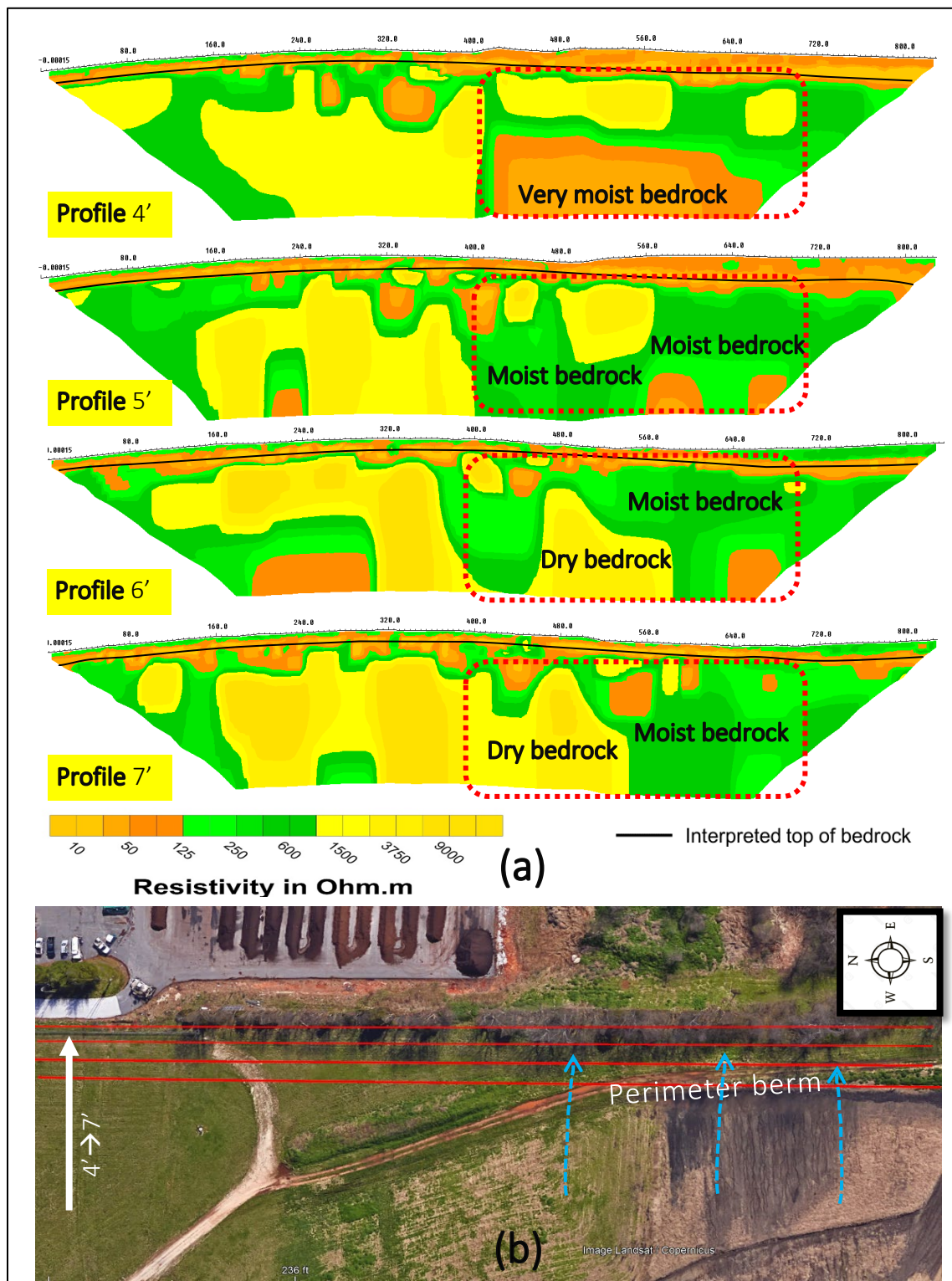


Figure 7.13. ERT profiles acquired at the east toe of the landfill. (a) Interpreted ERT profiles 4', 5' and 6' and 7'. (b) Aerial view (Google Earth image) of ERT traverses 4', 5' and 6' and 7' and the perimeter berm.

The 3-D ERT profiles (Figure 7.14) 614-615, 615-616, 616-617 and 618-619 represent the assumed “ERT profiles” that were “acquired” along the “ERT traverses” in between traverses 614-615, 615-616, 616-617 and 618-619. As Figure 7.14 illustrates, seepage pathways identified on the four profiles are attributed to run-off and surface rainwater temporarily accumulating by man-made and natural features. The identified seepage pathways are consistent with those identified on ERT profile 1 (Figure 7.5) and ERT profile 10 (Figure 7.11).

ERT profile 8' (Figure 7.15) was acquired essentially at the same location as ERT profile 1 (with a slightly longer array), but at a different time of year. ERT profile 8' was acquired in early February. Precipitation and snowmelt in the winter month were limited and as a result, run-off significantly decreased. Subsurface bedrock immediately adjacent to the north toe of the landfill and anthropogenic features, is mostly characterized by dry bedrock (resistivities > 900 ohm-m), indicating very little moisture has seeped through the subsurface in these areas. On the contrary, ERT profile 1 was acquired in early September and as a result, run-off increased from significant rain-fall in the later summer month. Subsurface bedrock immediately adjacent to the same area (the north toe of the landfill and anthropogenic features) is mostly characterized by moist bedrock (125 ohm-m $<$ resistivities < 900 ohm-m), indicating relatively more moisture has seeped through the subsurface in these areas.

MASW data were acquired primarily to identify the top-of-rock and correlate with ERT top-of-rock. In places where CCR is not present and subsurface is relatively dry, the depth of the top-of-rock are readily identified on the 1-D shear-wave velocity profiles, and generally is consistent with interpreted ERT top-of rock.

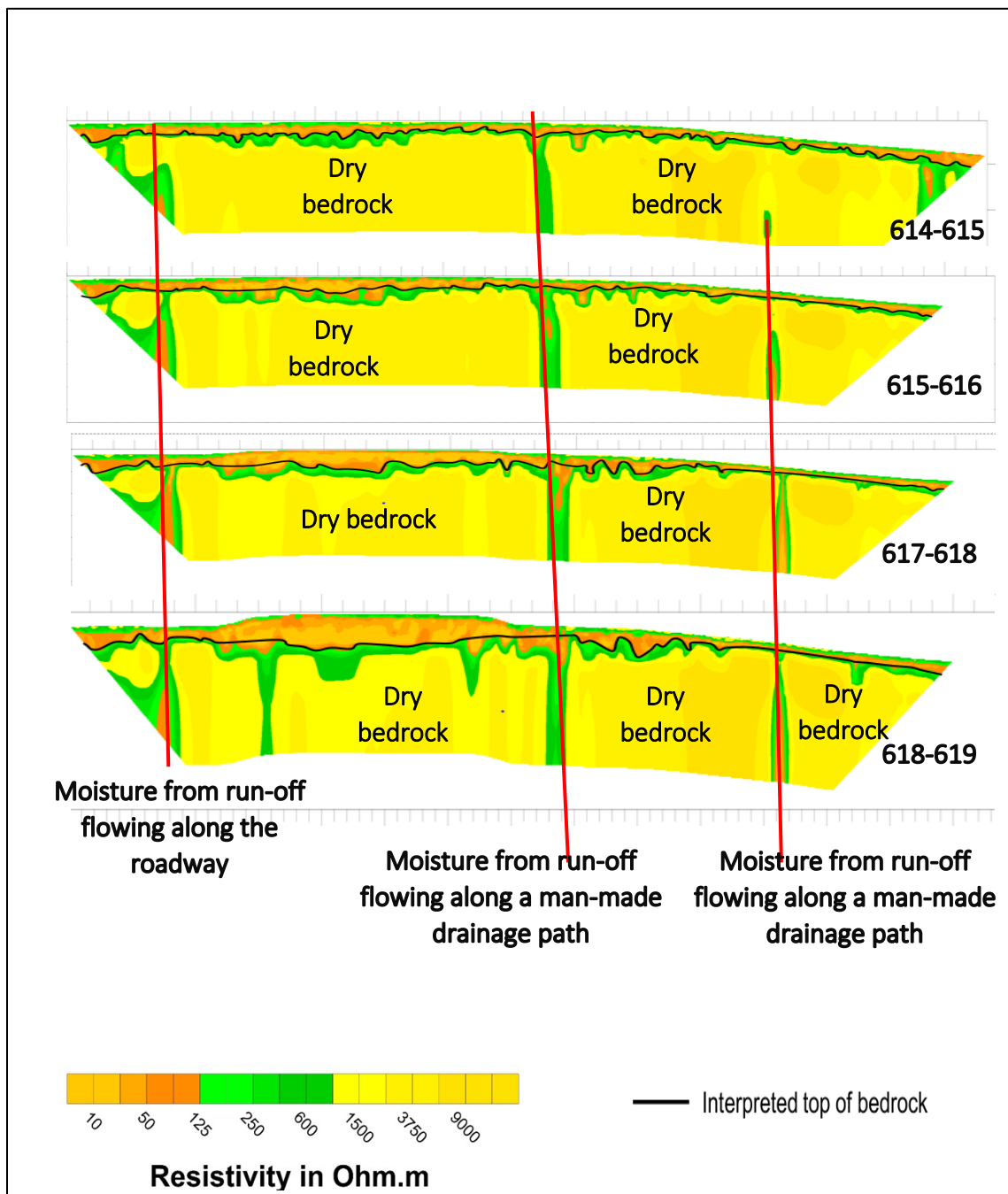


Figure 7.14. 3-D ERT profiles 614-615, 615-616, 616-617. These profiles show moisture seeping into the subsurface fractured bedrock overlain or immediately adjacent to man-made features.

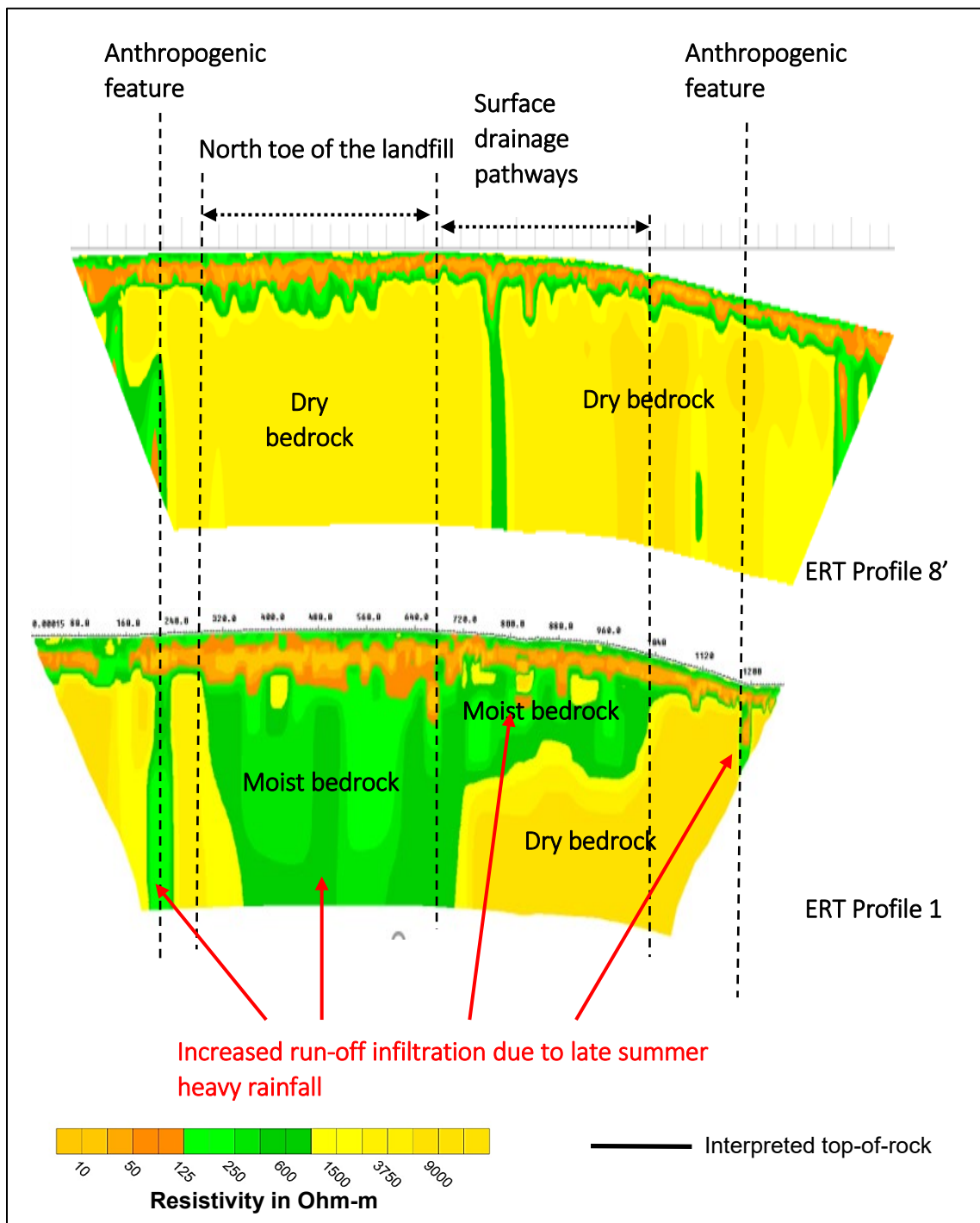


Figure 7.15. Moisture content comparison between ERT profile 8' and ERT profile 1.

As Figure 7.16 illustrates, on 3-D ERT profile 601, at ERT station 440, the interpreted ERT top-of-rock is 9 ft which is consistent with the MASW top-of-rock identified on the 1-D shear-wave velocity profile acquired at this station. Additionally, on 3-D ERT profile 601, at ERT station 240, the interpreted ERT top-of-rock is 15 ft. The MASW top-of-rock identified on the 1-D shear-wave velocity profile acquired at this location is 20 ft (Figure 7.17). The difference in top-of-rock between ERT and MASW at this location could be attributed to resolution differences between ERT and MASW. Generally, ERT has a higher resolution by using resistivity contrasts, while MASW has a relatively lower resolution by using acoustic properties contrasts.

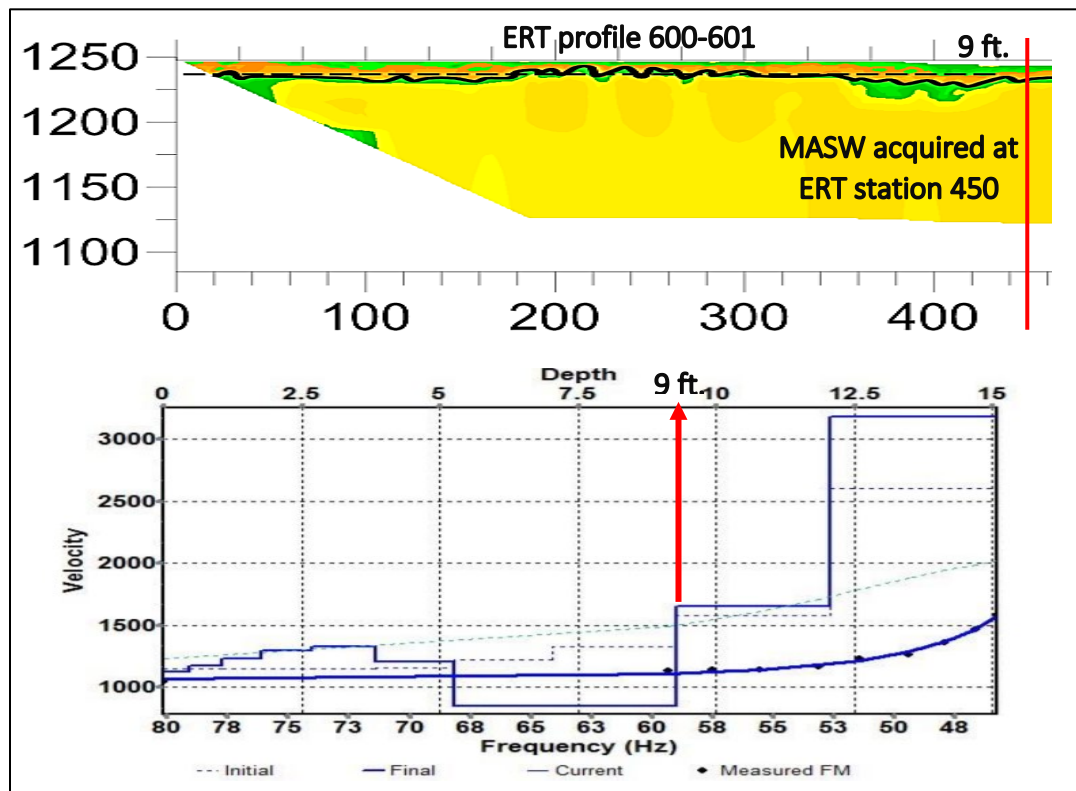


Figure 7.16. ERT top-of-rock is consistent with MASW top-of-rock at ERT station 450 on 3-D ERT profile 600-601.

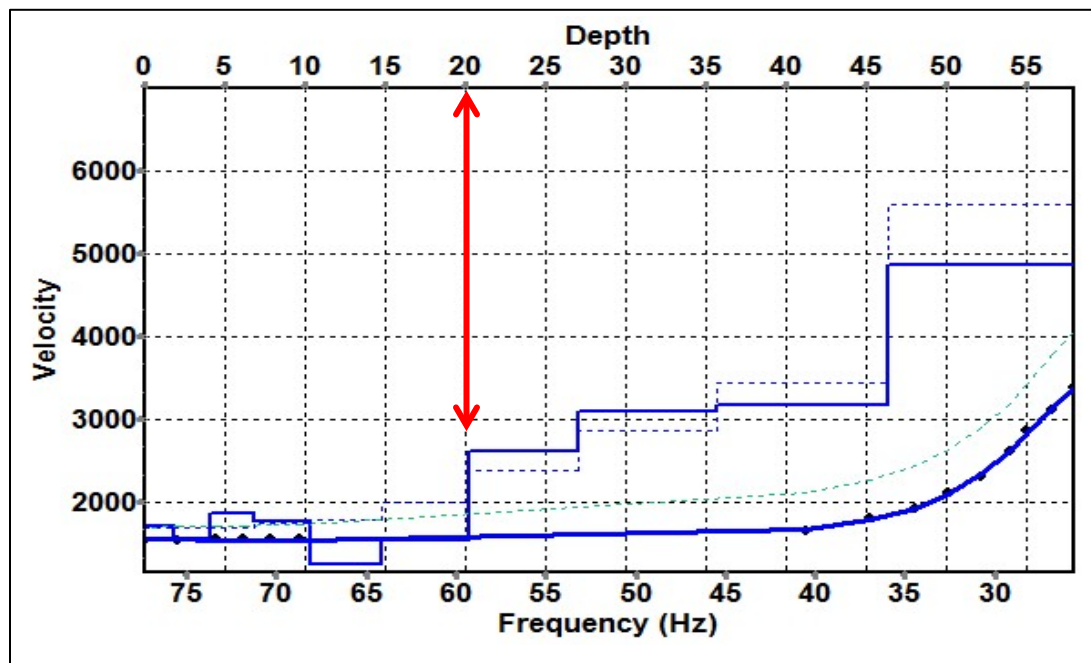


Figure 7.17. MASW top-of-rock is 20 ft at ERT station 240 on 3-D ERT profile 600-601.

Based on MASW data, the subsurface rock in the study area typically has a shear-wave velocity ranges from 1500 ft/s to over 5000 ft/s, which indicates that the shallower bedrock is likely pervasively fractured, and the deeper bedrock is relatively intact. This is consistent with the ERT interpretations that run-off seeps into the subsurface fractured bedrock in close proximity to the landfill.

8. CONCLUSIONS

The 2015 U.S. Environment Protection Agency CCR rule addressed the safe disposal and containment of coal combustion residual in landfills. Although by the time of this research states are not required to enforce this rule, it is reasonable to believe more and more states are making an effort to adopt at least the minimum criteria. This research presents a cost-effective, non-invasive and reasonably accurate geophysical investigation system, to evaluate karst subsurface and possible seepage pathways with regard to CCR landfill safety and contamination control. The non-invasive ERT succeeded in investigating the study area with an average speed of 1200 ft /day, and caused no damage to the containment (e.g., cap cover, liner) of the landfill. The non-invasive MASW provided information about the engineering properties of the CCR, soil and rock, and caused no damage to the containment of the landfill. The successful acquisition of ERT and MASW data was found out to be crucial to interpretations. This research extensively illustrated a streamline of ERT and MASW field operations, and listed the common issues associated with data acquisition over large tracts of land and suggested solutions for these issues.

In the study area, soil is generally characterized by resistivities less than 125 ohm-m, except in areas where the soil is dry. CCR is generally characterized by resistivities less than 125 ohm-m, except in areas where the CCR is dry. Rock is generally characterized by resistivities greater than 900 ohm-m, except in areas where rock is moist and transported silt & clay may be present. In such areas, rock resistivities may be as low as less than 125 ohm-m.

This research sufficiently mapped the top-of-rock (the interval between soil and rock, and the interval between soil/CCR mixture and rock) in the subsurface in close proximity to and directly underneath the CCR landfill. Except beneath the CCR landfill, the pre-development residual soil profile is approximately 20 ft thick. The soil/rock contact is relatively easy to identify on ERT data, except in areas where upper Burlington-Keokuk limestone is pervasively fractured and moist, and top-of-rock could not be confidently mapped as soil and rock are anomalously moist and have comparable resistivity values. Generally, the top-of-rock correlates well with the 125 ohm-m resistivity interval. The CCR/clay liner, clay liner/soil and soil/rock contacts beneath the landfill cannot be confidently mapped using ERT data. Resolution of ERT layers are about 12 ft high and the upper rock beneath the CCR is very moist and has comparable resistivity values to overlying moist soil and CCR.

Soil is generally characterized by shear wave velocity less than 1500 ft/s, except in areas where soil is relatively rigid. Shear wave velocity of soil generally increases with soil depth. CCR is generally characterized by shear wave velocity less than 1500 ft/s, except in areas where CCR is dense and compacted. Shear wave velocity of the CCR generally increases with CCR burial. Rock is generally characterized by shear wave velocity ranging from 1500 ft/s to over 5000 ft/s. Shear wave velocity of rock generally increases with rock depth. Except beneath the CCR landfill, soil/rock contact generally correlates well with the 1500 ft/s shear wave velocity interval. The soil/rock contact is relatively easy to identify on MASW data except in areas where upper bedrock is pervasively weathered and overlying soil is relatively rigid. The CCR/clay liner, clay liner/soil and soil/rock contacts beneath the landfill cannot be confidently mapped using

MASW data. Resolution of MASW layers is about 20 ft high and the upper rock underneath the CCR is very fractured and has comparable shear wave velocity values to overlying compacted soil and CCR.

Overall, MASW top-of-rock data correlates reasonably well with the ERT top-of-rock data. Differences between ERT and MASW data appear to be caused by the resolution difference between the two survey techniques.

Some rainfall seems to seep into the CCR deposit. The calcium sulfate in the FGD materials, and the initial moisture in the CCR could both contribute to the relatively low resistivity of the CCR. The most prominent seepage pathways are immediately adjacent to the toe of the landfill. All other identified seepage pathways are associated with anthropogenic features such as drainage ditches and perimeter berms. Seepage at the toe of the landfill tends to percolate vertically into the subsurface. But, there also appears to be a lateral component to seepage, both towards and away from the landfill. The overall resistivity of the bedrock appears to decrease with increasing distance from the landfill toe. The overall resistivity of the bedrock appears to decrease with increasing distance from anthropogenic features.

Resistivity of the subsurface varies seasonally with precipitation. At several locations, the resistivity of shallow limestone overall was lower on the data acquired after heavy precipitation.

No karst features that could be affected by the seepage, such as solution widened joints in the subsurface underneath and in proximity to the landfill, were found on the ERT profiles. No karst features such as air-filled voids that are significant enough to potentially cause landfill structure failures were found on the ERT profiles.

BIBLIOGRAPHY

- ACAA. (2016). Fly Ash Production and Use with Percent. Retrieved from <https://www.aaa-usa.org/Portals/9/Files/PDFs/2016-Charts.pdf>
- Advanced Geoscience Incorporated. (2005). The SuperSting™ with Swift™ automatic resistivity and IP system Instruction Manual, (512), 88.
- Alley, W. M., Reilly, T. E., & Franke, O. L. (1999). Sustainability of Ground-Water Resources, U.S. Geological Survey Circular 1186. U.S. Geological Survey Circular 1186, 79.
- Bell, J., Daly, K., & Shumpert, M. (2017). Practical Considerations for CCR Facility Design, Operations, and Maintenance. Retrieved from <http://www.flyash.info/2017/117-Leedy-woca2017p.pdf>
- Blair, R. (1986). GEO_CHAPTER_7.HTML. Retrieved July 9, 2018, from http://geoinfo.amu.edu.pl/wpk/geos/GEO_7/GEO_CHAPTER_7.HTML
- Brian Palmer. (2015). Coal Ash, Fly Ash, Bottom Ash, and Boiler Slag | NRDC. Retrieved from <https://www.nrdc.org/onearth/coal-ash-fly-ash-bottom-ash-and-boiler-slag>
- Briney, A. (2017). Overview of Aquifers and the Ogallala Aquifer. Retrieved July 17, 2018, from <https://www.thoughtco.com/ogallala-aquifer-1435307>
- British Geological Survey, N. (2017). Caves and karst | Foundations of the Mendips. Retrieved July 17, 2018, from https://www.bgs.ac.uk/mendips/caveskarst/karst_1.htm
- Butalia, T. S. (2011). Coal Combustion Products in Constructed Landfills. Retrieved from http://www.gseworld.com/content/documents/Coal_Ash_Seminar/Dr._Butalia.pdf
- Catawba Riverkeeper Foundation. (2018). Coal Ash. Retrieved July 16, 2018, from <https://www.catawbariverkeeper.org/state-of-the-river/coal-ash/>
- Chakradhar, V., & Katoch, S. S. (2016). Study of Fly Ash In Hydraulic Barriers In Landfills – A Review. International Refereed Journal of Engineering and Science, 5(4), 32–38. Retrieved from www.irjes.com
- Clark, J. T. (2017). Tennessee Landfills in Karst Environments.
- Cole, B., & Kuhn, J. (2017). Evaluating Compatibility of CCR with Leachate Collection System to Ensure Rule Compliance Introduction -Design and Site Conditions. Retrieved from <http://www.flyash.info/>

- Coppe. (2012). The sustainable future. Retrieved November 25, 2017, from http://www.coppe.ufrj.br/pdf_revista/rio20_ing.pdf
- Crum, B. (2018). CU efforts to expand John Twitty coal ash landfill stall. Retrieved July 16, 2018, from <https://www.news-leader.com/story/news/2018/02/22/cu-still-wants-expand-john-twitty-coal-ash-landfill-sierra-club-still-opposes/365270002/>
- D.W. Clark and D.W. Briar. (2001). What is Ground Water? Science for a Changing World, (April), 1–2. Retrieved from <http://pubs.usgs.gov/of/1993/ofr93-643/pdf/ofr93-643.pdf>
- De Carlo, L., Perri, M. T., Caputo, M. C., Deiana, R., Vurro, M., & Cassiani, G. (2013). Characterization of a dismissed landfill via electrical resistivity tomography and mise-à-la-masse method. *Journal of Applied Geophysics*, 98, 1–10. <https://doi.org/10.1016/j.jappgeo.2013.07.010>
- Delseaphysics1. (n.d.). Ohm's Law Notes. Retrieved from <https://sites.google.com/site/delseaphysics1/Home>
- Dey A. and Morrison H.F. 1979a. Resistivity modelling for arbitrary shaped two-dimensional structures. *Geophysical Prospecting* 27, 1020-1036.
- Duke Energy. (2016). Activists Lose Appeals of Coal Ash Landfill Permits | WFAE. Retrieved July 17, 2018, from <http://wfae.org/post/activists-lose-appeals-coal-ash-landfill-permits#stream/0>
- Earthjustice. org. (n.d.). Ashes: A Community's Toxic Inheritance | Earthjustice. Retrieved July 8, 2018, from <https://earthjustice.org/features/campaigns/photos-a-toxic-inheritance>
- Electric Power Research Institute, (EPRI), 1979, Coal ash disposal manual, FP-1257 Research Project 1404-1, 347 p.
- EPA. (2017). Frequent Questions about the Coal Ash Disposal Rule. Retrieved from <https://www.epa.gov/coalash/frequent-questions-about-coal-ash-disposal-rule>
- Fitts, C. (2013). Ground water Vadose zone Saturated zone. *Groundwater Science*, 1–19. Retrieved from <http://linkinghub.elsevier.com/retrieve/pii/B9780123847058000017>
- Freudebrich, C. (2000). Parts of a Landfill - How Landfills Work | HowStuffWorks. Retrieved July 17, 2018, from <https://science.howstuffworks.com/environmental/green-science/landfill6.htm>
- Galupino, J. G., & Dungca, J. R. (2015). Permeability characteristics of soil-fly ash mix. *ARPN Journal of Engineering and Applied Sciences*, 10(15), 6440–6447.

- Geology, T., & America, N. (2005). The goal of, 1–16. Retrieved from <http://www.landtecnica.com/wp-content/uploads/2014/12/RCRA-Subtitle-D-Regulations1.pdf>
- Geoscience, A. (2009). EarthImager 2D, (512), 139.
- Geotomo Software. (2011). Rapid 2-D Resistivity & IP inversion using the least-squares method.
- Ginzburg, A. (1974). Resistivity surveying. *Geophysical Surveys*, 1(3), 325–355. <https://doi.org/10.1007/BF01449118>
- Giroud, J. P. (1997). Equations for calculating the rate of liquid migration through composite liners due to geomembrane defects. *Geosynthetics International*, 4(March 1998), 3–4. <https://doi.org/10.1680/gein.4.0097>
- Gottfried, R. (n.d.). Burlington Formation. Retrieved November 26, 2017, from <http://www.lakeneosho.org/Miss26.html>
- Green, R. T., Painter, S. L., Sun, A., & Worthington, S. R. H. (2006). Groundwater contamination in karst terranes. *Water, Air, and Soil Pollution: Focus*, 6(1–2), 157–170. <https://doi.org/10.1007/s11267-005-9004-3>
- Hardin, C. D., Perrotta, N. L., & Haley, P. E. (2011). Operations and Maintenance Guidelines for Coal Ash Landfills. In *World of Coal Ash Conference*. Retrieved from <http://www.flyash.info/2011/127-Hardin-2011.pdf>
- Herman, R. (2001). An introduction to electrical resistivity in geophysics. *American Journal of Physics*, 69(9), 943–952. <https://doi.org/10.1119/1.1378013>
- Herrmann, I., Svensson, M., Ecke, H., Kumpiene, J., Maurice, C., Andreas, L., & Lagerkvist, A. (2009). Hydraulic conductivity of fly ash-sewage sludge mixes for use in landfill cover liners. *Water Research*, 43(14), 3541–3547. <https://doi.org/10.1016/j.watres.2009.04.052>
- Kalyoncu, R. S. (1997). Coal combustion products. Retrieved from <https://www.aaa-usa.org/Portals/9/Files/PDFs/News-Release-Coal-Ash-Production-and-Use-2015.pdf>
- Kansas Geological Survey. (2014). Retrieved from <http://www.kgs.ku.edu/software/surfseis/masw.html>
- Kaufmann, J. (2007). Sinkholes Catastrophic Sinkhole Collapse in Missouri. Retrieved from <https://pubs.usgs.gov/fs/2007/3060/pdf/FS2007-3060.pdf>
- Keller G.V. and Frischknecht F.C., 1966. Electrical methods in geophysical prospecting. Pergamon Press Inc., Oxford.

- Kentucky Geological Survey, University of Kentucky, Green, R. T., Painter, S. L., Sun, A., & Worthington, S. R. H. (2006). Groundwater contamination in karst terranes. *Water, Air, and Soil Pollution: Focus*, 6(1–2), 157–170.
<https://doi.org/10.1007/s11267-005-9004-3>
- Kim, B., Prezzi, M., & Salgado, R. (2005). Geotechnical Properties of Fly and Bottom Ash Mixtures for Use in Highway Embankments. *Journal of Geotechnical and Geoenvironmental Engineering*, 131(7), 914–924.
[https://doi.org/10.1061/\(ASCE\)1090-0241\(2005\)131:7\(914\)](https://doi.org/10.1061/(ASCE)1090-0241(2005)131:7(914))
- Kincaid, T. R. (2003). Groundwater Tracing | Global Underwater Explorers. Retrieved July 17, 2018, from <https://www.gue.com/groundwater-tracing>
- Koch, K. M. (2004). Application of electrical resistivity tomography (ERT) together with tracer data to identify hydrological process areas at a surface water / groundwater test site, Thesis, (August). Retrieved from http://www.hydrology.uni-freiburg.de/abschluss/Koch_K_2004_DA.pdf
- Lagmanson, M. (2005). Electrical Resistivity Imaging, 41.
- Loke, D. M. (1999). Electrical imaging surveys for environmental and engineering studies, 6574525(1999), 63. <https://doi.org/10.3390/su8111117>
- Loke, M. H. (2004). 2-D and 3-D Electrical Imaging Surveys. Tutorial, (July), 29. Retrieved from <http://citeseerx.ist.psu.edu/viewdoc/download?doi=10.1.1.454.4831&rep=rep1&type=pdf>
- Marshall, S. (2006). Electrical Methods Resistivity Surveying Chapter 12. Retrieved from www.appstate.edu/~marshallst/GLY3160/lectures/12_Resistivity.pptx
- MDNR. (2016). Coal Combustion Residual Storage and Disposal Sites in Missouri Division of Environmental Quality. Retrieved from <https://dnr.mo.gov/env/swmp/docs/CCRWhitePaper7-29-16.pdf>
- Mull, D. S. (1993). Use of Dye Tracing to Define the Direction of Ground-Water Flow from a Superfund Waste-Disposal Site in Karst Terrane, Near Auburn, Kentucky. Retrieved from <https://pubs.usgs.gov/wri/1992/4195/report.pdf>
- Nebraska, S. O. F. (2008). Department of Natural Resources. Water, (2), 2–4. Retrieved from <https://dnr.mo.gov/geology/wrc/groundwater/education/provinces/springfieldplatprovince.htm?/env/wrc/groundwater/education/provinces/springfieldplatprovince.htm>
- Neil L. Anderson, Derek B. Apel and Ahmed Ismail. (2006). “Assessment of Karst activity at Highway Construction Sites Using the Electrical Resistivity Method,” unpublished report for MoDOT.

- Nwokebuihe, S. C. (2014). The description of an effective sinkhole investigation approach: A case study of two sites in Greene County, Missouri. 27th Annual Symposium on the Application of Geophysics to Engineering and Environmental Problems (SAGEEP), 304–318. Retrieved from <http://adsabs.harvard.edu/abs/2014PhDT.....36N>
- Palmer, B. (2015). Coal Ash, Fly Ash, Bottom Ash, and Boiler Slag | NRDC. Retrieved July 8, 2018, from <https://www.nrdc.org/onearth/coal-ash-fly-ash-bottom-ash-and-boiler-slag>
- Peppler, R. A. (2012). Constructing and Managing Coal Ash Landfills. Retrieved July 8, 2018, from <http://www.powermag.com/constructing-and-managing-coal-ash-landfills/>
- Pettijohn, F.J. (1975) Sedimentary Rocks. 2nd Edition, Harper and Row Publishers, New York, 628 p.
- Prashanth J., Sivapullaiah P. and Sridharan A. 2001. Pozzolanic fly ash as a hydraulic barrier in landfills. Engineering Geology, Vol. 60, pp. 245-252.
- Recycled Materials Resource Center. (n.d.). UG-Mat Coal Bottom Ash/Boiler Slag | Recycled Materials Resource Center. Retrieved July 8, 2018, from <http://rmrc.wisc.edu/ug-mat-coal-bottom-ashboiler-slag/>
- Remediation Technologies Screening Matrix. (2016). 4-26 Landfill Cap. Retrieved July 8, 2018, from <https://frtr.gov/matrix2/section4/4-27.html>
- Roberts, M., Flanders, S., & Gumm, M. (2017). Utilizing Alternative Caps that meet Subtitle D Equivalency Requirements for CCP Landfill and Impoundment Closures to Gain Significant Savings and Secondary Use Opportunities. Retrieved from <http://www.flyash.info/>
- Rogers, J. D. (1998). Hydrocompression and Hydroswell-News Terms in the Geotechnical Dictionary.
- Rogers, J.D. (2016). GE 5441 Engineering Geology and Geotechnics lecture notes. Missouri University of Science and Technology.
- Rosano, B. M. (2017). How sinkholes form, 1–6.
- Rosenberg, M. (2018). Karst Topography and Sinkholes. Retrieved November 13, 2018, from <https://www.thoughtco.com/karst-topography-and-sinkholes-1435334>
- Ruhl, L., Vengosh, A., Dwyer, G. S., Hsu-Kim, H., Deonarine, A., Bergin, M., & Kravchenko, J. (2009). Survey of the potential environmental and health impacts in the immediate aftermath of the coal ash spill in Kingston, Tennessee. Environmental Science and Technology, 43(16), 6326–6333. <https://doi.org/10.1021/es900714p>

- Shanahan, P. (2004). 1.34 Waste Containment and Remediation Technology. Massachusetts Institute of Technology: MIT OpenCourseWare, <https://ocw.mit.edu>. License: Creative Commons BY-NC-SA.
- Shepard, E. M., 1898, A report on Greene County: Mo. Geol. Survey, 1st Ser. v. 12, p. 13-245.
- Silvester P.P. and Ferrari R.L., 1990. Finite elements for electrical engineers (2nd. ed.). Cambridge University Press.
- Site, I. (2011). FINAL CLOSURE AND POST CLOSURE PLAN COAL ASH LANDFILL COVER SYSTEM ASH LANDFILL PERMIT SW-09 / 01 Prepared for:, 058210(2).
- Soto, & Limaris R. (n.d.). Karst Topography Paper Model. Retrieved from <http://www.nature.nps.gov/geology/index.cfm>
- Teirstein, Z. (2018). Roses are red, violets are blue, America to coal: I might dump you. | Grist. Retrieved July 16, 2018, from <https://grist.org/briefly/roses-are-red-violets-are-blue-america-to-coal-i-might-dump-you/>
- Tenenbaum, D. (2009). Trash or treasure? Putting coal combustion waste to work. Environmental health perspectives, 117(11), A490-7.
- Tobergte, D. R., & Curtis, S. (2013). Chapter 3: Engineering practices of coal ash placement. Journal of Chemical Information and Modeling, 53(9), 1689–1699. <https://doi.org/10.1017/CBO9781107415324.004>
- U.S. Environmental Protection Agency (EPA). (2015). Final Rule: Disposal of Coal Combustion Residuals from Electric Utilities Rule History, 1–4. Retrieved from https://www.epa.gov/sites/production/files/2017-11/documents/frequent_questions_on_the_implementation_of_the_ccr_final_rule_full_list.pdf
- U.S. EPA. (2015). Disposal of Coal Combustion Residuals (CCR) from Electric Utilities and Independent Power Producers, Overview of Final Rule, March 4, 2015. Retrieved from www2.epa.gov/coalash.
- United States Department of Transportation. (2016). Coal Fly Ash User Guideline Embankment or Fill User Guidelines for Waste and Byproduct Materials in Pavement Construction. <https://doi.org/Publication Number: FHWA-RD-97-148>
- United States Environmental Protection Agency (US EPA). (2008). Ground Water Contamination. Getting Up to Speed, 10. Retrieved from <https://www.epa.gov/sites/production/files/2015-08/documents/mgwc-gwc1.pdf>
- University of Kentucky Center for Applied Energy Research. (2017). Bottom Ash Explored - CCBs, coal, combustion, by-products, structural fill, clinker, concrete blocks - Kentucky Ash Education Site - UK CAER

- USGS. (2017). USGS Groundwater Information: Land Subsidence. Retrieved July 17, 2018, from <https://water.usgs.gov/ogw/subsidence.html>
- Vandike, J. E., & Sherman, L. D. (1994). Hydrogeologic Investigation of the Fulbright Area, Greene County, Missouri. Retrieved from <https://dnr.mo.gov/pubs/WR43.pdf>
- W.V. Abeele. (1985). Consolidation and Shear Failure Leading to Subsidence and Settlement Los Alamos National Laboratory Los Alamos. New Mexico 87545, (November).
- Waltham, T. (2008). Sinkhole hazard case histories in karst terrains. *Quarterly Journal of Engineering Geology and Hydrogeology*, 41(3), 291–300. <https://doi.org/10.1144/1470-9236/07-211>
- Western Taney County Fire Protection District. (2018). Retrieved from <https://www.kansascity.com/news/state/missouri/article206348524.html>
- Whitehead Construction Inc. (2017). An Overview of Baghouse Fabric Filters. Retrieved July 8, 2018, from <http://www.precip.com/baghouses.html>
- Wikimedia Foundation. (2017). Fly ash. Wikimedia Foundation. Retrieved from <https://www.aaaa-usa.org/aboutcoalash/whatareccps/flyash.aspx>
- William, R., Thiery, R. G., Schuller, R. M., & Subway, J. J. (1981). Coal fly ash: a review of the literature and proposed classification system with emphasis on environmental impacts. *Environmental Geology Notes*, 1–78. Retrieved from <https://www.ideals.illinois.edu/bitstream/handle/2142/78929/coalflyashreview96royw.pdf?sequence=>

VITA

Ruobai Zhao was born in the city of Wulumuqi, Xinjiang Province, China. He graduated from China University of Petroleum in 2007 with a bachelor's degree in Petroleum Engineering. He was admitted to Missouri University of Science and Technology in 2011 and graduated in 2012 with a master's degree in Petroleum Engineering. He continued his study in Missouri University of Science and Technology and received a master's degree in Geological Engineering in 2017.

He worked as a graduate research assistant, a graduate teaching assistant and a graduate assistant during his study in Missouri University of Science and Technology. He actively participated in numerous engineering projects utilizing his knowledge in geotechnical engineering, engineering geophysics and engineering geology. He spent most of his time working in the field and conducting research in the lab.

In December 2018, he received his Ph.D. in Geological Engineering from Missouri University of Science and Technology.